CHALMERS
UNIVERSITY OF TECHNOLOGY

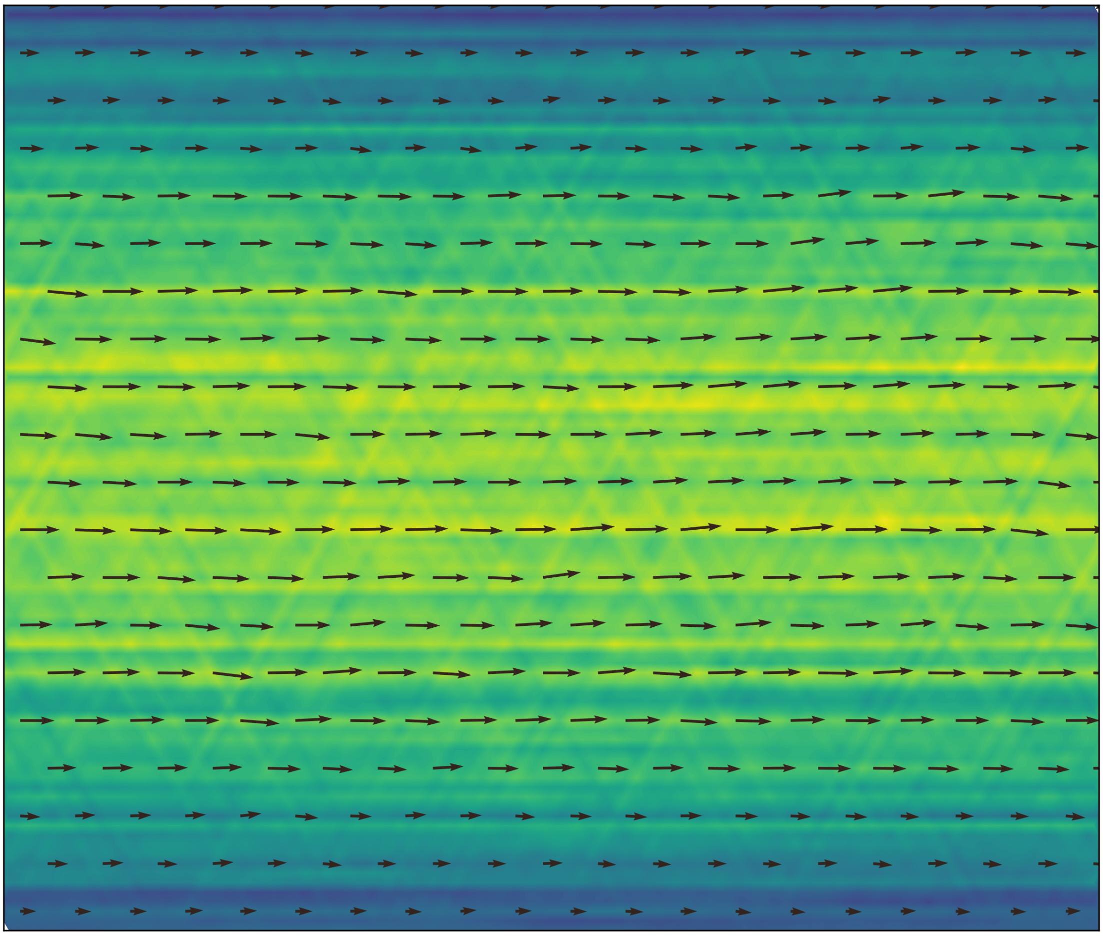

A Lattice Gas Cellular Automaton with Tomographic Dynamics

Master's thesis in Complex Adaptive Systems

SACKARIAS LUNMAN

DEPARTMENT OF PHYSICS
CHALMERS UNIVERSITY OF TECHNOLOGY
Gothenburg, Sweden 2026
www.chalmers.se

Master's thesis 2026

A Lattice Gas Cellular Automaton with Tomographic Dynamics

SACKARIAS LUNMAN

CHALMERS
UNIVERSITY OF TECHNOLOGY

Department of Physics
Chalmers University of Technology
Gothenburg, Sweden 2026

A Lattice Gas Cellular Automaton with Tomographic Dynamics
SACKARIAS LUNMAN

Supervisor: Johannes Hofmann, Department of Physics, University of Gothenburg
Examiner: Johannes Hofmann, Department of Physics, University of Gothenburg

Master's Thesis 2026
Department of Physics
Chalmers University of Technology
SE-412 96 Gothenburg
Telephone +46 31 772 1000

Cover: Velocity field from a lattice gas cellular automaton simulating flow in a channel.

Typeset in LaTeX
Printed by Chalmers Reproservice
Gothenburg, Sweden 2026

A Lattice Gas Cellular Automaton with Tomographic Dynamics
SACKARIAS LUNMAN
Department of Physics
Chalmers University of Technology

Abstract

We study the tomographic effect in lattice gas cellular automata, which are simple discrete models for hydrodynamics. The tomographic effect is predicted in two-dimensional Fermi liquids whenever head-on scattering dominates, leading to inefficient angular relaxation due to Pauli blocking. As a result, odd-parity deformations of the Fermi surface are anomalously long-lived compared to even-parity ones. We find an analogous effect in two-dimensional triangular lattice gas automata, which exhibit a single discrete odd-parity mode that we call the hexapolar mode. We analyze the relaxation times of the linearized lattice gas dynamics, and find that at low densities, head-on collisions dominate and the odd-parity mode is long-lived, resulting in a two-step relaxation of the system. At higher densities, three-body interactions set the dominant decay channel and the odd-parity mode becomes short-lived. We then analyze a reduced model of the lattice gas with a long-lived hexapolar mode, and derive the equilibrium distribution via entropy maximization. Using a small perturbation approximation and a multi-scale expansion, we derive a set of macroscopic equations that incorporate the hexapolar mode. We show that the odd-parity mode couples anisotropically to the momentum, leading to direction-dependent dynamics. We analyze the linear hydrodynamic modes and solve for the velocity profile in a channel (Poiseuille flow). We then compare our findings with the expected behavior for a two-dimensional Fermi liquid that exhibits the tomographic effect. Using the linearized kinetic equation for a two-dimensional homogeneous electron gas, we derive a set of linearized macroscopic equations. We conclude by discussing the limitations of the model due to its discrete nature and lack of full rotational symmetry.

Keywords: lattice gas cellular automata, hydrodynamics, electron transport, Fermi liquid

Acknowledgements

I first and foremost want to express my sincere gratitude to my supervisor, Johannes Hofmann, for his guidance and support. I also want to thank his doctoral students, Enrique Rozas Garcia and Viktor Frilén, as well as all the other members of the Department of Physics at the University of Gothenburg, for providing great company throughout this year.

Furthermore, I have had the privilege of meeting many international collaborators during this time. I want to thank Andrew Allocca, Sriram Ganeshan, and Gustavo Machado Monteiro for the productive discussions on lattice gas automata. I also want to express my gratitude to Nitay Ben-Shachar and Jeffrey Maki, whom I had the pleasure of meeting at the 855th WE-Heraeus Seminar in Hamburg, for the discussions on Fermi liquids and collective modes. I thank the Wilhelm and Else Heraeus Foundation for sponsoring the seminar.

Finally, I want to thank my friends and family. Thank you!

Sackarias Lunman, Gothenburg, June 2026

Contents

1

Introduction

What do the flow of air across the wing of an airplane, the convection of plasma in the sun, and the motion of a crowd of people have in common? They all demonstrate *hydrodynamic behavior*, one of the few universal truths in physics. Originally, hydrodynamics was the study of the viscous motion of liquids, such as water. Nowadays, fluids are studied through the branch of physics known as fluid mechanics, where the term fluid encompasses gases, liquids, and plasmas. Hydrodynamics, meanwhile, has broadened and appears in many seemingly disparate places in physics.

The success of hydrodynamics as a universal limiting behavior is due to its inherent simplicity and generality. In a system with many interacting components, where the interactions are sufficiently fast and leave some part of the system unchanged, one may expect hydrodynamic behavior. The parts of the system that are unchanged are known as *conserved quantities*, which are commonly the fundamental properties of mass, momentum, energy, and charge. More specifically, hydrodynamics describes the dynamics of conserved quantities near local equilibrium. The other parts of the system are assumed to decay fast and are effectively "integrated out." This is why one may approximate a crowd of people that are all bumping into each other as a fluid.

Fluid mechanics describes the motion of fluids using the continuity equations and the Navier-Stokes equations. The latter is a system of nonlinear partial differential equations (PDEs), originally developed by Claude-Louis Navier and George G. Stokes during the early 19th century. The equations are famously hard to solve except for very simple flows. For instance, the velocity profile of a fluid in a flat channel, known as Poiseuille flow, is fully solvable. Combining the fluid mechanical equations with Maxwell's equations allows one to describe electrically conducting fluids. This model is called magnetohydrodynamics, which is used to describe the motion of charged plasmas in stars.

Although originally devised phenomenologically, the fluid mechanical equations can be derived from an underlying microscopic description of interacting particles. Instead of describing every particle in a fluid individually, one can assume that the particles are interchangeable and describe the distribution of particles. Such a model is called a *kinetic theory*. To go from a kinetic description to a macroscopic description, such as the continuity and the Navier-Stokes equations, one can use a method called the *Chapman-Enskog expansion*.

1.1 Electron Hydrodynamics

Another place where one finds interacting particles and currents is in electronic systems. Historically, through the lens of solid state and condensed matter physics, electrical conductance has been understood using the classical kinetic theory proposed by Paul Drude in 1900 [1, 2]. The Drude model describes electrons, somewhat akin to billiard balls, that are accelerated by an electric field and bounce off immobile impurities, such as positively charged ions. Collisions with impurities cause the electrons to scatter off in random directions and lose momentum.

In 1927, Arnold Sommerfeld developed a quantum mechanical description of electrons known as the Drude-Sommerfeld model, or the free electron model [3]. Electrons are fermions and obey Pauli's exclusion principle, such that every quantum state can only be occupied by at most a single electron. Thus, the electrons are distributed according to the *Fermi-Dirac distribution function* at equilibrium. For temperatures $T \ll T_F$, where T_F is called the *Fermi temperature*, quantum fluctuations become dominant over thermal fluctuations. At these temperatures, the Fermi-Dirac distribution develops a sharp edge known as the *Fermi surface*. As $T \to 0$, all quantum states below the Fermi surface become occupied. If one assumes momentum relaxation by inhomogeneities in the lattice, such as impurity atoms or phonons, both the free electron model and the Drude model predict the same conductivity for Ohm's law.

The Drude and Sommerfeld pictures of electron flow in a metal are fundamentally different from the viscous flow of water. Both models ignore electron-electron interactions, which facilitate exchange of momentum between the particles. A fluid description of electron transport was first developed by Lev Landau in 1956 using his *Fermi liquid theory* [4]. Instead of individual electrons, the theory describes long-lived excitations called *quasiparticles*. Quasiparticles are fermions that have the same spin, charge, and momentum as electrons. Fermi liquid theory describes the kinetics of the quasiparticles that live close to the Fermi surface, including inter-quasiparticle interactions.

In 1963, Radii M. Gurzhi theorized a hydrodynamic electron regime [5]. The argument relies on the relation of different length scales in the system. The lengths ℓ_i and ℓ_{ee} are the mean free paths of an electron before it scatters off an impurity or with another electron, respectively. If one considers a system with a typical length scale l, there are three different limits with qualitatively different behaviors. For $l \ll \ell_{ee}, \ell_i$ we have the ballistic regime: Individual electrons move unimpeded by inhomogeneities and other electrons through the medium. For $l \gg \ell_{ee}, \ell_i$, we have the diffusive regime: The electrons quickly scatter and lose momentum. This is the regime of the Drude model and free electron model. Hydrodynamic behavior emerges when $\ell_{ee} \ll \ell_i, l$. In this regime, the dominant relaxation mechanism is electron-electron scattering which conserves momentum. Gurzhi calculated that the resistance will have a non-monotonic dependence on temperature in the hydrodynamic regime, which is now known as the Gurzhi effect.

In 2004, Konstantin S. Novoselov and Andre K. Geim described the electric field effect of graphene [6], a two-dimensional layer of densely packed carbon atoms. The material was found to be semimetallic, stable (down to a single atomic layer), and remarkably impurity-clean. The fabrication of graphene and other ultraclean materials with very large ℓ_i has sparked great interest in electron hydrodynamics [7, 8]. These experimental and theoretical studies make it possible to develop new high-mobility electronic devices that utilize hydrodynamic effects.

In 2017, Kumar *et al.* [9] measured the resistance of electron flow through a graphene constriction, which showed the same non-monotonic temperature dependence that Gurzhi predicted. In 2019, Sulpizio *et al.* [10] probed the Hall field of electron flow through a channel of graphene. The resulting Hall voltage across the channel showed a Poiseuille profile. In 2022, Aharon-Steinberg *et al.* [11] imaged the electron flow in a circular chamber. Inside the chamber, the current develops vortices, a phenomenon that appears in hydrodynamics. Finally, a recent experiment by Geurs *et al.* [12] studied electron flow through an electronic de Laval nozzle. In this compressible and nonlinear regime, the electrons are pushed beyond the electronic speed of sound and create shock waves.

Interestingly, electrons in two-dimensional Fermi liquids are theoretically predicted to have another transport regime that lies in between ballistic and hydrodynamic. To understand this, one needs to understand electron-electron scattering in two dimensions. For a Fermi liquid with $T \ll T_F$, the Fermi surface is very sharp. We also assume that the electron gas is sufficiently dilute such that we only need to consider pairwise scattering. Due to Pauli blocking, the states below the Fermi surface are mostly occupied, which constrains the allowed scattering configurations. For a two-dimensional Fermi liquid, there are two scattering types: small-angle scattering and head-on scattering (Fig. 1.1) [13, 14]. In small-angle scattering, both incoming quasiparticles rotate by a small angle $\Delta\theta \sim T/T_F \ll 1$ such that both outgoing particles are still close to the Fermi surface. This relaxation process therefore involves very slow angular diffusion, known as angular subdiffusion. In contrast, head-on scattering has zero total momentum, allowing both outgoing particles to rotate by an arbitrary $\Delta\theta$, leading to very quick angular relaxation.

Gurzhi *et al.* [14] realized that head-on scattering in two-dimensional Fermi liquids only relaxes the inversion-symmetric parts of the quasiparticle distribution. The symmetric parts of the distribution relax quickly, while the antisymmetric parts relax via the slow small-angle collisions. Another way of picturing this is by considering a linear perturbation around an isotropic two-dimensional Fermi surface. This perturbation may be expanded in Fourier modes, as illustrated in Fig. 1.2. The zeroth and first modes (in a trigonometric basis) represent a shift in density and momentum, respectively. The *even-parity modes* are symmetric and relax quickly on a length scale ℓ_e. Conversely, the *odd-parity modes* are antisymmetric and relax slowly on a longer length scale ℓ_o. The odd-parity deformation modes can therefore be regarded as long-lived collective excitations, which preserve sharp local features of the Fermi surface. This is called the odd-even effect, or the *tomographic effect*. The tomographic transport regime $\ell_e \ll l \ll \ell_o, \ell_i$ constitutes a mix of ballistic odd-parity modes and hydrodynamic even-parity modes.

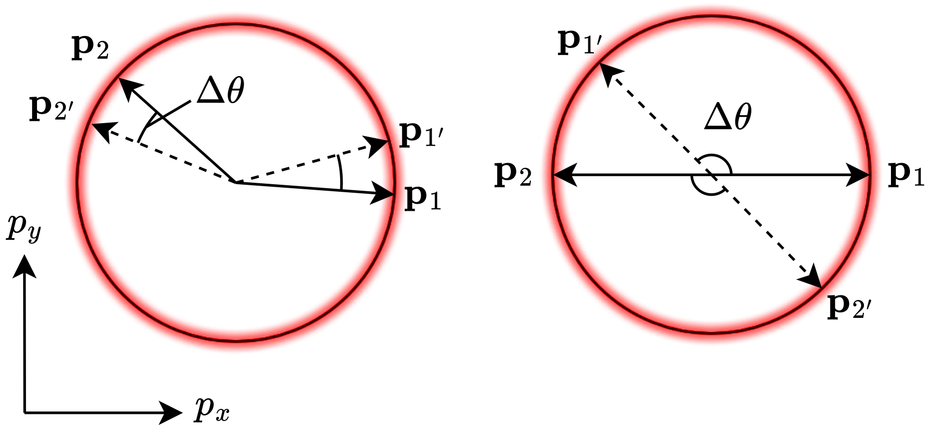

Figure 1.1: The two relaxation mechanisms available to quasiparticles in a two-dimensional Fermi liquid. The black circle is the Fermi surface and the red outline is the thermal window. The vector pairs $(\mathbf{p}_1, \mathbf{p}_2)$, and $(\mathbf{p}_1', \mathbf{p}_2')$ are the momentum vectors of two quasiparticles before and after scattering. The change in the angle of the momentum vectors after scattering is $\Delta\theta$. The left picture shows small-angle scattering and the right picture shows head-on scattering.

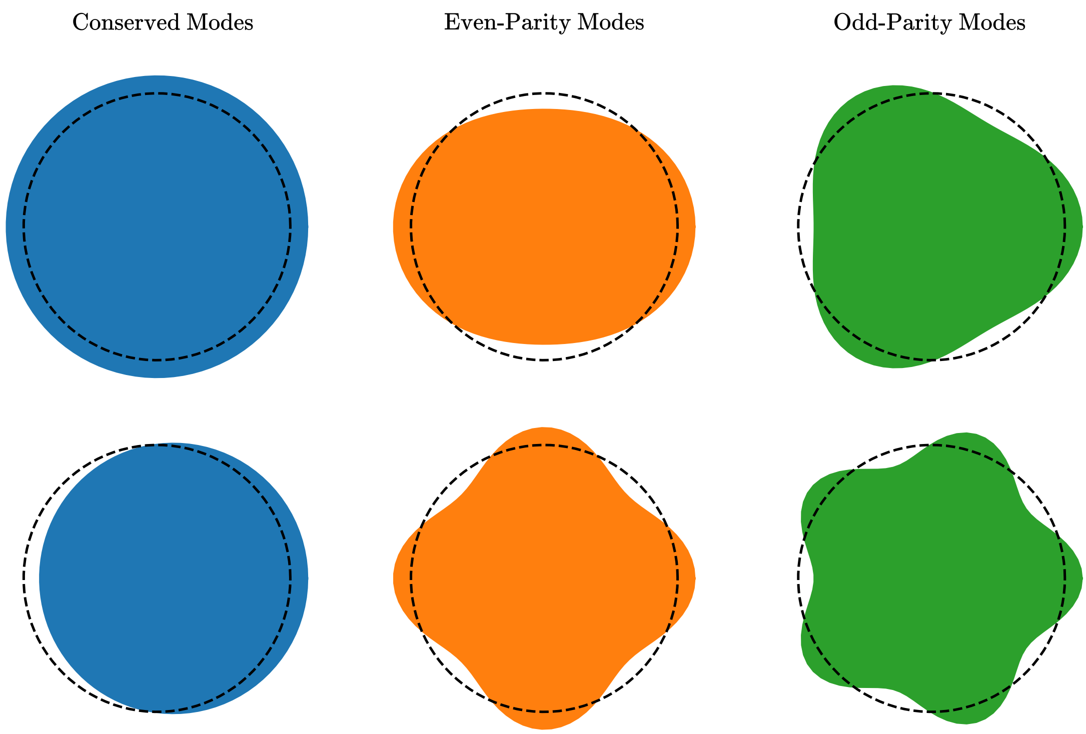

Figure 1.2: Fourier modes of a linear perturbation around a two-dimensional Fermi surface (black dashed line). The filled colored areas are occupied states.

1.2 Discrete Fluids

Due to the difficulties involved in solving the Navier-Stokes equations analytically in complex flows, physicists and fluid dynamicists often resort to numerical solutions. The subfield of computational fluid mechanics has devised many computational methods, such as the finite volume method and finite element method. These methods can be regarded as *top-down approaches*, since the starting point is to discretize the macroscopic Navier-Stokes equations, and not the underlying microscopic picture. Another way to numerically model fluids is the *bottom-up approach*. Instead of discretizing partial differential equations, we model the microscopic dynamics such that the average behavior approaches the macroscopic equations. One such method is *molecular dynamics*, which involves simulating the microscopic particles that make up the fluid using Newton's laws, or some approximation thereof. Due to the large number of particles involved, this method is computationally extremely expensive for large systems.

In the late 1940s and early 1950s, John von Neumann and Stanisław M. Ulam introduced the *cellular automaton*[1]. The two mathematicians developed the idea in order to study self-replicating machines [19, 20]. Cellular automata (CA) are models consisting of elements, or cells, with states. The states change in time based on an update rule. Straightforward examples of CA are the elementary cellular automata studied by Stephen Wolfram in the 1980s [21]. These automata consist of a one-dimensional grid of cells that have binary states that are either zero or one. One may also think of the states as *Boolean*, with values false or true. The time is discrete and the update rule is local, such that the state at position r at time $(t+1)$ depends on the state at positions $(r-1)$, r, and $(r+1)$ at time t, where r and t are integers. Thus, there are in total $2^{(2^3)} = 256$ possible rules for elementary cellular automata, three of which are illustrated in Fig. 1.3.

After the introduction of cellular automata, physicists started thinking about using them to model fluids. This idea was realized in 1973 by Jean Hardy, Yves Pomeau, and Olivier de Pazzis when they introduced the first in a class of models known as *lattice gas cellular automata* (LGCA) [22]. This model, later named the *HPP model* after its authors, simulates fluid particles that propagate throughout a two-dimensional square lattice. The particles have a discrete velocity, such that they hop to a neighboring lattice site at each time step. The update rule describes inter-particle collisions that obey the conservation of mass, momentum, and energy. Similar to molecular dynamics, LGCA is a bottom-up approach. In 1986, Uriel Frisch, Brosl Hasslacher, and Yves Pomeau developed an LGCA with a triangular lattice, which is now known as the *FHP model* [23]. Further work by Dominique d'Humières and Pierre Lallemand extended LGCA to three dimensions [24].

The early LGCA employ a regular lattice and a Boolean representation of the automaton state: At each site, there are b outgoing edges to neighboring sites. For every edge, there may be zero or one particle with a velocity in the direction of

[1] The work on cellular automata by von Neumann was left unfinished due to his premature death in 1957. What is left is a series of lectures on the topic [15, 16], some of which were compiled into the book *The Computer and the Brain* [17]. The unfinished manuscripts for his systematic theory of cellular automata were later edited and completed by Arthur Burks [18].

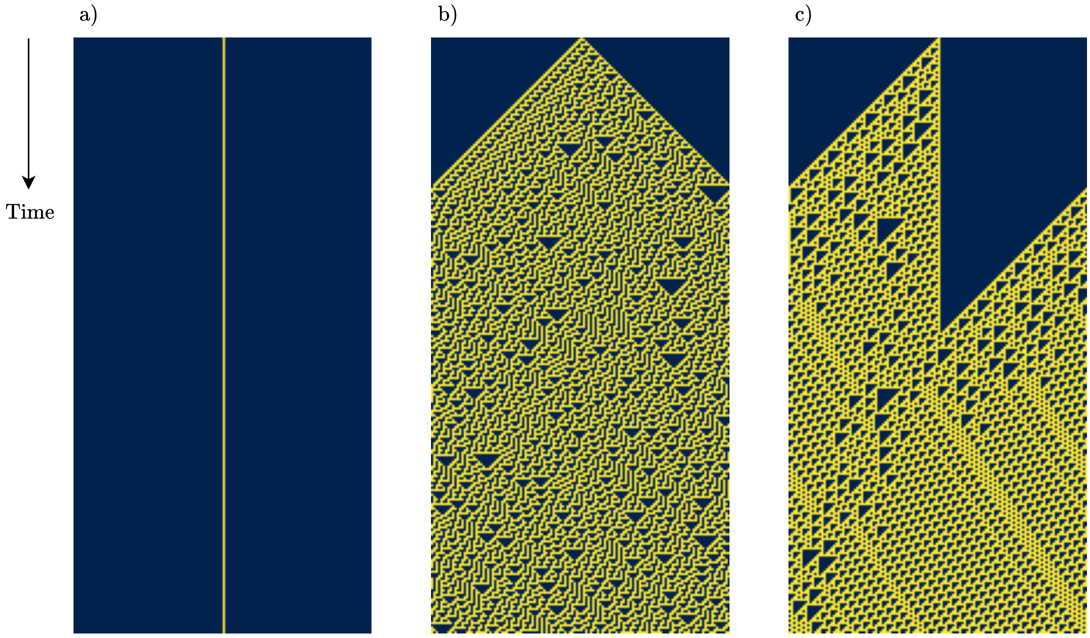

Figure 1.3: The evolution of elementary cellular automata obeying different update rules with periodic boundary conditions, where dark (light) squares indicate state zero (one). The initial condition is a single cell with state one. The horizontal axis is the discrete positions of the cells. The vertical axis is the discrete time. Using Wolfram's naming convention, the shown update rules are rule 4, 30, and 110 from left to right.

that edge. Thus, each node has 2^b possible states. Due to the Boolean nature of the particles, LGCA obey Fermi-Dirac statistics. Since at most one particle may occupy the same node and velocity, the particles obey Pauli exclusion. Due to the simple collision rules, the high degree of parallelization, and relatively few bits required, LGCA are very computationally efficient.

Later work on LGCA attempted to remove the fermionic properties and restore Maxwell-Boltzmann statistics. This resulted in the development of the *lattice Boltzmann method* (LBM), which describes the dynamics of the mean number of particles. These models were first used to simulate fluids by Guy R. McNamara and Gianluigi Zanetti in 1988 [25], and are still in use today to model complex fluids. There are also LGCA that remove Pauli exclusion and allow multiple particles to occupy the same state, such as integer lattice gas cellular automata [26].

The analogy of LGCA to Fermi liquids goes further. In the work of Frisch *et al.* [27], the existence of *spurious conservation laws* is mentioned. Specifically, the authors bring up that for the FHP model, if one only considers head-on collisions, the difference in particle numbers in any pair of opposite directions is conserved. This amounts to three new scalar conservation laws, besides the conservation of mass. This is very similar to tomographic transport in two-dimensional Fermi liquids, where head-on scattering gives rise to long-lived odd-parity modes.

1.3 Aim and Purpose

The aim of this thesis is to analyze the spurious conservation laws in LGCA. The goal is to show that these conserved quantities are equivalent to the long-lived odd-parity modes found in two-dimensional Fermi liquids. The purpose of the thesis is to establish a theoretical and computational model that can be used to study simple tomographic transport.

In Chapter 2, we review the existing work on LGCA. First, we provide the reader with the basic intuition of this class of models. We describe in detail the mechanics of HPP and FHP models. We then establish the mathematical formalism to describe the microscopic dynamics of the model. We introduce the collision function which describes the collision rules of the models. We then analyze the system using a probabilistic description. We introduce the lattice Boltzmann approximation and the linearized collision matrix.

In Chapter 3, we begin our analysis of the spurious conservation laws. We show that the three spurious scalar conservation laws in the FHP model are equivalent to the conservation of momentum and a scalar quantity called the hexapolar mode. The hexapolar mode is the cosine part of the third Fourier mode of a linear perturbation of the single-particle distribution function. We analyze the microscopic relaxation rates and show that at low densities, the FHP model exhibits a two-step relaxation process, analogous to the tomographic effect. We derive the macroscopic equations of the LGCA, i.e., the Navier-Stokes equations, using a multi-scale expansion similar to the Chapman-Enskog expansion. We derive an additional equation that describes the dynamics of the long-lived hexapolar mode, assuming that it is lightly damped. We analyze the linearized macroscopic equations to find the linear hydrodynamic modes. We end the chapter by analyzing flow in a channel.

In Chapter 4, we derive a set of macroscopic equations for a two-dimensional Fermi liquid. Using *adiabatic elimination*, we derive an equivalent set of PDEs to the LGCA with a long-lived hexapolar mode, although to linear order in the perturbations and without the lattice artifacts. We explain how to go from the hexapolar Fermi liquid equation to the hexapolar lattice gas equation, and the failures of the LGCA to model tomographic dynamics.

In Chapter 5, we conclude the thesis by discussing the applicability of using lattice gas models to simulate tomographic Fermi liquids. We then offer some possible future research directions for LGCA in condensed matter physics, as well as use cases for our derived Fermi liquid equations.

2

Lattice Gas Cellular Automata Background

This chapter introduces the existing body of work on LGCA. The theory in this chapter is derived from the work of Frisch *et al.* [27]. The article by Hasslacher [28] serves as an introduction to LGCA while providing a background on the relevant kinetic theory. The article also contains illustrations of lattice gas simulations in different flow scenarios. The book by Wolf-Gladrow [29] introduces cellular automata and covers a large number of different lattice gas and lattice Boltzmann models.

Going forward, the terms *lattice gas cellular automaton*, *lattice gas automaton*, *lattice gas*, and *automaton* will be used interchangeably. Similarly, the terms *site* and *node* are used interchangeably. The former term is preferred while the latter is used in conjunction with the term *edge* in order to describe the lattice as a graph. The term *cell* is instead used to describe a specific velocity channel at a site.

2.1 The HPP Model and FHP Models

Before delving into the theory, let us discuss how a lattice gas automaton works. To this aim, in the following we describe and illustrate the dynamics of LGCA, starting with the HPP model. In the HPP model, a number of particles occupy the sites of a 2D lattice. The particles are identical, have unit mass and move with a single speed c. The lattice here is a square grid. Each lattice site is connected to four neighboring sites to its north, east, south, and west. These directions constitute the four velocity channels that the particles are allowed to move along. Importantly, at a given site, at most one particle is allowed to occupy a velocity channel. In other words, an occupied velocity channel, or cell, constitutes a particle. This is a general feature of this class of models and prescribes the exclusion principle. As such, the occupation of each site can be represented by four bits. Empty cells are referred to as *holes*.

The dynamics is discrete in time with a unit time step and discrete time instant denoted by t_*. The dynamics can be split into two steps: collisions and streaming. Collisions occur on each site locally and are designed to conserve the local total mass (or simply particle number or particle density) and total momentum. Note that the conservation of energy is redundant here: the particle speed is fixed, making the conservation of mass equivalent to the conservation of energy. This limits collisions to configurations with two particles of opposite velocities. After scattering, the two particles rotate by 90°, flipping the occupation of the four velocity channels (see

Fig. 2.1). During the streaming step, also called the propagation step, the particles simply translate to the neighboring lattice site in the direction of their velocity channel. An illustration of the evolution of the HPP model for a single time step is seen in Fig. 2.2.

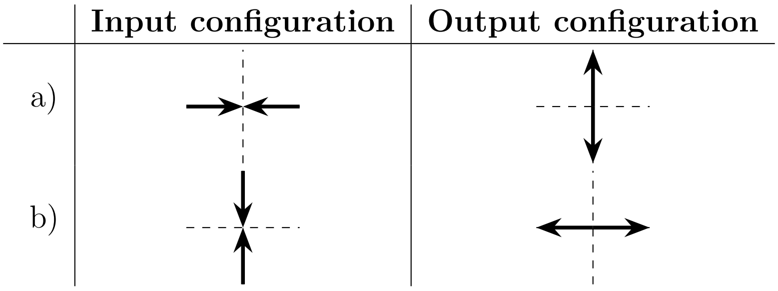

Figure 2.1: Collision rules for the HPP model. The arrows represent the occupied velocity channels.

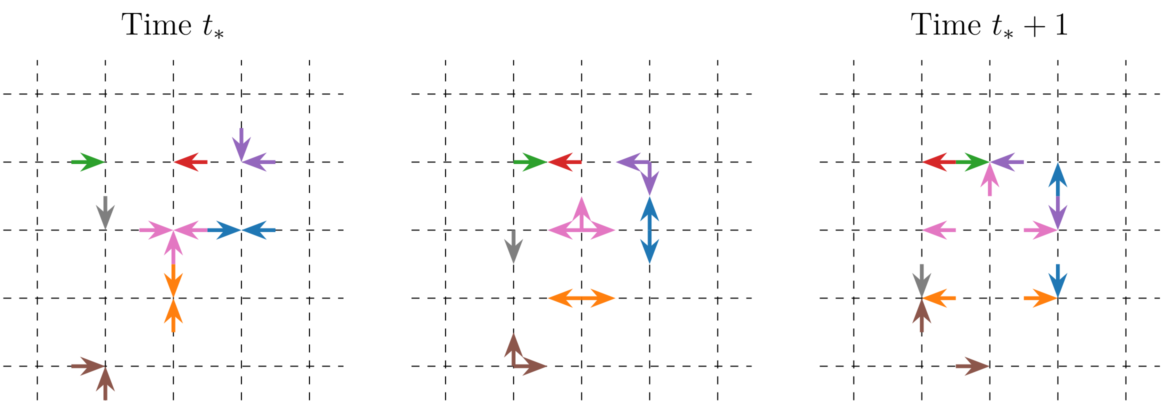

Figure 2.2: The evolution of the HPP model for a single time step. The intersections of the dashed lines are lattice sites and the arrows denote particles. The directions of the arrows are aligned with the respective velocities of the particles. Particles with the same color are located on the same lattice site at time t_*. The particles are illustrated to be placed on the edges during propagation and on the lattice sites during collisions. Two collisions are shown in the figure (the blue and orange particles). Note that some pairs of particles with opposite momenta appear to pass through one another, for instance the green and red particles. This is a consequence of the discrete nature of the model, as the particles are not at the same lattice site at the time of the collision step.

It turns out that when deriving the macroscopic equations of the HPP model some terms do not have the same tensor structure as the ones found in the Navier-Stokes equations [27]. The reason for this has to do with the square lattice. The FHP model meanwhile with its triangular lattice retrieves the correct tensors in its macroscopic equations. The additional symmetry axis of the triangular lattice means that many more scattering configurations are possible.

Historically, the collision rules of the FHP model have been categorized into three different variants [27]. We will focus on the one called FHP-I, which has four types of collisions. These are two-body collisions (see Fig. 2.3(a)), four-body collisions (see Fig. 2.3(b)), asymmetric three-body collisions (see Fig. 2.3(c)), and symmetric three-body collisions (see Fig. 2.3(d)).

In a two-body collision, there are two possible outcomes which represent a rotation by 30° clockwise or counterclockwise. The four-body collisions are equivalent to swapping the particles and the holes in two-body collisions. These collisions make the model particle-hole symmetric. Both types of three-body collisions are deterministic. The two-body, asymmetric three-body, and four-body collisions are head-on collisions. The evolution of the FHP-I model for a single time step is shown in Fig. 2.4.

In contrast to the HPP model, which is fully deterministic, the FHP model has non-deterministic collisions. We have introduced the probabilities p_2, p_{3s}, p_{3a}, and p_4 to have two-body, symmetric three-body, asymmetric three-body, or four-body collisions.

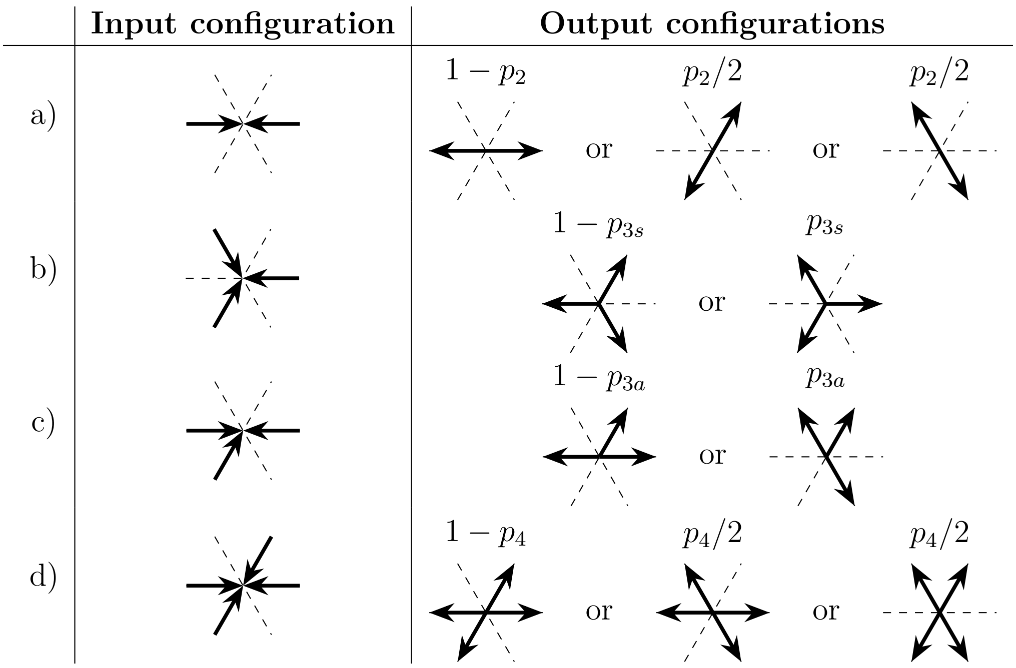

Figure 2.3: Types of collisions in the FHP-I model. The value above each output state is its transition probability, given the input state.

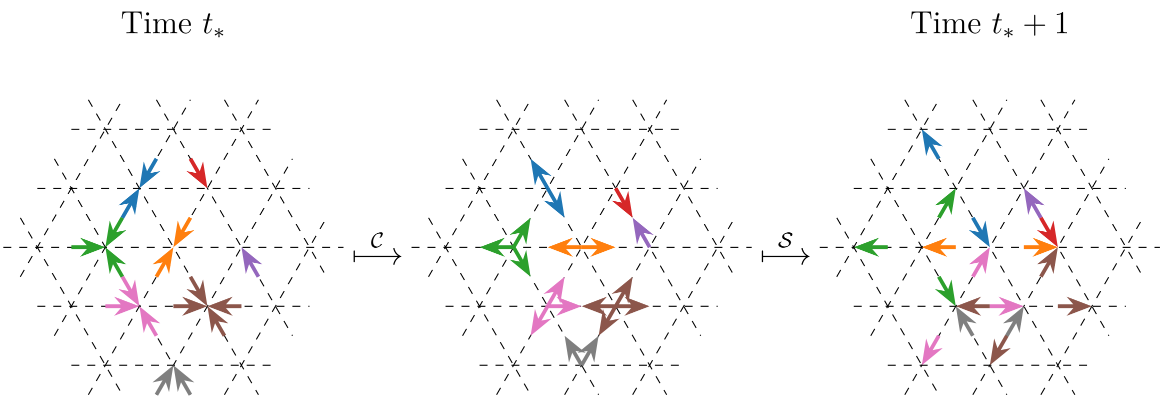

Figure 2.4: The evolution of the collision-saturated FHP-I model for a single timestep. The intersections of the dashed lines are lattice sites and the arrows denote particles. The directions of the arrows are aligned with the respective velocities of the particles. Particles with the same color are located on the same lattice site at time t_*. All four types of collisions are illustrated. These are two-body collisions with zero spectators (the blue and orange particles), three-body collisions (the green particles), two-body collisions with two spectator particles (the brown particles), and asymmetric three-body collisions (the pink particles).

2.2 Mathematical Formalism

We introduce a mathematical formalism to describe LGCA as a general class of hydrodynamic models. We assume the lattice is a d-dimensional Bravais lattice $\mathcal{L}$. We will later restrict ourselves to two-dimensional systems with $d = 2$. The lattice has sites, or nodes, interconnected by edges to their nearest neighbors. The lattice sites have a position vector $\mathbf{r}_*$ which is a linear combination of d independent generating vectors with integer coefficients.

Although LGCA with multiple allowed speeds have been studied [29], we will restrict ourselves to particles with a single speed, such as the HPP and FHP models. There are also models that incorporate *rest particles* with zero velocity. This includes both the FHP-II and FHP-III variants. We will not consider rest particles in this analysis.

We assume that there are b velocity vectors $\mathbf{c}_j$ for $j = 0, 1, \ldots, b-1$ with equal modulus c. For a site $\mathbf{r}_* \in \mathcal{L}$, the nearest set of neighbors is the set of $\mathbf{r}_* + \mathbf{c}_j$ for all j. Using the unit time step τ, we have the lattice constant $c\tau$. Further, any two sites can be connected by a finite chain of nearest neighbors. For a regular two-dimensional lattice, the velocity vectors are defined as

$$\mathbf{c}_j = c \begin{pmatrix} \cos(\theta_j) \\ \sin(\theta_j) \end{pmatrix}, \quad \text{for } j = 0, 1, \ldots, b-1, \tag{2.1}$$

where b is the number of outgoing edges at each site and

$$\theta_j = \frac{2\pi j}{b}. \tag{2.2}$$

Let the discrete time instant be denoted as t_*. We can represent the occupation state of each lattice site as a vector

$$\mathbf{n}(t_*, \mathbf{r}_*) = \{n_j(t_*, \mathbf{r}_*) \in \{0, 1\},\ j = 0, 1, \ldots, b-1\}, \tag{2.3}$$

where the elements n_j, referred to as cells, are Boolean variables. There are 2^b possible particle configurations at each site, which is the number of possible b-bit words. The particle in cell j has velocity $\mathbf{c}_j$.

To treat collisions, we introduce the collision transition probability $A(\mathbf{s}' \leftarrow \mathbf{s}) \geq 0$. It describes the probability of transitioning from an in-state $\mathbf{s} \in \{0, 1\}^b$ to an out-state $\mathbf{s}' \in \{0, 1\}^b$. The transition probability is node independent and normalized to one, such that

$$\sum_{\mathbf{s}'} A(\mathbf{s}' \leftarrow \mathbf{s}) = 1, \quad \forall \mathbf{s}. \tag{2.4}$$

Any real vector $\mathbf{a} \in \mathbb{R}^b$ that satisfies

$$\sum_j (s'_j - s_j) A(\mathbf{s}' \leftarrow \mathbf{s}) a_j = 0, \quad \forall j, \mathbf{s}, \mathbf{s}' \tag{2.5}$$

represents a conservation law. Eq. (2.5) states that the weighted sum, or observable, $\sum_j a_j s_j$ stays constant after applying collisions and is thus conserved. For hydrodynamic lattice gases, the only allowed values for the collision invariant vectors a_j are $a_j \propto 1, c_{j1}, \ldots, c_{jd}$ for all j, which are related to conservation of density and momentum. We further assume that the collisions satisfy semi-detailed balance, such that

$$\sum_{\mathbf{s}} A(\mathbf{s}' \leftarrow \mathbf{s}) = 1, \quad \forall \mathbf{s}'. \tag{2.6}$$

Eq. (2.6) and semi-detailed balance can be interpreted as saying that if every state has equal probability before collision, this remains true after collision.

Microdynamical Equations

In this section, we describe the microscopic dynamics of lattice gas cellular automata. The dynamics consists of collisions and propagation of the Boolean field $\mathbf{n}$ introduced in Eq. (2.3). We begin by writing the update of the HPP model in arithmetic form. This is done by introducing a collision function $\Delta_j(\mathbf{n})$ such that the propagated state $n_j(t_* + 1, \mathbf{r}_* + \mathbf{c}_j)$ only depends on the previous state at the neighboring cell $n_j(t_*, \mathbf{r}_*)$. Using the collision function, we write the update equation of n_j as

$$n_j(t_* + 1, \mathbf{r}_* + \mathbf{c}_j) = n_j(t_*, \mathbf{r}_*) + \Delta_j(\mathbf{n}). \tag{2.7}$$

This equation is called the microdynamical equation. The collision function can take the values 0 or ± 1, thus leaving the Boolean variable unchanged or incrementing or decrementing it by one. The propagation step is simply a translation $\mathbf{r}_* \mapsto \mathbf{r}_* + \mathbf{c}_j$.

For the HPP model, the collision function is written as

$$\Delta_j(\mathbf{n}) = n_{j+1} n_{j+3} (1 - n_j)(1 - n_{j+2}) - n_j n_{j+2} (1 - n_{j+1})(1 - n_{j+3}), \tag{2.8}$$

which holds for arbitrary indices modulo b, $\mathbf{r}_* \in \mathcal{L}$, and integer t_*. The function is fully deterministic. The first term is the gain term for bit j, which flips the bit from zero to one if both bits j and $j+2$ are empty and both bits of the opposite pair $j+1$ and $j+3$ are occupied (right column in Fig. 2.1). The second term is the loss term for bit j. It is negative one if both bits j and $j+2$ are unity and the opposite bits $j+1$ and $j+3$ are zero (left column in Fig. 2.1).

Unlike the HPP model, the collision function of FHP-I is non-deterministic. The full expression of the function including all four collision types is quite long. One can write a collision function with only two-body collisions and symmetric three-body collisions (Fig. 2.3 (a) and (d)) as

$$\begin{aligned}\Delta_j(\mathbf{n}) = {} & \xi_{t_*\mathbf{r}_*} n_{j+1} n_{j+4}(1-n_j)(1-n_{j+2})(1-n_{j+3})(1-n_{j+5}) \\ & + (1-\xi_{t_*\mathbf{r}_*}) n_{j+2} n_{j+5}(1-n_j)(1-n_{j+1})(1-n_{j+3})(1-n_{j+4}) \\ & - n_j n_{j+3}(1-n_{j+1})(1-n_{j+2})(1-n_{j+4})(1-n_{j+5}) \\ & + n_{j+1} n_{j+3} n_{j+5}(1-n_j)(1-n_{j+2})(1-n_{j+4}) \\ & - n_j n_{j+2} n_{j+4}(1-n_{j+1})(1-n_{j+3})(1-n_{j+5}),\end{aligned} \tag{2.9}$$

where we have introduced the random Boolean variable $\xi_{t_*\mathbf{r}_*}$ to account for the non-deterministic outcomes of the two-body collisions. The spatial dependence of $\xi_{t_*\mathbf{r}_*}$ ensures that only a single outcome configuration is possible at a given lattice site. This outcome should not be static throughout time, hence the time dependence. The first two terms of the function describe the two gain terms of the two-body collision, which is where the $\xi_{t_*\mathbf{r}_*}$ enters (right column of Fig. 2.3(a)). The third term is the loss term of the two-body collision (left column of Fig. 2.3(a)). The fourth and fifth terms are the gain and loss terms of the three-body collision (right and left columns of Fig. 2.3(d)), respectively.

Both the HPP and FHP-I models are invariant under discrete lattice rotations. This means that no lattice direction is preferred.

The collision function can be generalized for arbitrary non-deterministic models. For an arbitrary input and output pair $(\mathbf{s}, \mathbf{s}')$, we define the random Boolean variable $\xi_{\mathbf{s}'\mathbf{s}}(t_*, \mathbf{r}_*)$. This variable determines the outcome of transitioning to $\mathbf{s}'$ from state $\mathbf{s}$. We will omit the space and time dependence for brevity and assume that the average of $\xi_{\mathbf{s}'\mathbf{s}}$ has the form

$$\langle \xi_{\mathbf{s}'\mathbf{s}} \rangle = A(\mathbf{s}' \leftarrow \mathbf{s}), \quad \forall \mathbf{s}, \mathbf{s}', \tag{2.10}$$

and it is normalized to one as

$$\sum_{\mathbf{s}'} \xi_{\mathbf{s}'\mathbf{s}} = 1, \quad \forall \mathbf{s}. \tag{2.11}$$

Using this variable, and treating the propagation the same as before, we can define the update step as

$$n_j(t_* + 1, \mathbf{r}_* + \mathbf{c}_j) = \sum_{\mathbf{s}\mathbf{s}'} s'_j \xi_{\mathbf{s}'\mathbf{s}} \left[\prod_k n_k^{s_k} (1-n_k)^{1-s_k} \right]. \tag{2.12}$$

where we define $0^0 = 1$. Since $\xi_{\mathbf{s}'\mathbf{s}}$ is Boolean, a single outcome is selected over the summation of all possible pairs $(\mathbf{s}, \mathbf{s}')$. The product factor in the square bracket ensures that the pattern of n matches that of the input state $\mathbf{s}$, and the $\mathbf{s}'$ factor sets the output bits of $\mathbf{n}(t_* + 1)$. From this, one may read off the identity

$$\sum_{\mathbf{s}} s_j \prod_k n_k^{s_k} (1 - n_k)^{1-s_k} = n_j. \tag{2.13}$$

Using Eq. (2.13), the update step in Eq. (2.12) can be written as

$$n_j(t_* + 1, \mathbf{r}_* + \mathbf{c}_j) = n_j(t_*, \mathbf{r}_*) + \sum_{\mathbf{s}\mathbf{s}'} (s'_j - s_j) \xi_{\mathbf{s}'\mathbf{s}} \prod_k n_k^{s_k} (1 - n_k)^{1-s_k}. \tag{2.14}$$

Using the microdynamical equation (Eq. (2.7)), we identify $\Delta_j(\mathbf{n})$ as

$$\Delta_j(\mathbf{n}) = \sum_{\mathbf{s}\mathbf{s}'} (s'_j - s_j) \xi_{\mathbf{s}'\mathbf{s}} \prod_k n_k^{s_k} (1 - n_k)^{1-s_k}. \tag{2.15}$$

Local conservation relations of the collision function are described by the equations

$$\sum_j \Delta_j(\mathbf{n}) = 0, \quad \forall n \in \{0, 1\}^b, \tag{2.16}$$

$$\sum_j \mathbf{c}_j \Delta_j(\mathbf{n}) = 0, \quad \forall n \in \{0, 1\}^b, \tag{2.17}$$

where Eqs. (2.16) and (2.17) encode the local conservation of particle number and total momentum, respectively. Using the above equations and Eq. (2.7) one can derive

$$\sum_j n_j(t_* + 1, \mathbf{r}_*) = \sum_j n_j(t_*, \mathbf{r}_* - \mathbf{c}_j), \tag{2.18}$$

$$\sum_j \mathbf{c}_j n_j(t_* + 1, \mathbf{r}_*) = \sum_j \mathbf{c}_j n_j(t_*, \mathbf{r}_* - \mathbf{c}_j). \tag{2.19}$$

2.3 Probabilistic Description

With the introduced theory, we can describe the dynamics of the noisy Boolean fields $\mathbf{n}(t_*, \mathbf{r}_*)$. We want to study the average behavior of the system, preferably in a way that suppresses the noise. To do this, we introduce the mean occupation vector

$$\mathbf{N}(t_*, \mathbf{r}_*) = \{N_j(t_*, \mathbf{r}_*) \in [0, 1],\ j = 0, 1, \ldots, b - 1\}. \tag{2.20}$$

It is a single-particle distribution function that describes the mean number of particles that occupy a site $\mathbf{r}_*$ at time t_*. It is defined as the ensemble average of the occupation numbers of many trajectories on a finite lattice, written as $N_j(t_*, \mathbf{r}_*) = \langle n_j(t_*, \mathbf{r}_*) \rangle$. Details on the definition of the ensemble average are found in Appendix A.2.

Conserved Quantities

Using the mean occupations, we define the conserved quantities of the system. These are the density ρ and the particle current $\mathbf{j}$:

$$\rho(t_*, \mathbf{r}_*) = \sum_j N_j(t_*, \mathbf{r}_*), \tag{2.21}$$

$$\mathbf{j}(t_*, \mathbf{r}_*) = \sum_j \mathbf{c}_j N_j(t_*, \mathbf{r}_*). \tag{2.22}$$

Since the particles are assumed to have unit mass, ρ and $\mathbf{j}$ are equivalent to the mass density and mass current, or mean momentum. Ensemble averaging the conservation relations in Eqs. (2.18) and (2.19) gives the mean conservation relations

$$\sum_j N_j(t_* + 1, \mathbf{r}_* + \mathbf{c}_j) = \sum_j N_j(t_*, \mathbf{r}_*), \tag{2.23}$$

$$\sum_j \mathbf{c}_j N_j(t_* + 1, \mathbf{r}_* + \mathbf{c}_j) = \sum_j \mathbf{c}_j N_j(t_*, \mathbf{r}_*). \tag{2.24}$$

Further, we define the mean velocity as

$$\mathbf{u}(t_*, \mathbf{r}_*) = \mathbf{j}(t_*, \mathbf{r}_*)/\rho(t_*, \mathbf{r}_*). \tag{2.25}$$

Equilibrium Distribution

Having introduced the mean occupation numbers and the conserved quantities, we may now write down the equilibrium distribution, or steady-state solutions. Assuming a finite lattice $\mathcal{L}$ with periodic boundary conditions, we can assume that the steady-state solutions are translation invariant, such that every lattice site has the same distribution in equilibrium. The derivation of the steady-state solutions is found in Appendix A.3, in which we define the entropy H:

$$H = -\sum_j \left[N_j \ln N_j + (1 - N_j) \ln (1 - N_j)\right]. \tag{2.26}$$

The entropy is non-decreasing over time. Since the equilibrium is translation invariant, summing the local entropy $H(\mathbf{N})$ over every lattice site gives the global entropy, which is also non-decreasing over time. Maximizing the entropy gives the Fermi-Dirac distributed equilibrium solutions N_j^{eq}:

$$N_j^{\mathrm{eq}} = \frac{1}{1 + \exp\left(h + \mathbf{q} \cdot \mathbf{c}_j\right)}, \tag{2.27}$$

where $h \in \mathbb{R}$ and $\mathbf{q} \in \mathbb{R}^d$ are Lagrange multipliers. Since the particles obey Pauli exclusion, it is natural that their equilibrium distribution is Fermi-Dirac.

For an equilibrium with $\mathbf{u} = 0$, there is no dependence on the directional index j. In this case, we get an isotropic equilibrium distribution $N_j = \rho/b$.

Lattice Boltzmann Approximation

The LHS of Eq. (A.23) resembles the collision function, as defined in Eq. (2.15), only evaluated with n_j and $\xi_{\mathbf{s}'\mathbf{s}}$ replaced with their respective averaged quantities N_j and $A(\mathbf{s}' \leftarrow \mathbf{s})$. Meanwhile, the RHS of Eq. (A.23) is zero since there is no change to the mean occupations at equilibrium. Inspired by this, we aim to derive a time evolution of the mean occupations N_j. By ensemble averaging the microdynamical equation (Eq. (2.7)) one gets

$$N_j(t_* + 1, \mathbf{r}_* + \mathbf{c}_j) = N_j(t_*, \mathbf{r}_*) + \Omega_j(\mathbf{N}), \tag{2.28}$$

where $\Omega_j\left(\mathbf{N}(t_*, \mathbf{r})\right)$ is the lattice Boltzmann collision function, written as

$$\Omega_j(\mathbf{N}) = \sum_{\mathbf{s}\mathbf{s}'} (s'_j - s_j) A(\mathbf{s}' \leftarrow \mathbf{s}) \prod_k N_k^{s_k} (1 - N_k)^{1-s_k}. \tag{2.29}$$

The dynamics described by Eqs. (2.28) and (2.29) are referred to as the lattice Boltzmann approximation [27, 30]. This approximation assumes what is known as *molecular chaos*, or the Stoßzahlansatz, which assumes that particles collide frequently enough such that their velocities are uncorrelated and independent of position.

One can further approximate by assuming that the velocity is small ($|\mathbf{u}| \ll c$) such that we are close to the isotropic equilibrium. Linearizing $\Omega_j(N)$ around $N_j = \rho/b$ leads to

$$N_j(t_* + 1, \mathbf{r}_* + \mathbf{c}_j) = N_j(t_*, \mathbf{r}_*) + \sum_k \mathcal{L}_{jk} N_k(t_*, \mathbf{r}_*), \tag{2.30}$$

where $\mathcal{L}_{jk}$ is the $b \times b$ linearized collision matrix with elements

$$\mathcal{L}_{jk} = \left[\frac{\partial \Omega_j}{\partial N_k}\right]_{N_j = \rho/b}. \tag{2.31}$$

Using the derivation by Hénon [31], we can write the elements of $\mathcal{L}$ as

$$\mathcal{L}_{jk} = -\frac{1}{2} \sum_{\mathbf{s}\mathbf{s}'} (s_j - s'_j) A(\mathbf{s}' \leftarrow \mathbf{s}) \bar{n}^{\rho(\mathbf{s})-1} (1 - \bar{n})^{b-\rho(\mathbf{s})-1} (s_k - s'_k), \tag{2.32}$$

with $\rho(\mathbf{s}) = \sum_j s_j$ and

$$\bar{n} = \frac{\rho}{b}. \tag{2.33}$$

The FHP-I collision rules are invariant under reflections. Since the collision matrix is linearized around the isotropic equilibrium, the symmetries of the collision function are inherited by the linearized collision matrix. This implies that $\mathcal{L}$ is symmetric, such that the matrix elements $\mathcal{L}_{j,k} = \mathcal{L}_{j,b-k}$. Importantly, symmetric matrices have real eigenvalues. Since $\mathcal{L}$ has real-valued matrix elements (Eq. (2.32)), it satisfies

$$\mathcal{L}^* = \mathcal{L}, \tag{2.34}$$

where $\mathcal{L}^*$ is the complex conjugate of $\mathcal{L}$.

The collision rules are also invariant under discrete lattice rotations. Consequently, the matrix elements depend only on the relative velocity channel orientation, $j - k$. This implies that $\mathcal{L}$ is circulant. Circulant matrices are square matrices that have rows that are all composed of the same elements, where each row is right-shifted by one element relative to the preceding row. This is also confirmed by computing the terms using Eq. (2.32). Circulant matrices have eigenvectors $\boldsymbol{\psi}_m$ that are discrete Fourier modes, given by

$$\boldsymbol{\psi}_m = \frac{1}{\sqrt{b}} \begin{pmatrix} 1 & e^{i\theta_1 m} & e^{i\theta_2 m} & \cdots & e^{i\theta_{b-1} m} \end{pmatrix}, \quad \text{for } m = 0, 1, \ldots, b-1, \tag{2.35}$$

where b is the number of rows or columns of the matrix, i is the imaginary unit, and the angle θ_j is given by (2.2). The elements of the eigenvectors satisfy

$$e^{i\theta_j(b-m)} = \underbrace{e^{i2\pi j}}_{=1} e^{-i\theta_j m} = e^{-i\theta_j m} \tag{2.36}$$

for any integer j. This means that

$$\boldsymbol{\psi}_m = \boldsymbol{\psi}^*_{-m}, \tag{2.37}$$

where $\boldsymbol{\psi}^*$ is the complex conjugate of $\boldsymbol{\psi}$ and $-m$ is modulo b due to the cyclic nature of the discrete Fourier modes. The eigenvalues λ_m of circulant matrices are given by

$$\lambda_m = \sum_{j=0}^{b-1} \mathcal{L}_{0j} e^{-i\theta_j m}, \quad \text{for } m = 0, 1, \ldots, b-1, \tag{2.38}$$

where $\mathcal{L}_{0j}$ is the first row of the circulant matrix. Using Eqs. (2.34) and (2.37), one finds that

$$\begin{aligned} \lambda_m \boldsymbol{\psi}_m &= \mathcal{L}\boldsymbol{\psi}_m \\ &= \mathcal{L}\boldsymbol{\psi}^*_{-m} \\ &= \left(\mathcal{L}\boldsymbol{\psi}_{-m}\right)^* \\ &= \left(\lambda_{-m}\boldsymbol{\psi}_{-m}\right)^* \\ &= \lambda^*_{-m}\boldsymbol{\psi}_m. \end{aligned} \tag{2.39}$$

Since the eigenvalues are real, it is clear from Eq. (2.39) that

$$\lambda_m = \lambda_{-m}. \tag{2.40}$$

3

Tomographic Lattice Gas Dynamics

Frisch *et al.* [27] noted, during the development of the FHP model, that only including two-body collisions gives rise to an additional "spurious" conserved quantity. By evaluating the FHP-I collision function (Eq. (2.9)) with only two-body collisions and no symmetric three-body collisions, one indeed finds that the difference in number of particles in pairs of opposite directions, given by

$$n_j - n_{j+3}, \quad \text{for } j = 0, 1, 2, \tag{3.1}$$

are independently conserved. This is evident from inspecting Fig. 2.3, where it is clear that head-on collisions preserve the total particle flux along the three directions on the lattice. This is verified by the fact that $\Delta_j(\mathbf{n})$ satisfies the equations $0 = \Delta_j(\mathbf{n}) - \Delta_{j+3}(\mathbf{n})$ for all $\mathbf{n} \in \{0,1\}^b$ when excluding symmetric three-body collisions. Since this is not a physical behavior in the hydrodynamic regime, these conserved modes need to be removed to retrieve hydrodynamic behavior. To achieve this, symmetric three-body collisions were added, which introduces an exchange of momentum between all velocity channels. Furthermore, introducing rest particles or multiple allowed speeds also removes these modes.

In Sec. 3.1, we introduce the physical basis vectors to represent the mean occupations. We analyze the linearized collision matrix and the decay rates of its eigenvalues. We find that at low densities, the lattice gas exhibits a two-step relaxation process, with a long-lived scalar quantity ϕ, called the hexapolar mode. In Sec. 3.2, we analyze the three conserved scalar quantities. We find that these are equivalent to the conservation of momentum and the hexapolar mode. We discuss the connection to long-lived collective modes found in two-dimensional Fermi liquids.

In Sec. 3.3, we derive a quasi-equilibrium distribution with a dynamic hexapolar mode. We derive a small perturbation approximation to the distribution, up to second order in the small parameters, the density fluctuation $\delta\rho$, velocity $\mathbf{u}$, and hexapolar mode ϕ. In Sec. 3.4, we derive a set of macroscopic equations of motion of the density, momentum, and hexapolar mode. We assume that the hexapolar mode is long-lived but lightly damped. These equations are equivalent to the continuity and Navier-Stokes equations used in fluid mechanics, although modified to include ϕ. We find that the hexapolar mode introduces anisotropic diffusive and advective terms.

In Sec. 3.5, we analyze the hydrodynamic modes of the linearized macroscopic equations. We assume that the small parameters are plane waves. We find the usual two acoustic modes and two anisotropic diffusive modes. For a conserved hexapolar mode, we find that one of these diffusive modes is zero for wave vectors with certain angles. Finally, in Sec. 3.6, we study solutions to the macroscopic equations for flow in a rectangular channel.

3.1 Physical Basis

Using the linearized lattice Boltzmann approximation introduced in Sec. 2.3, we can establish a b-dimensional *physical basis* of the LGCA [30]. In contrast to the mean occupations N_j which make up the *direction basis*, the physical basis consists of a set of vectors that represent physical quantities, such as the density and momentum. The former is described by the b-long vector $\mathbf{1}$ consisting of only ones. The latter is described by the vectors $\mathbf{c}_\alpha = \{c_{j\alpha},\ \text{for } j = 0, 1, \ldots, b-1\}$, where $\alpha = 1, \ldots, d$. Due to the conservation of density and momentum, these three vectors are eigenvectors of $\mathcal{L}$ and have eigenvalues that are zero:

$$\mathcal{L} \cdot \mathbf{1} = 0, \quad \mathcal{L} \cdot \mathbf{c}_\alpha = 0. \tag{3.2}$$

Using the traceless symmetric second-order tensor $Q_{j\alpha\beta}$, defined as

$$Q_{j\alpha\beta} = c_{j\alpha} c_{j\beta} - \frac{c^2}{d} \delta_{\alpha\beta}, \tag{3.3}$$

we define the stress tensor $S_{\alpha\beta}$:

$$S_{\alpha\beta}(t_*, \mathbf{r}_*) = \sum_j Q_{j\alpha\beta} N_j(t_*, \mathbf{r}_*), \tag{3.4}$$

where $\delta_{\alpha\beta}$ is the Kronecker delta function. For single-speed LGCA with sufficient symmetry, the vectors $\mathbf{Q}_{\alpha\beta} = \{Q_{j\alpha\beta},\ \text{for } j = 0, 1, \ldots, b-1\}$ are eigenvectors of $\mathcal{L}$ with negative eigenvalues $-\gamma_2$, where $\gamma_2 > 0$ [30]. Thus, the stress tensor decays at a rate γ_2, such that

$$\mathcal{L} \cdot \mathbf{Q}_{\alpha\beta} = -\gamma_2 \mathbf{Q}_{\alpha\beta}, \quad \forall \alpha, \beta. \tag{3.5}$$

Since $\mathbf{Q}_{\alpha\beta}$ is traceless and symmetric, there are $d(d+1)/2 - 1$ independent invariant vectors for all spatial components. Thus, the physical basis vectors $\mathbf{1}$, $\mathbf{c}_\alpha$, and $\mathbf{Q}_{\alpha\beta}$ consist of $d(d+3)/2$ independent vectors of the b-dimensional basis.

For the FHP model with $b = 6$ and $d = 2$, the six independent physical basis vectors are

$$\begin{aligned}
\mathbf{1} &= (1,1,1,1,1,1), & \mathbf{Q}_{xx} &= c^2\left(\frac{1}{2}, -\frac{1}{4}, -\frac{1}{4}, \frac{1}{2}, -\frac{1}{4}, -\frac{1}{4}\right), \\
\mathbf{c}_x &= c\left(1, \frac{1}{2}, -\frac{1}{2}, -1, -\frac{1}{2}, \frac{1}{2}\right), & \mathbf{Q}_{xy} &= c^2\left(0, \frac{\sqrt{3}}{4}, -\frac{\sqrt{3}}{4}, 0, \frac{\sqrt{3}}{4}, -\frac{\sqrt{3}}{4}\right), \\
\mathbf{c}_y &= c\left(0, \frac{\sqrt{3}}{2}, \frac{\sqrt{3}}{2}, 0, -\frac{\sqrt{3}}{2}, -\frac{\sqrt{3}}{2}\right), & \mathbf{w} &= (1,-1,1,-1,1,-1).
\end{aligned} \tag{3.6}$$

Since the density, momentum, and stress make up five out of the six independent degrees of freedom, the final degree of freedom is determined to be the $\mathbf{w}$ vector, with elements $w_j = (-1)^j$ for $j = 0, 1, \ldots, 5$. This eigenvector has the negative eigenvalue $-\gamma_3$, with $\gamma_3 > 0$, such that

$$\mathcal{L} \cdot \mathbf{w} = -\gamma_3 \mathbf{w} \tag{3.7}$$

This eigenvector represents a perturbation in a scalar quantity that we denote ϕ. It is defined as

$$\phi(t_*, \mathbf{r}_*) = \sum_j w_j N_j(t_*, \mathbf{r}_*), \tag{3.8}$$

where $w_j = (-1)^j$. Since $\mathcal{L}$ is circulant, these six eigenvectors are proportional to the Fourier modes (Eq. (2.35)). We show this explicitly by assuming a small perturbation δN_j such that

$$N_j(t_*, \mathbf{r}_*) = \frac{\rho_0}{6} + \delta N_j(t_*, \mathbf{r}_*). \tag{3.9}$$

Inserting Eq. (3.9) into Eq. (2.30) leads to

$$N_j(t_* + 1, \mathbf{r}_* + \mathbf{c}_j) = N_j(t_*, \mathbf{r}_*) + \sum_k \mathcal{L}_{jk} \delta N_k(t_*, \mathbf{r}_*). \tag{3.10}$$

The linearized collision matrix only acts on the perturbation δN_j since it is zero at equilibrium $N_j = \rho/b$. Since we know that $\mathcal{L}$ is symmetric circulant, we know that its eigenvectors are Fourier modes given by Eq. (2.35). We decompose δN_j into angular harmonics as

$$\delta N_j = \sum_{m=0}^{5} a_m e^{im\theta_j}, \tag{3.11}$$

where a_m is a complex coefficient. Since the perturbation is real-valued, we remove the imaginary parts by decomposing the exponential factors into cosine and sine factors. Writing $a_m = A_m + iB_m$, where both A_m and B_m are real, and using Eq. (2.36) leads to

$$\begin{aligned}
\delta N_j = A_0 + iB_0 &+ \sum_{m=1}^{2} \left[(A_m + A_{-m})\cos(m\theta_j) - (B_m - B_{-m})\sin(m\theta_j)\right] \\
&+ i \sum_{m=1}^{2} \left[(A_m - A_{-m})\sin(m\theta_j) + (B_m + B_{-m})\cos(m\theta_j)\right], \\
&+ A_3 \cos(3\theta_j) - B_3 \sin(3\theta_j) + i\left[A_3 \sin(3\theta_j) + B_3 \cos(3\theta_j)\right]
\end{aligned} \tag{3.12}$$

where $a_{6-m} = a_{-m}$ since the relation in Eq. (2.36) holds. Note that $\sin(3\theta_j) = \sin(\pi j) = 0$ for all integers j. For δN_j to be real, we need that $B_0 = B_3 = 0$. We also need that $A_{-m} = A_m$ and $B_{-m} = -B_m$. This means that a_{-m} is the complex conjugate of a_m, i.e., $a_{-m} = a_m^*$. This leads to

$$\delta N_j = A_0 + 2\sum_{m=1}^{2} \left[A_m \cos(m\theta_j) - B_m \sin(m\theta_j)\right] + A_3 \cos(3\theta_j). \tag{3.13}$$

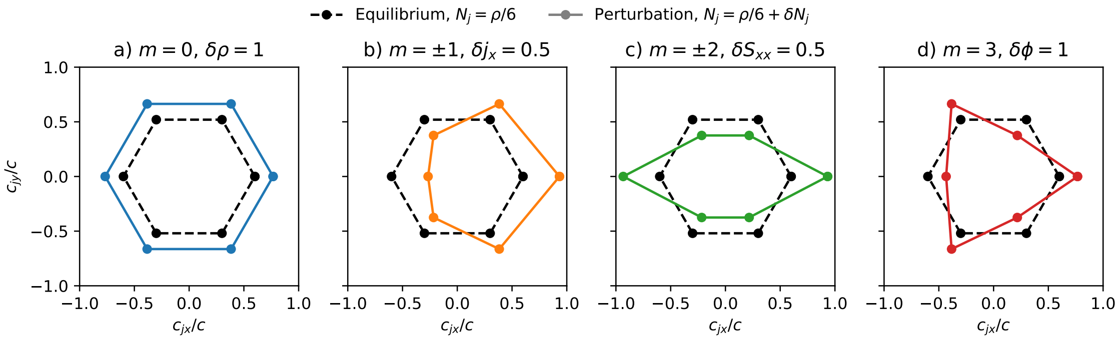

Figure 3.1: The figure shows individual angular harmonic perturbations around the isotropic equilibrium $N_j = \rho/6$ with $\rho = 3.6$.

We identify the physical meaning of the different terms. The A_0 term is proportional to the **1** vector and represents a shift in density. The A_1 and B_1 terms are proportional to the vectors c_{jx} and c_{jy}, as is evident from Eq. (2.1), and represent a shift in the momentum. The A_2 and B_2 terms are proportional to the two independent vectors $Q_{jxx} = (c^2/2)\cos(2\theta_j)$ and $Q_{jxy} = (c^2/2)\sin(2\theta_j)$, as can be seen by from inserting Eq. (2.1) into Eq. (3.3) and setting $\alpha = \beta = x$ and $\alpha = x, \beta = y$ respectively. These represent a shift in the two independent elements of the stress tensor, S_{xx} and S_{xy}. Finally, the A_3 term is proportional to the $\mathbf{w}$ vector, since $\cos(3\theta_j) = \cos(\pi j) = w_j$, and represents a shift in the quantity ϕ. Since $\cos(3\theta)$ has six extrema in the range $\theta \in [0, 2\pi)$, we call ϕ the hexapolar mode.

The coefficients can thus be relabeled as $A_0 = \delta\rho/6$, $A_1 = j_x/3$ and $-B_1 = j_y/3$ with $j_\alpha = (\rho_0 + \delta\rho)u_\alpha$, $A_2 = S_{xx}/3$ and $-B_2 = S_{xy}/3$, and $A_3 = \phi/6$, such that

$$\delta N_j = \frac{\delta\rho}{6} + \frac{2}{3}(\rho_0 + \delta\rho)c_{j\alpha}u_\alpha + \frac{4}{3}Q_{jx\alpha}S_{x\alpha} + w_j\frac{\phi}{6}, \tag{3.14}$$

where we sum over repeated Greek indices[1].

The perturbations of the quantities ρ, j_α, $S_{\alpha\beta}$, and ϕ in Eq. (3.14) correspond to angular harmonic perturbations of the isotropic equilibrium distribution. These perturbations are proportional to the vectors that make up the physical basis of the linearized collision matrix mentioned in Sec. 2.3. The perturbative effects on the distribution function are visualized in Fig. 3.1.

Relaxation Rates

Using Eqs. (2.32) and (2.38), we compute the eigenvalues $-\gamma_m$ of $\mathcal{L}$, shown in Tab. 3.1 and Fig. 3.2. The probabilities p_2, p_{3s}, p_{3a}, and p_4 are explained in Fig. 2.3. In the FHP-I model, the probabilities are all unity, i.e., $p_2 = p_{3s} = p_{3a} = p_4 = 1$. From Eq. (2.40), we know that $\gamma_{-m} = \gamma_m$. The collisions conserve density and momentum, so $\gamma_0 = \gamma_1 = 0$. The stress tensor decays with rate γ_2 and the hexapolar mode decays with rate γ_3.

[1]This notation is called *Einstein notation* or the *Einstein summation convention*. It was first introduced by Albert Einstein in 1916 in his foundation of general relativity.

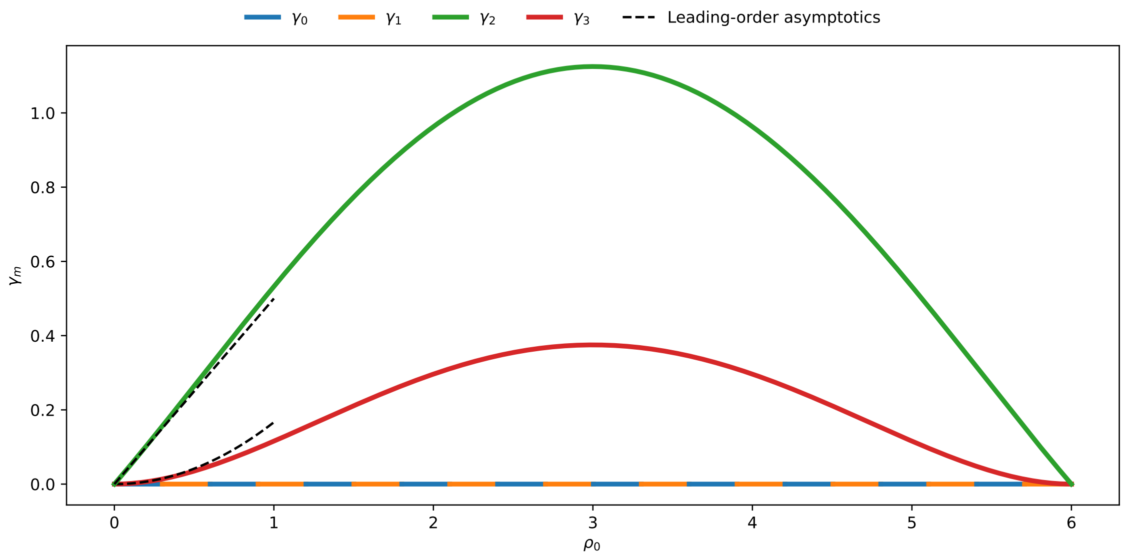

Figure 3.2: Eigenvalues of the linearized collision matrix $\mathcal{L}$ around the isotropic equilibrium distribution $N_j = \rho_0/6$.

These rates have different leading-order asymptotics for low densities $\bar{n} \approx 0$. At low densities, γ_3 increases quadratically with $\bar{n}$ while γ_2 increases linearly with $\bar{n}$. Thus, at low densities, ϕ becomes parametrically more long-lived than the stress tensor, by a factor $1/\bar{n}$. Since the hexapolar mode is an odd-parity Fourier mode, this effect is analogous to the tomographic effect found in two-dimensional Fermi liquids.

However, there are issues with reducing the density to get a long-lived ϕ. In the small ρ_0 limit, the molecular chaos ansatz breaks down. With few particles and collisions, the assumption that particle velocities are uncorrelated is no longer true.

m	γ_m	$\gamma_m\big\vert_{\rho_0=0}$
0	0	0
1	0	0
2	$3p_2\bar{n}(1-\bar{n})^3 + 12p_{3a}\bar{n}^2(1-\bar{n})^2 + 3p_4\bar{n}^3(1-\bar{n})$	$3p_2\bar{n}$
3	$6p_{3s}\bar{n}^2(1-\bar{n})^2$	$6p_{3s}\bar{n}^2$

Table 3.1: Eigenvalues $-\gamma_m$ of the linearized collision matrix $\mathcal{L}$.

To demonstrate the two-step relaxation process and breakdown of molecular chaos, we simulated the FHP-I model with particle densities (Fig. 3.4). We used a 400×400 lattice with nodes placed uniformly on a square with wraparound periodic boundary conditions (Fig. 3.3). The three simulations show an increasing separation of lifetimes between the stress tensor elements, S_{xx} and S_{xy}, and the hexapolar mode ϕ when ρ_0 decreases. However, for $\rho_0 = 0.01$, the perturbations initially follow the decay rates of their respective eigenvalues until they reach a sudden plateau.

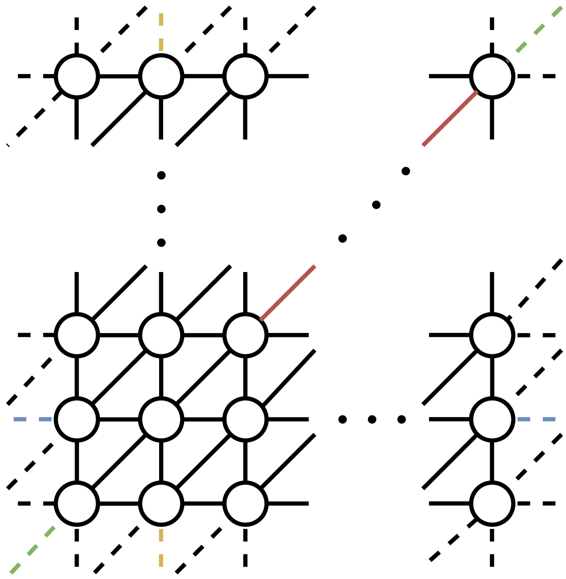

Figure 3.3: A schematic of the square lattice used to simulate the two-step relaxation process. Circles represent lattice sites and lines represent edges to neighboring sites. Dashed lines represent edges at the periodic boundaries. For instance, the two lines sharing the same color (blue, yellow, or green) represent the same edge. However, the two red lines are not the same edge, unless it is a 4×4 lattice.

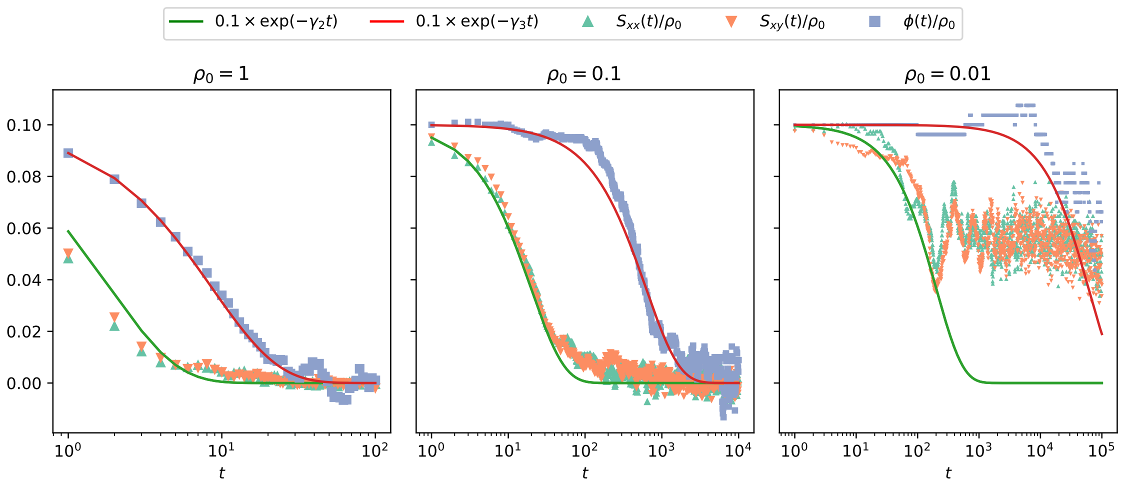

Figure 3.4: The resulting stress tensor elements, S_{xx} and S_{xy}, and hexapolar mode ϕ for three different background particle densities ρ_0, with $c = 1$ and $u_x = u_y = \delta\rho = 0$. We use a 400×400 lattice with periodic boundary conditions (Fig. 3.3). The mean occupations N_j were computed by ensemble averaging the occupations n_j over all lattice sites. At time $t = 0$, the small perturbations started with the values $0.1\rho_0$. The solid lines show the predicted decays of the stress tensor elements and the hexapolar mode using their respective eigenvalues, $-\gamma_2$ and $-\gamma_3$.

3.2 “Spurious” Conservation Laws

We return to the initial hook of this chapter: without symmetric three-body collisions, the FHP model has the three additional conserved scalar quantities (Eq. (3.1)). This raises two questions: Are the collision invariant vectors describing the conservation of density and momentum linearly independent of the invariants? And how many conservation laws are there in addition to the conservation of density and momentum?

We begin by inspecting the linear independence of the spurious conservation laws from the physical basis vectors, given by Eq. (3.6). These basis vectors are pairwise orthogonal with respect to the scalar product, such that for any pair of invariant vectors their scalar product is zero. This in turn means that they are linearly independent.

We define the three vectors related to the spurious conservation laws in Eq. (3.1) as

$$\begin{aligned} \mathbf{v}_1 &= (1,0,0,-1,0,0)\,, \\ \mathbf{v}_2 &= (0,1,0,0,-1,0)\,, \\ \mathbf{v}_3 &= (0,0,1,0,0,-1)\,. \end{aligned} \tag{3.15}$$

These vectors are also pairwise orthogonal with respect to the scalar product, and are thus linearly independent. Since they are linearly independent, the three vectors have a span with dimensionality three: $\dim \operatorname{span}\{\mathbf{v}_1,\mathbf{v}_2,\mathbf{v}_3\} = 3$.

By computing the pairwise scalar products between the physical basis vectors (Eq. (3.6)) and the spurious invariant vectors (Eq. (3.15)), we find that the only nonzero scalar products are $\mathbf{c_x}\cdot\mathbf{v}_1$, $\mathbf{c_x}\cdot\mathbf{v}_2$, $\mathbf{c_x}\cdot\mathbf{v}_3$, $\mathbf{c_y}\cdot\mathbf{v}_2$, $\mathbf{c_y}\cdot\mathbf{v}_3$, $\mathbf{w}\cdot\mathbf{v}_1$, $\mathbf{w}\cdot\mathbf{v}_2$, and $\mathbf{w}\cdot\mathbf{v}_3$. Since the spurious invariants are not orthogonal to the velocity vectors and $\mathbf{w}$, we need to check for linear dependence. Indeed, we see that

$$\begin{aligned} \mathbf{c}_x &= c\left(\mathbf{v}_1 + \frac{1}{2}\mathbf{v}_2 - \frac{1}{2}\mathbf{v}_3\right), \\ \mathbf{c}_y &= \frac{\sqrt{3}}{2}c\left(\mathbf{v}_2 + \mathbf{v}_3\right), \\ \mathbf{w} &= \mathbf{v}_1 - \mathbf{v}_2 + \mathbf{v}_3. \end{aligned} \tag{3.16}$$

Since $\mathbf{c}_x$, $\mathbf{c}_y$, and $\mathbf{w}$ are linearly dependent on the spurious vectors, they span a subspace of the span of the spurious vectors, i.e., $\operatorname{span}\{\mathbf{c}_x,\mathbf{c}_y,\mathbf{w}\} \subseteq \operatorname{span}\{\mathbf{v}_1,\mathbf{v}_2,\mathbf{v}_3\}$. However, since they are also linearly independent vectors, their span also has dimensionality three: $\dim \operatorname{span}\{\mathbf{c}_x,\mathbf{c}_y,\mathbf{w}\} = 3$. Any subspace of the same finite dimensionality must be equal, so the two sets of vectors span the same subspace: $\operatorname{span}\{\mathbf{c}_x,\mathbf{c}_y,\mathbf{w}\} = \operatorname{span}\{\mathbf{v}_1,\mathbf{v}_2,\mathbf{v}_3\}$.

Since the subspace spanned by the spurious vectors is fully conserved, the subspace spanned by the velocity vectors and $\mathbf{w}$ must be conserved. The spurious conservation laws are thus equivalent to the conservation of momentum and the scalar conservation law

$$0 = \sum_j w_j \Delta_j(\mathbf{n}), \quad \forall \mathbf{n} \in \{0,1\}^b, \tag{3.17}$$

where $\Delta_j(\mathbf{n})$ is the collision function given by Eq. (2.15). By this conservation law, the scalar quantity ϕ (defined in Eq. (3.8)) is conserved.

Looking back at the eigenvalues (Tab. 3.1), this fact becomes rather obvious. The decay rate of the hexapolar mode, γ_3, is directly proportional to the probability of symmetric three-body scattering p_3. Setting $p_3 = 0$ thus conserves ϕ.

Therefore, we have two ways of reducing symmetric three-body scattering to create a long-lived hexapolar mode. To set $\gamma_3 \ll \gamma_2$, we can either reduce the density, or set $p_3 \ll 1$ while keeping the head-on scattering processes fast. The latter method is preferable since reducing the density causes the breakdown of the molecular chaos ansatz, which makes the particles behave ballistically rather than hydrodynamically.

3.3 Quasi-Equilibrium

In this section, we derive the equilibrium distribution of the mean occupations N_j^{eq} with the assumption that ϕ is long-lived. In Sec. 2.3, the equilibrium distribution was introduced. It is translation invariant and Fermi-Dirac distributed. Further, the local entropy H is introduced and defined in Eq. (2.26). Due to translation invariance, maximizing entropy locally subject to the long-lived quantities ρ, $\rho\mathbf{u}$ and ϕ yields the equilibrium distribution N_j^{eq}. The maximization is performed using Lagrange multipliers with the Lagrangian function,

$$\mathscr{L} = H + h\left(\rho - \sum_j N_j\right) + \mathbf{q} \cdot \left(\rho\mathbf{u} - \sum_j \mathbf{c}_j N_j\right) + z\left(\phi - \sum_j w_j N_j\right), \tag{3.18}$$

where $h \in \mathbb{R}$, $\mathbf{q} \in \mathbb{R}^2$, and $z \in \mathbb{R}$ are Lagrange multipliers that depend on ρ, $\mathbf{u}$, and ϕ. To maximize the Lagrangian, we evaluate the partial derivative of $\mathscr{L}$ with respect to N_j as

$$\frac{\partial \mathscr{L}}{\partial N_j} = -\ln \frac{N_j}{1 - N_j} - h - q_\alpha c_{j\alpha} - z w_j. \tag{3.19}$$

Setting the partial derivative in Eq. (3.19) to zero and solving for N_j in terms of the Lagrange multipliers yields a Fermi-Dirac distribution of the form

$$N_j^{\text{eq}} = \frac{1}{1 + \exp\left(h + \mathbf{q} \cdot \mathbf{c}_j + z w_j\right)}. \tag{3.20}$$

The equilibrium distribution without the hexapolar deformation is recovered by setting z to zero.

Small Perturbation Approximation

To determine the Lagrange multipliers in Eq. (3.20), we derive a small perturbation approximation of the equilibrium distribution. We assume that the mean density has a small perturbation $\delta\rho$ such that $\rho = \rho_0 + \delta\rho$ where $|\delta\rho| \ll 1$. The mean velocity $|\mathbf{u}| = u \ll c$ and the hexapolar mode $|\phi| \ll 1$ are also small. We closely follow the derivation outlined by Frisch *et al.* [27] and begin by expanding the Lagrange multipliers in small $\delta\rho$, u, and ϕ. This task is simplified by considering that parity invariance conserves occupation numbers when $\mathbf{c}_j, \mathbf{u} \mapsto -\mathbf{c}_j, -\mathbf{u}$, such that

$$\begin{aligned} N_j^{\text{eq}}(\rho, -\mathbf{u}, \phi) = N_j^{\text{eq}}(\rho, \mathbf{u}, \phi) &= f_{\text{FD}}\left(h(\rho, -\mathbf{u}, \phi) + \mathbf{q}(\rho, -\mathbf{u}, \phi) \cdot (-\mathbf{c}_j) + z(\rho, -\mathbf{u}, \phi) w_j\right) \\ &= f_{\text{FD}}\left(h(\rho, \mathbf{u}, \phi) + \mathbf{q}(\rho, \mathbf{u}, \phi) \cdot \mathbf{c}_j + z(\rho, \mathbf{u}, \phi) w_j\right), \end{aligned} \tag{3.21}$$

where f_{FD} is the Fermi-Dirac distribution function, defined as

$$f_{\text{FD}}(x) = \frac{1}{1+e^x}. \tag{3.22}$$

This means that h and z are even in $\mathbf{u}$ while $\mathbf{q}$ is odd in $\mathbf{u}$:

$$\begin{aligned} h(\rho, -\mathbf{u}, \phi) &= h(\rho, \mathbf{u}, \phi), \\ \mathbf{q}(\rho, -\mathbf{u}, \phi) &= -\mathbf{q}(\rho, \mathbf{u}, \phi), \\ z(\rho, -\mathbf{u}, \phi) &= z(\rho, \mathbf{u}, \phi). \end{aligned} \tag{3.23}$$

Further, the distribution is also invariant when $w_j, \phi \mapsto -w_j, -\phi$, such that

$$\begin{aligned} N_j(\rho, \mathbf{u}, -\phi) = N_j(\rho, \mathbf{u}, \phi) &= f_{\text{FD}}\left(h(\rho, \mathbf{u}, -\phi) + \mathbf{q}(\rho, \mathbf{u}, -\phi) \cdot \mathbf{c}_j + z(\rho, \mathbf{u}, -\phi)(-w_j)\right) \\ &= f_{\text{FD}}\left(h(\rho, \mathbf{u}, \phi) + \mathbf{q}(\rho, \mathbf{u}, \phi) \cdot \mathbf{c}_j + z(\rho, \mathbf{u}, \phi) w_j\right), \end{aligned} \tag{3.24}$$

which means that h and $\mathbf{q}$ are even in ϕ while z is odd in ϕ:

$$\begin{aligned} h(\rho, \mathbf{u}, -\phi) &= h(\rho, \mathbf{u}, \phi), \\ \mathbf{q}(\rho, \mathbf{u}, -\phi) &= \mathbf{q}(\rho, \mathbf{u}, \phi), \\ z(\rho, \mathbf{u}, -\phi) &= -z(\rho, \mathbf{u}, \phi). \end{aligned} \tag{3.25}$$

We now Taylor expand $h(\rho, \mathbf{u}, \phi)$ in small $\delta\rho$, u and ϕ, up to second order in the small parameters, which leads to

$$\begin{aligned} h(\rho, \mathbf{u}, \phi) = h(\rho_0, 0, 0) &+ \partial_{\delta\rho} h\Big|_{\delta\rho,u,\phi=0} \delta\rho + \frac{1}{2}\partial^2_{\delta\rho} h\Big|_{\delta\rho,u,\phi=0} \delta\rho^2 + \frac{1}{2}\partial_{u_\alpha}\partial_{u_\beta} h\Big|_{\delta\rho,u,\phi=0} u_\alpha u_\beta \\ &+ \frac{1}{2}\partial^2_{\phi} h\Big|_{\delta\rho,u,\phi=0} \phi^2 + \mathcal{O}(\delta^3) \\ = h^{(0)}(\rho_0) &+ h^{(\delta\rho)}(\rho_0)\delta\rho + h^{(\delta\rho,\delta\rho)}(\rho_0)\delta\rho^2 + h^{(u,u)}_{\alpha\beta}(\rho_0) u_\alpha u_\beta \\ &+ h^{(\phi,\phi)}(\rho_0)\phi^2 + \mathcal{O}(\delta^3) \\ = h^{(0)}(\rho_0) &+ h^{(\delta\rho)}(\rho_0)\delta\rho + h^{(\delta\rho,\delta\rho)}(\rho_0)\delta\rho^2 + h^{(u,u)}(\rho_0) u^2 \\ &+ h^{(\phi,\phi)}(\rho_0)\phi^2 + \mathcal{O}(\delta^3), \end{aligned} \tag{3.26}$$

where repeated Greek indices are summed over. The notation $\mathcal{O}(\delta^n)$ denotes terms of order n and higher of the small parameters. All odd-ordered terms in u and ϕ disappear due to h being even in both expanded variables. Note that the tensor $h^{(u,u)}_{\alpha\beta}$ is assumed to be proportional to $\delta_{\alpha\beta}$. According to isotropy arguments made earlier, this must be the only choice for j-independent second-order tensor. This is not evident however with the long-lived hexapolar mode. It is however apparent that this is the correct ansatz for the tensor when we identify the expansion coefficients in Appendix B.1. The expansion of $\mathbf{q}$ is written as

$$\begin{aligned} q_\alpha(\rho,\mathbf{u},\phi) &= \partial_{u_\beta} q_\alpha \Big|_{\delta\rho,u,\phi=0} u_\beta + \partial_{\delta\rho}\partial_{u_\beta} q_\alpha \Big|_{\delta\rho,u,\phi=0} \delta\rho u_\beta + \mathcal{O}(\delta^3) \\ &= q^{(u)}_{\alpha\beta}(\rho_0) u_\beta + q^{(\delta\rho,u)}_{\alpha\beta}(\rho_0)\delta\rho u_\beta + \mathcal{O}(\delta^3) \\ &= q^{(u)}(\rho_0) u_\alpha + q^{(\delta\rho,u)}(\rho_0)\delta\rho u_\alpha + \mathcal{O}(\delta^3), \end{aligned} \tag{3.27}$$

where only terms that are odd in u and even in ϕ are nonzero. To second order, only the term linear in u survives. Similarly, the second-order tensor $q^{(u)}_{\alpha\beta}$ is proportional to $\delta_{\alpha\beta}$. Lastly, the expansion of z is

$$\begin{aligned} z(\rho,\mathbf{u},\phi) &= \partial_\phi z \Big|_{\delta\rho,u,\phi=0} \phi + \partial_{\delta\rho}\partial_\phi z \Big|_{\delta\rho,u,\phi=0} \delta\rho\phi + \mathcal{O}(\delta^3) \\ &= z^{(\phi)}(\rho_0)\phi + z^{(\delta\rho,\phi)}(\rho_0)\delta\rho\phi + \mathcal{O}(\delta^3), \end{aligned} \tag{3.28}$$

where only terms that are odd in ϕ and even in u are nonzero. To second order, only the term that is linear in ϕ survives. In the following, we drop the dependence on ρ_0 in the expansion coefficients.

The equilibrium distribution for $\rho = \rho_0$, $u = 0$, and $\phi = 0$ reduces to $\rho_0/6$, since there is no dependence on the velocity channel j. Thus, we write the isotropic equilibrium as

$$N_j(\rho_0, 0, 0) = f_{\mathrm{FD}}\left(h^{(0)}\right) = \frac{\rho_0}{6}. \tag{3.29}$$

We now write an ansatz for the small perturbation equilibrium up to second order in $\delta\rho$, u, and ϕ by expanding the Fermi-Dirac distribution around $h^{(0)}$ as

$$\begin{aligned} N_j &= f_{\mathrm{FD}}\Big(h^{(0)} + h^{(\delta\rho)}\delta\rho + h^{(\delta\rho,\delta\rho)}\delta\rho^2 + h^{(u,u)}u^2 + h^{(\phi,\phi)}\phi^2 + \left(q^{(u)} + q^{(\delta\rho,u)}\delta\rho\right) c_{j\alpha}u_\alpha \\ &\qquad + \left(z^{(\phi)} + z^{(\delta\rho,\phi)}\delta\rho\right) w_j\phi\Big) + \mathcal{O}(\delta^3) \\ &= \frac{\rho_0}{6} + f_0^{(1)}\Big[h^{(\delta\rho)}\delta\rho + h^{(\delta\rho,\delta\rho)}\delta\rho^2 + h^{(u,u)}u^2 + h^{(\phi,\phi)}\phi^2 + \left(q^{(u)} + q^{(\delta\rho,u)}\delta\rho\right) c_{j\alpha}u_\alpha \\ &\qquad + \left(z^{(\phi)} + z^{(\delta\rho,\phi)}\delta\rho\right) w_j\phi\Big] + \mathcal{O}(\delta^3) \\ &\qquad + \frac{1}{2} f_0^{(2)}\left[(q^{(u)})^2 c_{j\alpha}c_{j\beta}u_\alpha u_\beta + 2q^{(u)}z^{(\phi)}c_{j\alpha}w_j u_\alpha\phi + (z^{(\phi)})^2\phi^2\right] + \mathcal{O}(\delta^3), \end{aligned} \tag{3.30}$$

where

$$f_0^{(k)} = \frac{\mathrm{d}^k}{\mathrm{d}x^k} f_{\mathrm{FD}}(x)\Big|_{x=h^{(0)}}, \quad \text{for } k = 0, 1, 2, \ldots. \tag{3.31}$$

The derivatives $f_0^{(1)}$, $f_0^{(2)}$ and the expansion coefficients are determined in Appendix B.1. The coefficients are found by utilizing properties of evaluating sums involving $c_{j\alpha}$ and w_j (Appendix A.1) and the definitions of the mean quantities (Eqs. (2.21), (2.22), (2.25) and (3.8)). The result is the small perturbation equilibrium

$$N_j^{(0)} = \frac{\rho}{6} + w_j\frac{\phi}{6} + \frac{\rho}{3c^2}c_{j\alpha}u_\alpha + c^2G(\rho_0)c_{j\alpha}w_ju_\alpha\phi + \rho_0G(\rho_0)Q_{j\alpha\beta}u_\alpha u_\beta + \mathcal{O}\left(\delta^3\right), \tag{3.32}$$

where $\rho = \rho_0 + \delta\rho$ and $Q_{j\alpha\beta}$ is given by Eq. (3.3), with

$$G(\rho_0) = \frac{1}{3c^4}\frac{2\rho_0 - 6}{\rho_0 - 6}. \tag{3.33}$$

A discussion of Eq. (3.32) is warranted. By setting ϕ to zero, one recovers the low-velocity approximation without the hexapolar deformation, as described by Frisch *et al.* [27]. The solution contains a term proportional to $w_j\phi$, which is expected since this is simply a linear perturbation of the $m = 3$ mode. This term already appeared in our physical basis expansion with a small linear perturbation (Eq. (3.14)). The solution also contains a term proportional to $c_{j\alpha}w_ju_\alpha\phi$. This term is nonlinear and couples the $m = \pm 1$ and $m = 3$ modes, and thus induces nonlinear advection of the hexapolar mode.

3.4 Macroscopic Equations

In this section, we derive a set of macroscopic equations using a multi-scale expansion. We follow a similar derivation by Frisch *et al.* [27], while also including a long-lived hexapolar mode. We assume that the relaxation of the stress tensor is much faster than the relaxation of the hexapolar mode, such that $\gamma_3 \ll \gamma_2$.

To derive the macroscopic equations, we imagine the fluid continuum as a gluing of local equilibria distributed throughout all of space. These local equilibria depend on parameters that are slowly varying in space and time, the dynamical quantities ρ, $\mathbf{u}$, and ϕ.

Consider a lattice with density $\rho(t_*, \mathbf{r}_*)$, velocity $\mathbf{u}(t_*, \mathbf{r}_*)$, and hexapolar mode $\phi(t_*, \mathbf{r}_*)$ at time t_* and node $\mathbf{r}_*$. We assume that the quantities vary on a spatial scale ϵ^{-1}, where ϵ is small enough for the purpose of calculating derivatives. We will eventually let $\epsilon \to 0$. We therefore move from a discrete to a continuous description, and consequently write the continuous time and spatial coordinates as t and $\mathbf{r}$ respectively. Three phenomena of different time scales are expected:

1. Relaxation to local equilibrium on time scale ϵ^0,
2. Acoustic and advective effects on time scale ϵ^{-1},
3. Diffusive, or viscous, effects on time scale ϵ^{-2}.

The assumption that phenomena occur on time scales in powers of ϵ is the namesake of the "multi-scale" expansion. It may also be called a Chapman-Enskog expansion, which is commonly used to go from a kinetic equation to macroscopic equations. In Chapman-Enskog theory, the small expansion parameter is called the *Knudsen number*. It is the mean free path of the particles divided by the typical length scale of the system.

We use our small perturbation approximation (Eq. (3.32)), which approximates the quasi-equilibrium distribution (Eq. (3.20)) up to second order in the small parameters $\delta\rho$, $\mathbf{u}$, and ϕ. We therefore capture advective terms up to $O(\epsilon\delta^2)$, which is cubic in ϵ and the small parameters. To be consistent, we only keep diffusive terms up to $\mathcal{O}(\epsilon^2\delta)$.

We use a three-time formalism, t_*, $t_1 = \epsilon t_*$ and $t_2 = \epsilon^2 t_*$, with the latter two treated as continuous variables. We use two space variables, $\mathbf{r}_*$ and $\mathbf{r}_1 = \epsilon\mathbf{r}_*$. The former is discrete and the latter is continuous. The mean populations $N_j(t, \mathbf{r})$ are described by a power series in ϵ as

$$N_j = N_j^{(0)}(t, \mathbf{r}) + \epsilon N_j^{(1)}(t, \mathbf{r}) + \mathcal{O}(\epsilon^2). \tag{3.34}$$

The first term $N_j^{(0)}$ is the small perturbation approximation based on the local values of ρ, $\mathbf{u}$, and ϕ, and is defined in Eq. (3.32). The $N_j^{(1)}$ contribute with non-equilibrium corrections in the linear response regime. These have no effect on the local density, momentum, or hexapolar mode. These relations are thus written as

$$\sum_j N_j^{(1)}(t, \mathbf{r}) = 0, \quad \sum_j \mathbf{c}_j N_j^{(1)}(t, \mathbf{r}) = 0, \quad \text{and} \quad \sum_j w_j N_j^{(1)}(t, \mathbf{r}) = 0. \tag{3.35}$$

We assume that the lattice Boltzmann approximation holds. We Taylor expand the first term in the LHS of Eq. (2.28) around t and $\mathbf{r}$ up to second-order, replacing the discrete coordinates with the continuous ones. We write the time derivative as ∂_t and space derivatives as $\partial_{\mathbf{r}} = \{\partial_\alpha,\ \alpha = 1, \dots, d\}$:

$$\begin{aligned} N_j(t_* + 1, \mathbf{r}_* + \mathbf{c}_j) = N_j(t, \mathbf{r}) &+ \partial_t N_j + c_{j\beta}\partial_\beta N_j + \frac{1}{2}\partial_t\partial_t N_j \\ &+ \frac{1}{2}c_{j\beta}c_{j\gamma}\partial_\beta\partial_\gamma N_j + c_{j\beta}\partial_t\partial_\beta N_j + \mathcal{O}(\partial^3 N_j). \end{aligned} \tag{3.36}$$

Inserting Eq. (3.36) into the lattice Boltzmann equation (Eq. (2.28)) leads to

$$\partial_t N_j + c_{j\beta}\partial_\beta N_j + \frac{1}{2}\partial_t\partial_t N_j + \frac{1}{2}c_{j\beta}c_{j\gamma}\partial_\beta\partial_\gamma N_j + c_{j\beta}\partial_t\partial_\beta N_j = \Omega_j(\mathbf{N}). \tag{3.37}$$

Multiplying Eq. (3.37) by 1, $c_{j\alpha}$, and w_j and summing over j leads to

$$\begin{aligned} \sum_j \begin{Bmatrix} 1 \\ c_{j\alpha} \\ w_j \end{Bmatrix} &\left[\partial_t N_j + c_{j\beta}\partial_\beta N_j + \frac{1}{2}\partial_t\partial_t N_j + \frac{1}{2}c_{j\beta}c_{j\gamma}\partial_\beta\partial_\gamma N_j + c_{j\beta}\partial_t\partial_\beta N_j\right] \\ &= \sum_j \begin{Bmatrix} 1 \\ c_{j\alpha} \\ w_j \end{Bmatrix} \Omega_j(\mathbf{N}). \end{aligned} \tag{3.38}$$

The RHS of Eq. (3.38) is the collision term. We linearize the collision function $\Omega_j(\mathbf{N})$, which leads to

$$\begin{aligned}\sum_j \begin{Bmatrix} 1 \\ c_{j\alpha} \\ w_j \end{Bmatrix} \sum_k \mathcal{L}_{jk} N_k &= \sum_k \left[\sum_j \begin{Bmatrix} 1 \\ c_{j\alpha} \\ w_j \end{Bmatrix} \mathcal{L}_{jk} \right] \left(N_k^{(0)} + \epsilon N_k^{(1)} \right) \\ &= \sum_k \begin{Bmatrix} 0 \\ 0 \\ -\gamma_3 w_j \end{Bmatrix} N_k^{(0)} \\ &= \begin{Bmatrix} 0 \\ 0 \\ -\gamma_3 \phi \end{Bmatrix}. \end{aligned} \tag{3.39}$$

The vectors $\mathbf{1}$, $\mathbf{c}_\alpha$, and $\mathbf{w}$ are eigenvectors of $\mathcal{L}$. Technically, they are left eigenvectors of $\mathcal{L}$, which are equivalent to the right eigenvectors since $\mathcal{L}$ is symmetric. Thus, one may replace $\sum_j \mathcal{L}_{jk}$ with the corresponding eigenvalues, 0, 0, and $-\gamma_3$, inside the square bracket. We used the relations in Eq. (3.35) to remove the $N_j^{(1)}$ terms.

We now expand the time and space derivatives in powers of ϵ, as

$$\partial_t \to \epsilon \partial_{t_1} + \epsilon^2 \partial_{t_2}, \quad \partial_{\mathbf{r}} \to \epsilon \partial_{\mathbf{r}_1}. \tag{3.40}$$

To account for diffusive effects, terms up to second order in ϵ need to be included. Inserting the expanded derivatives (Eq. (3.40)) into the conservation relations in Eq. (3.38) results in the three equations

$$\begin{aligned}\begin{Bmatrix} 0 \\ 0 \\ -\gamma_3 \phi \end{Bmatrix} = \sum_j \begin{Bmatrix} 1 \\ c_{j\alpha} \\ w_j \end{Bmatrix} \Big[&\epsilon \partial_{t_1} N_j^{(0)} + \epsilon c_{j\beta} \partial_{1\beta} N_j^{(0)} + \epsilon^2 \partial_{t_2} N_j^{(0)} + \epsilon^2 \frac{1}{2} \partial_{t_1} \partial_{t_1} N_j^{(0)} \\ &+ \epsilon^2 \frac{1}{2} c_{j\beta} c_{j\gamma} \partial_{1\beta} \partial_{1\gamma} N_j^{(0)} + \epsilon^2 c_{j\beta} \partial_{t_1} \partial_{1\beta} N_j^{(0)} \\ &+ \epsilon^2 \partial_{t_1} N_j^{(1)} + \epsilon^2 c_{j\beta} \partial_{1\beta} N_j^{(1)} \Big] + \mathcal{O}(\epsilon^3). \end{aligned} \tag{3.41}$$

In the following, we evaluate the sums in Eq. (3.41), first to linear order in ϵ and then to second order in ϵ. We combine these equations to get the macroscopic equations for the lattice gas.

First-Order Corrections

To get the first-order contributions to our macroscopic equations, we collect the terms in Eq. (3.41) that are linear in ϵ, which leads to

$$\partial_{t_1} \sum_j N_j^{(0)} + \partial_{1\beta} \sum_j c_{j\beta} N_j^{(0)} = 0, \tag{3.42}$$

$$\partial_{t_1} \sum_j c_{j\alpha} N_j^{(0)} + \partial_{1\beta} \sum_j c_{j\alpha} c_{j\beta} N_j^{(0)} = 0, \tag{3.43}$$

$$\partial_{t_1} \sum_j w_j N_j^{(0)} + \partial_{1\beta} \sum_j w_j c_{j\beta} N_j^{(0)} = 0. \tag{3.44}$$

Using the definitions of the dynamic quantities in Eqs. (2.21), (2.22), (2.25), and (3.8), we get our analogue for the Euler equations,

$$\partial_{t_1} \rho + \partial_{1\beta} (\rho u_\beta) = 0, \tag{3.45}$$

$$\partial_{t_1} (\rho u_\alpha) + \partial_{1\beta} P_{\alpha\beta} = 0, \tag{3.46}$$

$$\partial_{t_1} \phi + \partial_{1\beta} Y_\beta = 0, \tag{3.47}$$

where $P_{\alpha\beta}$ and Y_β are the momentum- and hexapolar-flux tensors respectively. The momentum-flux tensor is defined as

$$P_{\alpha\beta} = \sum_j c_{j\alpha} c_{j\beta} N_j^{(0)} = \frac{c^2}{2} \rho \delta_{\alpha\beta} + c^2 R_{\alpha\beta\gamma} G(\rho_0) u_\gamma \phi + T_{\alpha\beta\gamma\delta} \rho_0 G(\rho_0) u_\gamma u_\delta + \mathcal{O}\left(\epsilon \delta^3\right) \tag{3.48}$$

where $T_{\alpha\beta\gamma\delta}$ is a symmetric isotropic fourth-order tensor given by

$$T_{\alpha\beta\gamma\delta} = \sum_j c_{j\alpha} c_{j\beta} Q_{j\gamma\delta}, \tag{3.49}$$

and $Q_{j\gamma\delta}$ is given by Eq. (3.3). Here, we have introduced the anisotropic tensor $R_{\alpha\beta\gamma}$, defined as

$$\begin{aligned} R_{\alpha\beta\gamma} &= \sum_j w_j c_{j\alpha} c_{j\beta} c_{j\gamma} \\ &= \frac{3c^3}{2} \left(\delta_{\alpha x} \delta_{\beta x} \delta_{\gamma x} - \delta_{\alpha x} \delta_{\beta y} \delta_{\gamma y} - \delta_{\alpha y} \delta_{\beta x} \delta_{\gamma y} - \delta_{\alpha y} \delta_{\beta y} \delta_{\gamma x} \right). \end{aligned} \tag{3.50}$$

Eq. (3.48) is derived using properties of sums over j with terms that include factors of $c_{j\alpha}$ and w_j (Appendix A.1). Similarly, the hexapolar flux tensor Y_β is defined as

$$Y_\beta = \sum_j w_j c_{j\beta} N_j^{(0)} = 3c^2 G(\rho_0) u_\beta \phi + R_{\alpha\beta\gamma} \rho_0 G(\rho_0) u_\gamma u_\delta + \mathcal{O}\left(\epsilon \delta^3\right), \tag{3.51}$$

and derived in a similar way.

We now compare our first-order equations to those in [27]. As expected, the conservation of density leads to the continuity equation Eq. (3.45). The momentum equation however has a new term that contains anisotropic nonlinear advection of the ϕ field. The anisotropic coupling is described using the tensor $R_{\alpha\beta\gamma}$. Conversely, Y_β has an isotropic advection term for the ϕ field and an anisotropic momentum advection term.

Second-Order Corrections

The macroscopic equations to second order in ϵ describe the diffusive dynamics of ρ, $\rho\mathbf{u}$, and ϕ. The derivation of these equations is rather lengthy and is found in Appendix B.2. To systematically capture the diffusive effects, we neglect terms on the order of $\mathcal{O}(\epsilon^2\delta^2)$. The resulting equations are

$$\partial_{t_2}\rho = 0, \tag{3.52}$$

$$\begin{aligned}\rho_0\partial_{t_2}u_\alpha + T_{\alpha\beta\gamma\delta}\partial_{1\beta}\left[\left(\psi(\rho_0)+\frac{1}{6c^2}\right)\rho_0\partial_{1\gamma}u_\delta\right]&\\ + R_{\alpha\beta\gamma}\partial_{1\beta}\left(\xi(\rho_0)+\frac{1}{12}\right)\partial_{1\gamma}\phi = \mathcal{O}\left(\epsilon^2\delta^2\right),&\end{aligned} \tag{3.53}$$

$$\begin{aligned}\partial_{t_2}\phi + 3c^2\partial_{1\beta}\left(\xi(\rho_0)+\frac{1}{12}\right)\partial_{1\beta}\phi&\\ + R_{\beta\gamma\delta}\partial_{1\beta}\left(\psi(\rho_0)+\frac{1}{6c^2}\right)\rho_0\partial_{1\gamma}u_\delta + \gamma_3\phi = \mathcal{O}\left(\epsilon^2\delta^2\right),&\end{aligned} \tag{3.54}$$

where $\psi(\rho_0)$ and $\xi(\rho_0)$ are arbitrary real coefficients. These appear in our ansatz for $N_j^{(1)}$:

$$N_j^{(1)} = \psi(\rho_0)Q_{i\alpha\beta}\rho_0\partial_{1\alpha}u_\beta + \xi(\rho_0)c_{j\alpha}w_j\partial_{1\alpha}\phi, \tag{3.55}$$

This ansatz emerges when solving for $N_j^{(1)}$ using the continuous lattice Boltzmann equation (Eq. (3.37)). In Appendix B.2, we show that the coefficients can be written as

$$\psi(\rho_0) = \frac{1}{3c^2}\frac{\sum_{j\alpha\beta}Q_{j\alpha\beta}^2}{\sum_{jk\alpha\beta}Q_{j\alpha\beta}\mathcal{L}_{jk}Q_{k\alpha\beta}}, \tag{3.56}$$

$$\xi(\rho_0) = \frac{1}{6}\frac{\sum_{j\alpha}c_{j\alpha}^2 w_j^2}{\sum_{jk\alpha}c_{j\alpha}w_j\mathcal{L}_{jk}c_{k\alpha}w_k}, \tag{3.57}$$

The first equation (Eq. (3.52)) states that there is no mass diffusion, which is expected. Mass diffusion occurs in media with several species of particles. These are classically described by Fick's laws, where the particle flux of a certain species is proportional to the gradient of the species' concentration.

The second equation (Eq. (3.53)) describes momentum diffusion over long time scales t_2. There is a non-hydrodynamic term proportional to $R_{\alpha\beta\gamma}$. It describes an anisotropic diffusive coupling to ϕ. The third equation (Eq. (3.54)) describes diffusion of ϕ over long time-scales and has an anisotropic diffusive coupling to the momentum.

Transport Coefficients

To determine the coefficients $\psi(\rho_0)$ and $\xi(\rho_0)$ in Eqs. (3.56) and (3.57), we use our analysis of the eigenvectors and eigenvalues of the linearized collision matrix $\mathcal{L}$. We know that $Q_{j\alpha\beta}$ is an eigenvector of $\mathcal{L}$. Indeed, this second-order tensor, written in matrix form, is

$$Q_{j\alpha\beta} = \frac{c^2}{2}\begin{pmatrix}\cos(2\theta_j) & \sin(2\theta_j)\\ \sin(2\theta_j) & -\cos(2\theta_j)\end{pmatrix}. \tag{3.58}$$

The $\cos(2\theta_j)$ and $\sin(2\theta_j)$ are the cosine- and sine-factors of the $m = 2$ Fourier mode, which decays with rate γ_2. Thus, Eq. (3.56) reduces to

$$\psi(\rho_0) = \frac{1}{3c^2}\frac{\sum_{j\alpha\beta} Q_{j\alpha\beta}^2}{\sum_{j\alpha\beta} Q_{j\alpha\beta}\left[-\gamma_2(\rho_0)Q_{j\alpha\beta}\right]} = -\frac{1}{3c^2\gamma_2(\rho_0)}. \tag{3.59}$$

Similarly, the factor $c_{j\alpha}w_j$ can be written in vector form as

$$c_{j\alpha}w_j = \frac{c}{2}\begin{pmatrix}\cos(2\theta_j)+\cos(4\theta_j)\\ \sin(4\theta_j)-\sin(2\theta_j)\end{pmatrix} = c\begin{pmatrix}\cos(2\theta_j)\\ -\sin(2\theta_j)\end{pmatrix}. \tag{3.60}$$

Here we used that $\cos(4\theta_j) = \cos(2\theta_j)$ and $\sin(4\theta_j) = -\sin(2\theta_j)$. We see that $c_{j\alpha}w_j$ is also proportional to the $m = 2$ Fourier mode. Thus, Eq. (3.57) reduces to

$$\xi(\rho_0) = \frac{1}{6}\frac{\sum_{j\alpha} c_{j\alpha}^2 w_j^2}{\sum_{j\alpha} c_{j\alpha}w_j\left[-\gamma_2(\rho_0)c_{j\alpha}w_j\right]} = -\frac{1}{6\gamma_2(\rho_0)}. \tag{3.61}$$

Both transport coefficients for the diffusion of momentum and the hexapolar mode are related to the $m = 2$ Fourier mode, i.e., the viscous stress tensor. The two coefficients are linked by the relation

$$c^2\psi(\rho_0) = 2\xi(\rho_0). \tag{3.62}$$

Final Equations

We finalize the macroscopic equations by inserting the equations for the first- and second-order corrections back into Eq. (3.41), combined with the equations for the transport coefficients.

First, we simplify the tensors. The tensor $T_{\alpha\beta\gamma\delta}$ is given by Eq. (3.49). For our lattice gas, it can be written using Kronecker delta functions [27] as

$$T_{\alpha\beta\gamma\delta} = \frac{3c^4}{4}\left(\delta_{\alpha\gamma}\delta_{\beta\delta} + \delta_{\alpha\delta}\delta_{\beta\gamma} - \delta_{\alpha\beta}\delta_{\gamma\delta}\right). \tag{3.63}$$

The tensor $R_{\alpha\beta\gamma}$ is defined in Eq. (3.50). We replace $R_{\alpha\beta\gamma}$ with the dimensionless tensor $V_{\alpha\beta\gamma}$:

$$V_{\alpha\beta\gamma} = \frac{2}{3c^3}R_{\alpha\beta\gamma} = \delta_{\alpha x}\delta_{\beta x}\delta_{\gamma x} - \delta_{\alpha x}\delta_{\beta y}\delta_{\gamma y} - \delta_{\alpha y}\delta_{\beta x}\delta_{\gamma y} - \delta_{\alpha y}\delta_{\beta y}\delta_{\gamma x}. \tag{3.64}$$

The factor $G(\rho)$ is replaced with the dimensionless factor $g(\rho_0)$:

$$g(\rho_0) = \frac{3c^4}{2}G(\rho_0) = \frac{1}{2}\frac{2\rho_0 - b}{\rho_0 - b}. \tag{3.65}$$

Putting it all together, we end up with the final macroscopic equations of motion for the density, momentum, and hexapolar mode:

$$\partial_t\rho + \partial_\beta(\rho u_\beta) = 0 \tag{3.66}$$

$$\begin{aligned}\partial_t(\rho u_\alpha) + \partial_\alpha\left(c_s^2\rho - \frac{\rho_0 g(\rho_0)}{2}u^2\right) + cg(\rho_0)V_{\alpha\beta\gamma}\partial_\beta\left(u_\gamma\phi\right) + g(\rho_0)\rho_0\partial_\beta\left(u_\alpha u_\beta\right)\\ = \nu(\rho_0)\partial_\beta\left(\rho_0\partial_\alpha u_\beta + \rho_0\partial_\beta u_\alpha - \delta_{\alpha\beta}\rho_0\partial_\gamma u_\gamma\right) + c\nu(\rho_0)V_{\alpha\beta\gamma}\partial_\beta\partial_\gamma\phi\\ + \mathcal{O}\left(\epsilon\delta^3\right) + \mathcal{O}\left(\epsilon^2\delta^2\right) + \mathcal{O}\left(\epsilon^3\delta\right),\end{aligned} \tag{3.67}$$

$$\begin{aligned}\partial_t\phi + \frac{2}{c^2}g(\rho_0)\partial_\beta\left(u_\beta\phi\right) + \frac{1}{c}g(\rho_0)V_{\beta\gamma\delta}\rho_0\partial_\beta\left(u_\gamma u_\delta\right)\\ = 2\nu(\rho_0)\partial_\beta\partial_\beta\phi + \frac{2}{c}\nu(\rho_0)V_{\beta\gamma\delta}\rho_0\partial_\beta\partial_\gamma u_\delta - \gamma_3\phi\\ + \mathcal{O}\left(\epsilon\delta^3\right) + \mathcal{O}\left(\epsilon^2\delta^2\right) + \mathcal{O}\left(\epsilon^3\delta\right),\end{aligned} \tag{3.68}$$

where $c_s^2 = c^2/2$ and $\nu(\rho_0)$ is the kinematic viscosity, defined as

$$\nu(\rho_0) = \nu_c(\rho_0) + \nu_p. \tag{3.69}$$

The first term is the "collision" viscosity:

$$\nu_c(\rho_0) = \frac{c^2}{4\gamma_2(\rho_0)}. \tag{3.70}$$

It is positive and proportional to both transport coefficients $\psi(\rho_0)$ and $\xi(\rho_0)$ (Eqs. (3.59) and (3.61)). It is thus inversely proportional to the decay rate γ_2, which in turn depends on the details of the collisions.

The second term is the "propagation":

$$\nu_p = -\frac{c^2}{8}. \tag{3.71}$$

It is negative and does not depend on the nature of the collisions. It is purely an artifact from the discreteness of the lattice.

We now discuss the macroscopic equations in detail. The density equation (Eq. (3.66)) is just the continuity equation. The momentum equation contains factors of $g(\rho_0)$, which are well known in the literature [27]. The hexapolar equation also contains factors of $g(\rho_0)$ in the advection terms. These factors break Galilean invariance. These can effectively be removed by assuming the fluid is incompressible, such that $\rho(t,\mathbf{r}) = \rho_0$, and simultaneously rescaling the time coordinate as $t \mapsto t/g(\rho_0)$ and the viscosity as $\nu(\rho_0) \mapsto g(\rho_0)\nu(\rho_0)$

We identify the second term in the momentum equation as the pressure term. We define the pressure as $p = c_s^2\rho$. The u^2 term is not physical and is known in the LGCA literature. Ignoring the u^2 term, we see that this is an isothermal pressure relationship with speed of sound

$$c_s = \frac{c}{\sqrt{2}}. \tag{3.72}$$

Due to the single-speed nature of the model, the stress tensor is traceless and there is no bulk viscosity. Introducing rest particles would add a bulk viscosity term to the second-order equations.

Both the diffusion of ϕ and of the momentum are proportional to $\nu(\rho_0)$. This is because both equations couple to the $m = 2$ mode, i.e., the stress tensor. However, in the ϕ-equation, there are additional factors of 2 in the advection and diffusion terms of ϕ. The source of these factors will be discussed in Chapter 4, where we will derive similar macroscopic equations for an isotropic Fermi liquid. We will extend our procedure to derive equations for all angular modes, although only up to linear order in the small parameters.

The hexapolar corrections to linear order were derived by Frisch [32]. The ϕ terms were considered "irrelevant in the hydrodynamic limit" by the author, which is true. In the tomographic limit, however, these corrections are long-lived and on the same scale as the velocity, and must thus be kept. How these terms change the dynamics of the fluid is still unclear.

3.5 Linear Hydrodynamic Modes

The nonlinear terms in the macroscopic equations (Eqs. (3.66), (3.67), and (3.68)) are difficult to analyze. In this section, we study the hydrodynamic modes of the linearized macroscopic equations. We assume the small parameters $\delta\rho$, $\mathbf{u}$, and ϕ are sufficiently small such that we may ignore quadratic terms. Keeping only the linear terms in Eqs. (3.66), (3.67), and (3.68) leads to the linearized macroscopic equations:

$$\partial_t \delta\rho + \rho_0 \partial_\beta u_\beta = 0, \tag{3.73}$$

$$\rho_0 \partial_t u_\alpha + c_s^2 \partial_\alpha \delta\rho = \rho_0 \nu_0 \partial_\beta^2 u_\alpha + c\nu_0 \partial_{\alpha x}^2 \phi, \tag{3.74}$$

$$\partial_t \phi = 2\nu_0 \partial_\beta^2 \phi + \frac{2}{c} \rho_0 \nu_0 \bar{\partial}_{x\beta}^2 u_\beta - \gamma_3 \phi, \tag{3.75}$$

where $\nu_0 \equiv \nu(\rho_0)$. We have used that $\partial_\beta \partial_\alpha u_\beta + \partial_\beta^2 u_\alpha - \delta_{\alpha\beta} \partial_\beta \partial_\gamma u_\gamma = \partial_\beta^2 u_\alpha$. The tensor $V_{\alpha\beta\gamma}$ has been contracted with the derivatives to form two anisotropic differential operators $\partial_{\alpha x}^2$ and $\bar{\partial}_{x\beta}^2$, defined as

$$\partial_{\alpha x}^2 = \bar{\partial}_{x\alpha}^2 = V_{\alpha\beta\gamma} \partial_\beta \partial_\gamma = \begin{pmatrix} \partial_x^2 - \partial_y^2 \\ -2\partial_x \partial_y \end{pmatrix}. \tag{3.76}$$

The former maps a scalar to a vector quantity. The latter maps a vector to a scalar quantity. We assume the perturbations are plane waves of the form

$$\begin{aligned} \delta\rho(t, \mathbf{r}) &= \delta\rho e^{i\mathbf{k}\cdot\mathbf{r} - i\omega t}, \\ \mathbf{u}(t, \mathbf{r}) &= \mathbf{u} e^{i\mathbf{k}\cdot\mathbf{r} - i\omega t}, \\ \phi(t, \mathbf{r}) &= \phi e^{i\mathbf{k}\cdot\mathbf{r} - i\omega t}, \end{aligned} \tag{3.77}$$

where $\mathbf{k}$ is the wave vector and ω is the frequency of the perturbation. This allows us to replace the time and space derivatives with

$$\partial_t \to -i\omega, \quad \partial_\alpha \to ik_\alpha. \tag{3.78}$$

The $V_{\alpha\beta\gamma}$ tensor introduces anisotropic couplings, which make the dispersion relations dependent on the direction of the wave vector. We introduce the longitudinal and transverse basis vectors, $\hat{\mathbf{e}}_\parallel$ and $\hat{\mathbf{e}}_\perp$, defined as

$$\hat{\mathbf{e}}_\parallel = \begin{pmatrix} \cos(\theta) \\ \sin(\theta) \end{pmatrix}, \quad \hat{\mathbf{e}}_\perp = \begin{pmatrix} -\sin(\theta) \\ \cos(\theta) \end{pmatrix}, \tag{3.79}$$

where θ is the angle of the wave vector relative to the x-axis. The former is parallel to the wave vector and the latter is perpendicular to it. We may thus write the wave vector as

$$\mathbf{k} = k\hat{\mathbf{e}}_\parallel. \tag{3.80}$$

We define the longitudinal and transverse velocities $u_\parallel$ and $u_\perp$ as

$$u_\parallel = \hat{\mathbf{e}}_\parallel \cdot \mathbf{u}, \quad u_\perp = \hat{\mathbf{e}}_\perp \cdot \mathbf{u}. \tag{3.81}$$

The x- and y-components of $\mathbf{u}$ are expressed using the longitudinal and transverse velocities as

$$u_x = u_\parallel \cos(\theta) - u_\perp \sin(\theta), \quad u_y = u_\parallel \sin(\theta) + u_\perp \cos(\theta). \tag{3.82}$$

This gives us the equations

$$-i\omega\delta\rho + i\rho_0 k_\beta u_\beta = 0, \tag{3.83}$$

$$-i\rho_0\omega\mathbf{u} + ic_s^2\mathbf{k}\delta\rho = -\rho_0\nu_0 k^2\mathbf{u} - c\nu_0 \begin{pmatrix} k_x^2 - k_y^2 \\ -2k_xk_y \end{pmatrix} \phi, \tag{3.84}$$

$$-i\omega\phi = -2\nu_0 k^2\phi - \frac{2}{c}\rho_0\nu_0 \begin{pmatrix} k_x^2 - k_y^2 \\ -2k_xk_y \end{pmatrix} \cdot \mathbf{u} - \gamma_3\phi. \tag{3.85}$$

Using the first equation (3.83), we solve for $\delta\rho$ as

$$\delta\rho = \frac{\rho_0 k}{\omega} u_\parallel. \tag{3.86}$$

Inserting Eq. (3.86) into (3.84) and using the substitutions $k_x = k\cos(\theta)$ and $k_y = k\sin(\theta)$ leads to

$$-i\rho_0\omega\mathbf{u} + i\frac{c_s^2\rho_0 k}{\omega}\mathbf{k}u_\parallel = -\rho_0\nu_0 k^2\mathbf{u} - c\nu_0 k^2 \begin{pmatrix} \cos(2\theta) \\ -\sin(2\theta) \end{pmatrix} \phi. \tag{3.87}$$

The usual procedure is to get an equation for the longitudinal velocity and one for the transverse velocity, as both decouple. The difference is that we have an additional coupling to $\delta\rho$ in both equations. To get the longitudinal and transverse velocity equations, we project Eq. (3.87) onto $\hat{\mathbf{e}}_\parallel$ and $\hat{\mathbf{e}}_\perp$ respectively, which gives

$$-i\rho_0\omega u_\parallel + i\frac{\rho_0 c_s^2 k^2}{\omega}u_\parallel = -\rho_0\nu_0 k^2 u_\parallel - c\nu_0 k^2\cos(3\theta)\phi, \tag{3.88}$$

$$-i\rho_0\omega u_\perp = -\rho_0\nu_0 k^2 u_\perp + c\nu_0 k^2 \sin(3\theta)\phi. \tag{3.89}$$

The hexapolar equation (Eq. (3.85)) is expressed using $u_\parallel$ and $u_\perp$ as

$$\left(i\omega - 2\nu_0 k^2 - \gamma_3\right)\phi = \frac{2}{c}\rho_0\nu_0 k^2\left(\cos(3\theta)u_\parallel - \sin(3\theta)u_\perp\right). \tag{3.90}$$

Eqs. (3.89) and (3.90) can be written as a matrix equation:

$$M\begin{pmatrix} u_\parallel \\ u_\perp \\ \phi \end{pmatrix} = 0 \tag{3.91}$$

where

$$M = \begin{pmatrix} -i\rho_0\omega^2 + i\rho_0 c_s^2 k^2 + \rho_0\nu_0 k^2\omega & 0 & c\nu_0 k^2\omega\cos(3\theta) \\ 0 & -i\rho_0\omega + \rho_0\nu_0 k^2 & -c\nu_0 k^2\sin(3\theta) \\ -\frac{2}{c}\rho_0\nu_0 k^2\cos(3\theta) & \frac{2}{c}\rho_0\nu_0 k^2\sin(3\theta) & i\omega - \gamma_3 - 2\nu_0 k^2 \end{pmatrix}. \tag{3.92}$$

Small k dispersions

We solve for the dispersion relations approximately by expanding ω in small k. Since the hexapolar mode spreads diffusively in the linearized equations, we assume that its damping rate is proportional to k^2 by making the ansatz $\gamma_3 = \hat{\gamma}_3 k^2$. Looking at the bottom right element of M, we see that both the hexapolar relaxation rate and viscosity terms are on the same order $\mathcal{O}(k^2)$. This particular limit does not represent the full range of the tomographic regime [33], but it is chosen due to its simplicity.

We expand ω as

$$\omega = \omega_0 + \omega_1 k + \omega_2 k^2 + \ldots. \tag{3.93}$$

Using the ansatz for ω, we solve for the dispersion using the equation $\det(M) = 0$. We find four solutions using Mathematica, up to second order in k:

$$\omega_{s,\pm} = \pm c_s k - i\frac{\nu_0}{2}k^2 + \mathcal{O}(k^3), \tag{3.94}$$

$$\omega_{d,\pm} = -i\tilde{\nu}_\pm(\theta)k^2 + \mathcal{O}(k^4). \tag{3.95}$$

where we have defined an anisotropic diffusive constant

$$\tilde{\nu}_\pm(\theta) = \frac{1}{2}\left(3\nu_0 + \hat{\gamma}_3 \pm \sqrt{\left(\nu_0 + \hat{\gamma}_3\right)^2 + 8\nu_0^2\sin^2(3\theta)}\right). \tag{3.96}$$

The dispersions $\omega_{s,\pm}$ (Eq. (3.94)) are the acoustic modes. These describe density waves, or sound, that propagate linearly in time at the speed of sound c_s. The imaginary part of $\omega_{s,\pm}$ gives the damping, which is negative and therefore corresponds to stable decay.

The dispersions $\omega_{d,\pm}$ (Eq. (3.95)) are the diffusive modes, which describe decay (or possibly growth) of the plane waves. We now determine if the diffusive modes are stable, which requires that $\tilde{\nu}_\pm(\theta) > 0$. Since $\nu_0, \hat{\gamma}_3 > 0$ and $\sin^2(3\theta) \geq 0$, the positive branch is always positive. The negative branch is stable if the expression inside the parentheses in Eq. (3.96) is positive, which is given by the inequality

$$3\nu_0 + \hat{\gamma}_3 > \sqrt{(\nu_0 + \hat{\gamma}_3)^2 + 8\nu_0^2 \sin^2(3\theta)}. \tag{3.97}$$

Squaring and removing equal terms on both sides of Eq. (3.97) leads to

$$8\nu_0 + 4\hat{\gamma}_3 > 8\nu_0 \sin^2(3\theta). \tag{3.98}$$

The maximum value of $\sin^2(3\theta)$ is unity. Thus, the requirement for $\omega_{d,-}$ to be stable is to have $\hat{\gamma}_3 > 0$. For the cases where $\sin^2(3\theta) = 0$, the anisotropic diffusive constant has the values $\tilde{\nu}_+(\theta = n\pi/3) = 2\nu_0 + \hat{\gamma}_3$ and $\tilde{\nu}_-(\theta = n\pi/3) = \nu_0$ for integers n.

For the marginally stable case of $\hat{\gamma}_3 = 0$, the anisotropic diffusive constant becomes

$$\tilde{\nu}_\pm(\theta)\Big|_{\hat{\gamma}_3=0} = \frac{\nu_0}{2}\left(3 \pm \sqrt{1 + 8\sin^2(3\theta)}\right). \tag{3.99}$$

In this limit, for $\sin^2(3\theta) = 1$, it has the values $\tilde{\nu}_+(\theta = \pi/6 + n\pi/3)|_{\hat{\gamma}_3=0} = 3\nu_0$ and $\tilde{\nu}_-(\theta = \pi/6 + n\pi/3)|_{\hat{\gamma}_3=0} = 0$.

Interestingly, the negative branch of the diffusive mode is zero for $\theta = \frac{\pi}{6} + \frac{n\pi}{3}$. These stationary plane waves correspond to the conserved hexapolar mode ϕ when $\hat{\gamma}_3 = 0$. As such, exciting the linearized system results in plane waves that decay at different rates depending on θ, with almost stationary waves at angles separated by 60°. These waves are marginally stable and require nonlinear stability analysis.

In standard hydrodynamics, there is a single diffusive mode $\omega = -i\nu_0 k^2$ called the shear mode. It is also called the transverse mode, since it only couples to the transverse velocity $u_\perp$. To find this, one only needs to assume that $\hat{\gamma}_3 \sim \mathcal{O}(1)$ and expand $\omega = \omega_0 + \omega_1 k + \omega_2 k^2$. Up to second order in k, this gives the acoustic modes, the shear mode, and a diffusive mode $\omega = -i\hat{\gamma}_3 - i2\nu_0 k^2$. Assuming $2\nu_0 k^2$ is much smaller than $\hat{\gamma}_3$, the former term dominates the relaxation of this mode.

Using the small k approximation for the dispersion, we solve for the amplitudes $\delta\rho$, $u_\parallel$, $u_\perp$, and ϕ. We begin with the sound modes and end with the diffusive modes.

Sound mode amplitudes

Inserting $\omega_{s,\pm}$ into Eq. (3.86) leads to

$$\left(\pm c_s - i\frac{\nu_0}{2}k\right)\delta\rho = \rho_0 u_\parallel. \tag{3.100}$$

To leading order in k, we see that $\delta\rho = \pm\frac{\rho_0}{c_s}u_\parallel$. The density waves simply follow the waves of the longitudinal velocity, with a smaller wave that is phase shifted by the factor of i.

Inserting the sound modes into the longitudinal equation (Eq. (3.88)) results in

$$\left(-i\rho_0\left(\pm c_s k - i\frac{\nu_0}{2}k^2\right) + i\frac{\rho_0 c_s^2 k}{\pm c_s - i\frac{\nu_0}{2}k} + \rho_0\nu_0 k^2\right)u_\parallel = -c\nu_0 k^2\cos(3\theta)\phi. \tag{3.101}$$

Taylor expanding the fraction term as $i\rho_0 c_s^2 k/(\pm c_s - i\frac{\nu_0}{2}k) = \pm i\rho_0 c_s k - \rho_0\frac{\nu_0}{2}k^2$ leads to

$$\mathcal{O}(k^3) = -c\nu_0 k^2\cos(3\theta)\phi. \tag{3.102}$$

The terms on the LHS cancel each other at order k^2, which means that $\phi \sim \mathcal{O}(k)$. Inserting the sound modes into the transverse equation (Eq. (3.89)) leads to

$$\left(\mp i\rho_0 c_s k + \rho_0\frac{\nu_0}{2}k^2\right)u_\perp = c\nu_0 k^2\sin(3\theta)\phi \tag{3.103}$$

To leading order in k, we find that $\mp i\rho_0 c_s u_\perp = c\nu_0 k\sin(3\theta)\phi$. The transverse velocity is driven by the ϕ perturbation and is very small, of order of k^2, and can be neglected. Thus, sound waves do not generate any significant transverse flow.

Finally, inserting the sound modes into the hexapolar equation (Eq. (3.90)) leads to

$$\left(i\left(\pm c_s k - i\frac{\nu_0}{2}k^2\right) - 2\nu_0 k^2 - \hat{\gamma}_3 k^2\right)\phi = \frac{2}{c}\rho_0\nu_0 k^2\left(\cos(3\theta)u_\parallel - \sin(3\theta)u_\perp\right). \tag{3.104}$$

Since $u_\perp \sim \mathcal{O}(k^2)$, we neglect the transverse velocity term. To leading order in k, we find that the hexapolar mode is driven as

$$\phi = \mp i\frac{2}{c_s c}\rho_0\nu_0 k\cos(3\theta)u_\parallel. \tag{3.105}$$

Thus, sound waves generate small hexapolar waves, but only in certain directions, which is mediated by the $\cos(3\theta)$ term.

Diffusive mode amplitudes

Inserting $\omega_{d,\pm}$ into Eq. (3.86) leads to

$$-i\tilde{\nu}_\pm(\theta)k\delta\rho = \rho_0 u_\parallel. \tag{3.106}$$

The density fluctuation is small in comparison to $u_\parallel$, and is driven anisotropically due to the factor of $\tilde{\nu}_\pm(\theta)$.

Inserting the diffusive modes into the longitudinal equation (Eq. (3.88)) leads to

$$\frac{\rho_0 c_s^2}{\tilde{\nu}_\pm(\theta)}u_\parallel = c\nu_0 k^2\cos(3\theta)\phi. \tag{3.107}$$

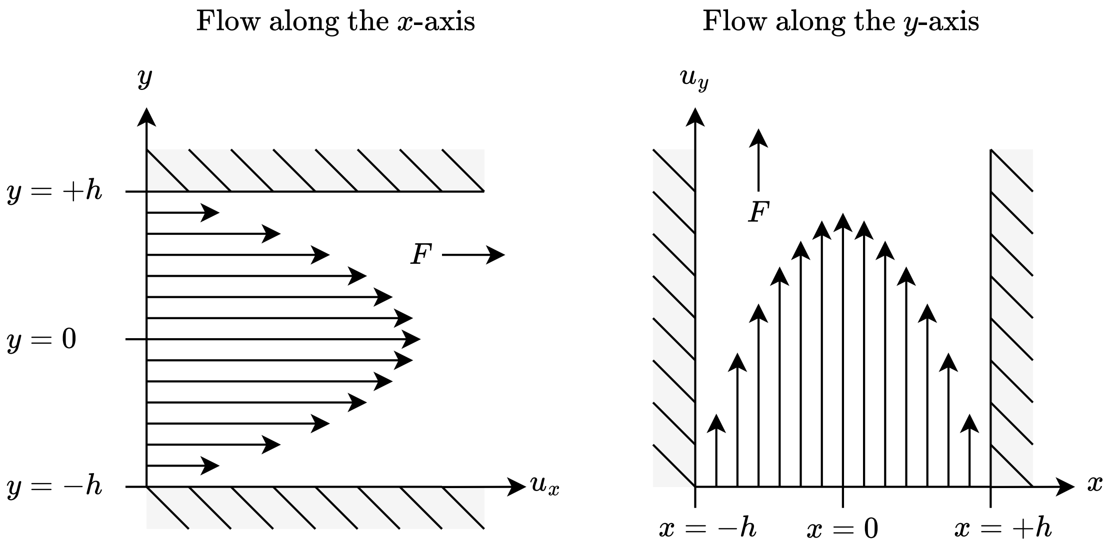

Figure 3.5: Illustrations of flow in a channel with different orientations.

The longitudinal velocity is tiny and negligible in comparison to the hexapolar mode, which in turn makes the density fluctuation even smaller.

Finally, inserting the diffusive modes into the transverse equation (Eq. (3.89)) and the hexapolar equation (Eq. (3.90)) leads to the matrix equation

$$\begin{pmatrix} \rho_0\left(\nu_0 - \tilde{\nu}_\pm(\theta)\right) & -c\nu_0 \sin(3\theta) \\ \frac{2}{c}\sin(3\theta) & \tilde{\nu}_\pm(\theta) - 2\nu_0 - \hat{\gamma}_3 \end{pmatrix} \begin{pmatrix} u_\perp \\ \phi \end{pmatrix} = \begin{pmatrix} 0 \\ 0 \end{pmatrix}. \tag{3.108}$$

The matrix equation is to leading order in k, as we have neglected the $u_\parallel$ term in the hexapolar equation. The hexapolar mode and the transverse velocity are on the same scale in this limit, and drive each other for most angles θ.

For angles $\theta = n\pi/3$ where n is an integer, the off-diagonal terms that contain a factor of $\sin(3\theta)$ become zero, such that $u_\perp$ and ϕ decouple. Further, the system also becomes degenerate at these angles. For the positive branch, the anisotropic diffusion constant $\tilde{\nu}_+ = 2\nu_0 + \hat{\gamma}_3$, which makes the bottom-right element zero and ϕ a free parameter. This forces $u_\perp$ to be zero. Conversely, for the negative branch we have that $\tilde{\nu}_- = \nu_0$, which makes the top-left element zero. This makes $u_\perp$ a free parameter and ϕ zero.

The solutions $\omega_{s,\pm}$ and $\omega_{d,\pm}$, along with the solutions to the amplitudes, contain anisotropic factors due to the influence of the hexapolar mode ϕ. In a Fermi liquid truncated to contain only a single odd-parity mode, a hexapolar mode with two components, we do not expect to see these anisotropic effects. This makes the LGCA weak as a simulation tool for tomographic Fermi liquids. However, we can still analyze the linear modes of the Fermi liquid in this truncated limit and find out if the modes of the LGCA are accurate for some angles θ.

3.6 Example: Flow in a Channel

Before leaving the macroscopic equations with a long-lived hexapolar mode (Eqs. (3.66), (3.67), and (3.68)), we solve a classic flow scenario from fluid mechanics: flow in a channel. Also known as Poiseuille flow, we assume that we have a fluid that flows in a rectangular channel, with one dimension taken to be infinitely long. Our analysis of the linear hydrodynamic modes showed that the diffusive modes behave differently for different orientations of the wave vector, so we expect different results based on the orientation of the channel. We consider flow along the x-axis and flow along the y-axis (Fig. 3.5). The channel has a width of $2h$ and we impose no-slip boundary conditions, such that the velocity field is zero at the boundaries.

To get analytically solvable solutions, we assume an incompressible fluid such that $\rho = \rho_0$. We also replace the gradient of the density in the momentum equations with a gradient of the pressure p, such that $\partial_\alpha p = c_s^2 \partial_\alpha \rho$. Inserting this into Eq. (3.66) leads to the incompressible continuity equation:

$$\partial_\beta u_\beta = 0. \tag{3.109}$$

Eq. (3.109) states that the velocity field is divergence free, such that there are no sources or sinks anywhere. This means that no fluid is created or destroyed.

Starting with flow along the x-axis, we solve for the steady state. We assume the flow is fully developed in the x-direction, such that $\mathbf{u}(y)$ and $\phi(y)$ have no dependence on x. Inserting this into the continuity equation (Eq. (3.109)) leads to $\partial_y u_y = 0$. This means that u_y is a constant along the y-direction. The no-slip boundary conditions impose $u_y(y = \pm h) = 0$, which means that $u_y(y) = 0$ for all y. This gives the equations

$$\rho_0 \partial_t u_x + \partial_x p = \rho_0 \nu_0 \partial_y^2 u_x - c\nu_0 \partial_y^2 \phi, \tag{3.110}$$

$$0 = \partial_y p - \frac{\rho_0 g(\rho_0)}{2} \partial_y u_x^2 - cg(\rho_0)\partial_y (u_x \phi), \tag{3.111}$$

$$\partial_t \phi = 2\nu_0 \partial_y^2 \phi - \frac{2}{c}\rho_0 \nu_0 \partial_y^2 u_x - \gamma_3 \phi. \tag{3.112}$$

The y-momentum equation (Eq. (3.111)) simply gives the pressure gradient $\partial_y p$, and it is ignored for now. To solve for the steady state, we set $\partial_t = 0$. Solving for $\partial_y^2 u_x$ in Eq. (3.110) and inserting it into Eq. (3.112) leads to

$$0 = \frac{2}{c}\rho_0 \nu_0 \partial_y^2 u_x - \frac{2}{c}\partial_x p - \frac{2}{c}\rho_0 \nu_0 \partial_y^2 u_x - \gamma_3 \phi. \tag{3.113}$$

The two $\partial_y^2 u_x$ terms perfectly cancel, and ϕ is determined as

$$\phi(y) = \frac{2F}{c\gamma_3}, \tag{3.114}$$

where $F = -\partial_x p$. The hexapolar mode is thus constant along the width of the channel. If γ_3 goes to zero, the ϕ field diverges, which suggests some instabilities in the macroscopic equations for very small γ_3.

Inserting the solution for ϕ back into Eq. (3.110) gives the usual quadratic velocity profile in $u_x(y)$, since $\partial_y^2\phi = 0$. Combined with the no-slip boundary conditions, this leads to

$$u_x(y) = \frac{F}{\rho_0\nu_0}\left(h^2 - y^2\right). \tag{3.115}$$

For flow along the y-axis (no dependence on y in u_y and ϕ, and $u_x = 0$), we get the equations

$$\partial_x p - \frac{\rho_0 g(\rho_0)}{2}\partial_x u_y^2 = c\nu_0\partial_x^2\phi, \tag{3.116}$$

$$\rho_0\partial_t u_y + \partial_y p - cg(\rho_0)\partial_x(u_y\phi) = \rho_0\nu_0\partial_x^2 u_y, \tag{3.117}$$

$$\partial_t\phi - \frac{\rho_0 g(\rho_0)}{c}\partial_x u_y^2 = 2\nu_0\partial_x^2\phi - \gamma_3\phi. \tag{3.118}$$

Setting $\partial_t = 0$ results in a set of coupled, nonlinear ordinary differential equations. These are generally difficult to solve analytically, and require a numerical solver. In this work, we will not dwell on these solutions.

4

Fermi Liquid Theory

The macroscopic lattice gas equations that were derived in Chapter 3 contained spatial derivative terms that featured an anisotropic symmetric tensor (cf. Eq. (3.64)). The question arises whether this tensor results from the discreteness of the lattice, or if it has a physical counterpart. To find out, we derive a set of similar equations for a homogeneous Fermi liquid, although to linear order in the perturbation. The resulting analysis shows that this tensor structure is not in fact a lattice artifact, but appears naturally in couplings between parity-even and parity-odd modes. The theory is adapted from the book by David Pines and Philippe Nozières [34]. The odd-even effect is described in the paper by Johannes Hofmann and Sankar Das Sarma [33].

In Sec. 4.1, we establish the kinetic theory for a two-dimensional Fermi liquid. We introduce the linearized kinetic equation, the Landau function, and the linearized collision integral. In Sec. 4.2, we introduce the mean quantities: the density and the current. We define angular projections on the distribution function and reestablish that the density and the current are the zeroth and first angular projections, and that the hexapolar mode is the cosine part of the third angular projection. In Sec. 4.3, we derive a macroscopic equation for every angular projection on the distribution function. We use adiabatic elimination to derive equations for only the conserved modes and the odd-parity modes. We discuss the similarities of these equations to those found in the lattice gas cellular automaton.

4.1 Kinetic Theory

The central object of Fermi liquid theory is the quasiparticle distribution function $n_{\mathbf{p}}(t, \mathbf{r})$. Similar to the single-particle distribution in LGCA, it gives the number of quasiparticles with momentum $\mathbf{p}$. It is parametrized by the time coordinate t and spatial coordinate $\mathbf{r}$. We assume that the Fermi liquid is a simple two-dimensional electron gas (2DEG) with a single circular Fermi surface. The equilibrium is Fermi-Dirac distributed as

$$n_0(\varepsilon_{\mathbf{p}}) = \frac{1}{1 + \exp\left[(\varepsilon_{\mathbf{p}} - \mu) / (k_B T)\right]}, \tag{4.1}$$

with the chemical potential μ, the Boltzmann constant k_B, and the temperature T. The quasiparticle energy is $\varepsilon_{\mathbf{p}} = p^2/(2m^*)$, where $p = |\mathbf{p}|$ and m^* is the effective mass of a quasiparticle.

We assume that $n_{\mathbf{p}}$ is close to equilibrium and that the quasiparticles are close to the Fermi surface. Quasiparticles at the Fermi surface have energy $\varepsilon_{\mathbf{p}} = \varepsilon_{p_F} = \mu$, where ε_{p_F} is the Fermi energy. Further, ignoring thermal fluctuations, we define the Fermi momentum $p_F = \sqrt{2m^* \varepsilon_{p_F}}$ and Fermi velocity $v_F = p_F/m^*$. We also define the Fermi temperature $T_F = \varepsilon_{p_F}/k_B$.

We further assume that the quasiparticle excitations are strongly concentrated near the Fermi surface, $|\mathbf{p}| = p_F$, such that the energy of the quasiparticles is only parametrized by θ, the angle of $\mathbf{p}$ relative to the x-axis. We write the momentum and velocity of the quasiparticles at the Fermi surface as $\mathbf{p}_\theta = p_F\left(\cos\theta, \sin\theta\right)$, and $\mathbf{v}_\theta = v_F\left(\cos(\theta), \sin(\theta)\right)$, respectively. The deformation of the Fermi surface can then be modeled by a small variation in chemical potential $\delta\mu(\theta; t, \mathbf{r}) = \varepsilon_\theta - \mu$.

Using these assumptions, we write the quasiparticle distribution function with a small linear perturbation $\delta n_{\mathbf{p}}$ as

$$n_{\mathbf{p}}(t, \mathbf{r}) = n_0(\varepsilon_{\mathbf{p}}) + \delta n_{\mathbf{p}}(t, \mathbf{r}), \tag{4.2}$$

where

$$\delta n_{\mathbf{p}}(\theta; t, \mathbf{r}) = \left(-\frac{\partial n_0}{\partial \varepsilon_{\mathbf{p}}}\right) \delta\mu(\theta; t, \mathbf{r}). \tag{4.3}$$

We assume that $\delta\mu$ is small enough such that we only need to keep terms up to linear order. In doing so, we are neglecting advective effects.

In Fermi liquid theory, one often encounters sums over momenta $\sum_{\mathbf{p}}$. Since we are looking at angular Fermi surface deformations that only depend on θ, these sums are essentially equivalent to sums over the angular indices j in lattice gases (cf. Eqs. (2.21) and (2.22)). To compute these sums, we will assume the momentum vector $\mathbf{p}$ is a continuous variable and convert the discrete sum into a continuous integral. We use the substitution $\mathrm{d}\varepsilon_{\mathbf{p}} = \frac{\mathrm{d}\varepsilon_{\mathbf{p}}}{\mathrm{d}p}\mathrm{d}p = (p/m^*)\mathrm{d}p$, which allows us to write the sums as functionals of an arbitrary function $\mathcal{F}_{\mathbf{p}}$:

$$\sum_{\mathbf{p}} \mathcal{F}_{\mathbf{p}} = g_s \int \frac{\mathrm{d}\mathbf{p}}{(2\pi\hbar)^2} \mathcal{F}_{\mathbf{p}} = \mathcal{N}_0 \int_0^\infty \mathrm{d}\varepsilon_{\mathbf{p}} \int_0^{2\pi} \frac{\mathrm{d}\theta}{2\pi} \mathcal{F}_{\mathbf{p}}, \tag{4.4}$$

where $g_s = 2$ is the spin-degeneracy factor and $\mathcal{N}_0 = m^* g_s/(2\pi\hbar^2)$ is the density of states of a 2D electron gas. In 1D and 3D, the density of states depends on energy.

The energy functional of the Fermi liquid and the time evolution of the quasiparticle distribution function are introduced in Appendices C.1 and C.2, respectively. The result is the linearized kinetic equation:

$$\frac{\partial}{\partial t}\delta n(\theta) + \mathbf{v}_\theta \cdot \frac{\partial}{\partial \mathbf{r}} \delta\bar{n}(\theta) = \mathcal{L}\left[\delta n(\theta)\right], \tag{4.5}$$

where $\delta\bar{n}$ is

$$\delta\bar{n}(\theta) = \delta n(\theta) + \left(-\frac{\partial n_0}{\partial \varepsilon_{\mathbf{p}}}\right) \delta\varepsilon(\theta). \tag{4.6}$$

It may be thought of as a deviation in the distribution function away from local equilibrium by a small deviation in energy $\delta\varepsilon(\theta)$, defined as

$$\delta\varepsilon(\theta) = \int_0^{2\pi} \frac{\mathrm{d}\theta'}{2\pi} F(\theta - \theta')\delta\mu(\theta'), \tag{4.7}$$

where $F(\theta)$ is the dimensionless Landau function. It describes the interaction energy between two quasiparticles. Due to isotropy, it only depends on the angular difference in the momentum of the quasiparticles.

We have also introduced the linearized collision integral $\mathcal{L}[\delta n(\theta)]$. The tomographic regime emerges from how the collision integral acts on Fermi surface deformations. To understand this, we must first expand $\delta\mu$ in Fourier modes as

$$\delta\mu(\theta) = \sum_{m=-\infty}^{\infty} \delta\mu_m e^{im\theta}. \tag{4.8}$$

By doing this, we interpret the variation in chemical potential as the sum of many different collective quasiparticle excitations, called collective modes or angular modes, that deform the Fermi surface. These modes describe local peaks on the Fermi surface that become sharper as m increases. Similarly, we decompose the Landau function $F(\theta)$ into Fourier modes as

$$F(\theta) = \sum_{m=-\infty}^{\infty} F_m e^{im\theta}. \tag{4.9}$$

The F_m are called Landau parameters, which describe the interaction energies between different collective modes. Since the Landau parameters are real, we have that $F_m = F_{-m}$.

Using the Fourier expansion, we rewrite the local quasiparticle energy in Eq. (4.7) as

$$\delta\varepsilon(\theta) = \int_0^{2\pi} \frac{d\theta'}{2\pi} \sum_{m=-\infty}^{\infty} F_m e^{im(\theta-\theta')} \delta\mu_m e^{im\theta'} = \sum_{m=-\infty}^{\infty} F_m \delta\mu_m e^{im\theta}. \tag{4.10}$$

Since the odd-parity and even-parity angular harmonics of the Fermi surface deformation are relaxed by different mechanisms, they have different relaxation times. In this work, we will consider a simple relaxation time approximation where each $\delta\mu_m$ decays with a single individual decay rate $\gamma_m > 0$:

$$\mathcal{L}\left[\delta\mu_m\right] = -\gamma_m \delta\mu_m \tag{4.11}$$

where the decay rates γ_m are given by

$$\gamma_m = \begin{cases} 0 & \\ \gamma_{m,\text{even}} & \text{for} \quad m = \pm 2, \pm 4, \pm 6, \ldots \\ \gamma_{m,\text{odd}} & \end{cases} \begin{matrix} m = 0, \pm 1 \\ \\ m = \pm 3, \pm 5, \pm 7, \ldots \end{matrix} \tag{4.12}$$

In this work, we do not specify the form of the decay rates in terms of m and T. We only assume that $\gamma_{\text{odd}} \ll \gamma_{\text{even}}$. This ensures that the odd-parity modes are collisionless and long-lived, while the even-parity modes decay quickly, giving a mix of ballistic and hydrodynamic behavior. Since the LGCA only has a single decaying even mode, the stress tensor, and a single long-lived odd-parity mode, the hexapolar mode, this description is sufficient.

4.2 Mean Quantities and Angular Projections

To go from a kinetic to a hydrodynamic description, we take averages, or moments, of the quasiparticle distribution $n(\theta)$. These are the quasiparticle density $\rho(t, \mathbf{r}) = \rho_0 + \delta\rho(t, \mathbf{r})$, the current $\mathbf{j}(t, \mathbf{r})$, and additional higher angular modes. We define the mean velocity $\mathbf{u}(t, \mathbf{r})$ as

$$\mathbf{u}(t, \mathbf{r}) = \frac{\mathbf{j}(t, \mathbf{r})}{\rho_0}. \tag{4.13}$$

We obtain the density by integrating the distribution function over all $\mathbf{p}$, which leads to

$$\rho(t, \mathbf{r}) = \sum_{\mathbf{p}} n(\theta; t, \mathbf{r}) = \mathcal{N}_0\mu + \mathcal{N}_0\delta\mu_0(t, \mathbf{r}), \tag{4.14}$$

We find that $\rho_0 = \mathcal{N}_0\mu$ and $\delta\rho(t, \mathbf{r}) = \mathcal{N}_0\delta\mu_0(t, \mathbf{r})$. The density is thus proportional to the zeroth moment of the distribution function. To get the current and angular modes, we need to compute higher-order moments of the distribution function. For this, the following relations are useful:

$$\int_0^{2\pi} \frac{\mathrm{d}\theta}{2\pi} \cos(m\theta) e^{im'\theta} = \frac{1}{2}\left(\delta_{m',-m} + \delta_{m',m}\right) \tag{4.15}$$

$$\int_0^{2\pi} \frac{\mathrm{d}\theta}{2\pi} \sin(m\theta) e^{im'\theta} = -\frac{i}{2}\left(\delta_{m',-m} - \delta_{m',m}\right). \tag{4.16}$$

Essentially, the $\cos(m\theta)$ and $\sin(m\theta)$ factors isolate the angular mode m under integration over θ. The current is the first moment and is found by multiplying the distribution function with the Fermi momentum $\mathbf{p}_\theta$ and integrating over all $\mathbf{p}$:

$$\begin{aligned}\mathbf{j}(t, \mathbf{r}) &= \sum_{\mathbf{p}} \frac{\mathbf{p}_\theta}{m_0} n(\theta; t, \mathbf{r}) = \sum_{\mathbf{p}} \frac{m^*}{m_0} \mathbf{v}_\theta n(\theta; t, \mathbf{r}) \\ &= \mathcal{N}_0 \frac{v_F}{2}\left(1 + F_1\right) \begin{pmatrix} \delta\mu_{-1}(t, \mathbf{r}) + \delta\mu_1(t, \mathbf{r}) \\ -i\left(\delta\mu_{-1}(t, \mathbf{r}) - \delta\mu_1(t, \mathbf{r})\right) \end{pmatrix}. \end{aligned} \tag{4.17}$$

Here, m_0 is the bare electron mass. We use that $F_1 = F_{-1}$ and assume Galilean invariance such that $m^*/m_0 = 1 + F_1$. The $m = \pm 1$ mode is proportional to the current. Specifically, the cosine part $\delta\mu_{-1} + \delta\mu_1$ is proportional to j_x and the sine part $-i\left(\delta\mu_{-1} - \delta\mu_1\right)$ is proportional to j_y. To bring the angular modes into the hydrodynamic description, we introduce the vectors

$$\hat{\mathbf{v}}_\theta^{(m)} = \begin{pmatrix} \cos(m\theta) \\ \sin(m\theta) \end{pmatrix}, \quad \text{for nonnegative integers } m. \tag{4.18}$$

The vector $\hat{\mathbf{v}}_\theta^{(1)}$ is the normalized Fermi velocity, i.e., $\mathbf{v}_\theta = v_F \hat{\mathbf{v}}_\theta^{(1)}$. Using these vectors, we define the angular projections $\mathbf{\Phi}^{(m)}$ for nonnegative integers m:

$$\mathbf{\Phi}^{(m)}(t, \mathbf{r}) = \sum_{\mathbf{p}} \hat{\mathbf{v}}_\theta^{(m)} n(\theta; t, \mathbf{r}) = \frac{\mathcal{N}_0}{2} \begin{pmatrix} \delta\mu_{-m}(t, \mathbf{r}) + \delta\mu_m(t, \mathbf{r}) \\ -i\left(\delta\mu_{-m}(t, \mathbf{r}) - \delta\mu_m(t, \mathbf{r})\right) \end{pmatrix}. \tag{4.19}$$

For the $m = 0$ projection, we find that $\Phi_x^{(0)}(t, \mathbf{r}) = \mathcal{N}_0 \delta\mu_0(t, \mathbf{r}) = \delta\rho(t, \mathbf{r})$ and $\Phi_y^{(0)}(t, \mathbf{r}) = 0$. This means that the $m = 0$ angular projection is essentially a scalar quantity, since the y-component is always zero. This is obvious since the zeroth mode is proportional to the density.

For the $m = 1$ projection, we find that $v_F (1 + F_1) \mathbf{\Phi}^{(1)}(t, \mathbf{r}) = \mathbf{j}(t, \mathbf{r})$. Since the angular projections are proportional to their exponential counterparts, they relax with the same decay rates γ_m.

4.3 Linearized Macroscopic Equations

In this section, we derive a set of macroscopic equations for the Fermi liquid. Since the kinetic equation (Eq. (4.5)) is linearized, a full Chapman-Enskog expansion is unnecessary. Instead, we derive a macroscopic equation for each angular projection $\mathbf{\Phi}^{(m)}$ with nonnegative integer m. The linearized continuity and Navier-Stokes equations are then recovered from the equations for $\mathbf{\Phi}^{(0)}$ and $\mathbf{\Phi}^{(1)}$. The equation for the $\mathbf{\Phi}^{(3)}$ projection is analogous to the hexapolar equation for the lattice gas.

We assume that the even angular modes are fully relaxed. This assumptions relies on the fact that the relaxation rate of the even modes $\gamma_{m,\text{even}}$ is large. We also assume that the even modes are not driven at frequencies that are much higher than $\gamma_{m,\text{even}}$. In that case, the even modes are overdamped and we can set $\partial_t \mathbf{\Phi}^{(m)} = 0$. Further, we assume that $\gamma_{m,\text{odd}}$ is very small, such that the odd-parity modes are long-lived, which effectively slaves the fast modes to the slow modes. This method is called adiabatic elimination.

We write the time derivative as ∂_t and spatial derivatives as $\partial_\mathbf{r} = \{\partial_\alpha, \alpha = x, y\}$, and $\hat{\mathbf{v}}_\theta^{(m)} = \left\{\hat{v}_{\theta,\alpha}^{(m)}, \alpha = x, y\right\}$, where Greek indices denote components. Using this notation, we write the linearized kinetic equation as

$$\partial_t n(\theta) + v_{\theta,\alpha} \partial_\alpha \left(n_0 + \delta\bar{n}(\theta)\right) = \mathcal{L}\left[n(\theta)\right]. \tag{4.20}$$

To obtain the macroscopic equations for the angular projections, we multiply Eq. (4.20) by $\hat{v}_{\theta,\alpha}^{(m)}$ and sum over $\mathbf{p}$. This leads to

$$\partial_t \sum_\mathbf{p} \hat{v}_{\theta,\alpha}^{(m)} n(\theta) + \partial_\beta \sum_\mathbf{p} \hat{v}_{\theta,\alpha}^{(m)} v_{\theta,\beta} \Big(n(\theta) + \delta\varepsilon(\theta)\Big) = \sum_\mathbf{p} \hat{v}_{\theta,\alpha}^{(m)} \mathcal{L}\left[n(\theta)\right]. \tag{4.21}$$

Using Eq. (4.19), the first term is simply $\partial_t \Phi_\alpha^{(m)}$. Due to linearity, the collision term reduces to

$$\sum_\mathbf{p} \hat{v}_{\theta,\alpha}^{(m)} \mathcal{L}\left[n(\theta)\right] = \mathcal{L}\left[\Phi_\alpha^{(m)}\right] = -\gamma_m \Phi_\alpha^{(m)}. \tag{4.22}$$

The propagation term describes the flux of the angular mode and requires more work. First, we evaluate the second-order tensor $\hat{v}_{\theta,\alpha}^{(m)} v_{\theta,\beta}$:

$$\begin{aligned} \hat{v}_{\theta,\alpha}^{(m)} v_{\theta,\beta} = \frac{v_F}{2} &\begin{pmatrix} \cos((m-1)\theta) & -\sin((m-1)\theta) \\ \sin((m-1)\theta) & \cos((m-1)\theta) \end{pmatrix} \\ &+ \frac{v_F}{2} \begin{pmatrix} \cos((m+1)\theta) & \sin((m+1)\theta) \\ \sin((m+1)\theta) & -\cos((m+1)\theta) \end{pmatrix}. \end{aligned} \tag{4.23}$$

Using Eq. (4.23), we evaluate the integral over the isotropic part of the distribution $n_0(\varepsilon)$:

$$\sum_{\mathbf{p}} \hat{v}^{(m)}_{\theta,\alpha} v_{\theta,\beta} n_0(\varepsilon_{\mathbf{p}}) = \mathcal{N}_0 \frac{v_F}{2} \mu \delta_{\alpha\beta} \delta_{m,1} = \frac{v_F}{2} \rho_0 \delta_{\alpha\beta} \delta_{m,1}. \tag{4.24}$$

This is essentially the isothermal pressure term, which only appears in the momentum flux tensor due to the Kronecker delta $\delta_{m,1}$. The integral over the deviation $\delta\bar{n}(\theta)$ is evaluated as

$$\begin{aligned}\sum_{\mathbf{p}} \hat{v}^{(m)}_{\theta,\alpha} v_{\theta,\beta} \delta\bar{n}(\theta) = \mathcal{N}_0 \frac{v_F}{4} \Bigg[&(1+F_{m-1}) \begin{pmatrix} \delta\mu_{-m+1} + \delta\mu_{m-1} & i\left(\delta\mu_{-m+1} - \delta\mu_{m-1}\right) \\ -i\left(\delta\mu_{-m+1} - \delta\mu_{m-1}\right) & \delta\mu_{-m+1} + \delta\mu_{m-1} \end{pmatrix} \\ &+ (1+F_{m+1}) \begin{pmatrix} \delta\mu_{-m-1} + \delta\mu_{m+1} & -i\left(\delta\mu_{-m-1} - \delta\mu_{m+1}\right) \\ -i\left(\delta\mu_{-m-1} - \delta\mu_{m+1}\right) & -\left(\delta\mu_{-m-1} + \delta\mu_{m+1}\right) \end{pmatrix} \Bigg].\end{aligned} \tag{4.25}$$

Here we have used that $F_{-m} = F_m$. The deviatoric part of the flux tensor couples to the $m \pm 1$ modes, which results in a tight-binding structure. For $m = 0$, Eq. (4.25) reduces to

$$\begin{aligned}\sum_{\mathbf{p}} \hat{v}^{(0)}_{\theta,\alpha} v_{\theta,\beta} \delta\bar{n}(\theta) &= \mathcal{N}_0 \frac{v_F}{2} (1+F_1) \begin{pmatrix} \delta\mu_1 + \delta\mu_{-1} & -i\left(\delta\mu_{-1} - \delta\mu_1\right) \\ 0 & 0 \end{pmatrix} \\ &= v_F (1+F_1) \begin{pmatrix} \Phi^{(1)}_x & \Phi^{(1)}_y \\ 0 & 0 \end{pmatrix}.\end{aligned} \tag{4.26}$$

As expected, the $m = 0$ mode only couples to the momentum. For $m > 0$, Eq. (4.25) reduces to

$$\sum_{\mathbf{p}} \hat{v}^{(m)}_{\theta,\alpha} v_{\theta,\beta} \delta\bar{n}(\theta) = \frac{v_F}{2} \left[(1+F_{m-1}) V^{-}_{\alpha\beta\gamma} \Phi^{(m-1)}_\gamma + (1+F_{m+1}) V^{+}_{\alpha\beta\gamma} \Phi^{(m+1)}_\gamma \right]. \tag{4.27}$$

In Eq. (4.27), we have introduced the two anisotropic third-order tensors $V^{\pm}_{\alpha\beta\gamma}$ defined as

$$V^{\pm}_{\alpha\beta\gamma} = \delta_{\alpha x}\delta_{\beta x}\delta_{\gamma x} \pm \delta_{\alpha x}\delta_{\beta y}\delta_{\gamma y} + \delta_{\alpha y}\delta_{\beta x}\delta_{\gamma y} \mp \delta_{\alpha y}\delta_{\beta y}\delta_{\gamma x}. \tag{4.28}$$

The tensors $V^{\pm}_{\alpha\beta\gamma}$ describe the anisotropic coupling to the $\Phi^{(m\pm1)}_\gamma$ modes. Contracting the tensors with the spatial derivative ∂_β creates two second-order differential operators:

$$\bar{\partial}_{\alpha\beta} = \partial_\beta V^{-}_{\alpha\beta\gamma} = \begin{pmatrix} \partial_x & -\partial_y \\ \partial_y & \partial_x \end{pmatrix}, \quad \partial_{\alpha\beta} = \partial_\beta V^{+}_{\alpha\beta\gamma} = \begin{pmatrix} \partial_x & \partial_y \\ -\partial_y & \partial_x \end{pmatrix}. \tag{4.29}$$

These derivatives are (excluding a factor of one half) the complex Wirtinger derivatives ∂_z and $\partial_{\bar{z}}$ where $z = x + iy$, defined to act on two-dimensional real-valued vectors instead of complex numbers. These operators satisfy $\partial^\top_{\alpha\beta} = \bar{\partial}_{\alpha\beta}$ and $\bar{\partial}^\top_{\alpha\beta} = \partial_{\alpha\beta}$. Using Eqs. (4.22), (4.24), and (4.27), the macroscopic equation for the $m > 0$ angular projection is

$$\partial_t \Phi^{(m)}_\alpha + \partial_\beta \hat{P}^{(m)}_{\alpha\beta} = -\gamma_m \Phi^{(m)}_\alpha. \tag{4.30}$$

where $\hat{P}^{(m)}_{\alpha\beta}$ is the generalized flux tensor, defined as

$$\hat{P}^{(m)}_{\alpha\beta} = \frac{v_F}{2}\left[\rho_0\delta_{\alpha\beta}\delta_{m,1} + \left(1+F_{m-1}\right)V^{-}_{\alpha\beta\gamma}\Phi^{(m-1)}_{\gamma} + \left(1+F_{m+1}\right)V^{+}_{\alpha\beta\gamma}\Phi^{(m+1)}_{\gamma}\right]. \quad (4.31)$$

This flux tensor does not assume that any Fourier mode decays quickly, and thus only couples to the $m \pm 1$ modes. To compare it to the momentum flux tensor, as well as the hexapolar flux tensor, we need to assume that the even-parity modes are fully relaxed.

Adiabatic Elimination

We now perform the adiabatic elimination for the even angular modes. Starting with Eq. (4.30) for even integers $m_e > 1$, we assume that $\Phi^{(m_e)}_{\alpha}$ is fully relaxed and has no dependence on t. This allows us to solve for $\Phi^{(m_e)}_{\alpha}$ in terms of the flux tensor $\hat{P}^{(m_e)}_{\alpha\beta}$, which leads to

$$\Phi^{(m_e)}_{\alpha} = -\frac{1}{\gamma_{m_e}}\partial_\beta\hat{P}^{(m_e)}_{\alpha\beta} = -\frac{v_F}{2\gamma_{m_e}}\left[\left(1+F_{m_e-1}\right)\bar{\partial}_{\alpha\beta}\Phi^{(m_e-1)}_{\beta} + \left(1+F_{m_e+1}\right)\partial_{\alpha\beta}\Phi^{(m_e+1)}_{\beta}\right]. \quad (4.32)$$

Having expressed $\Phi^{(m_e)}$ in terms of $\Phi^{(m_e\pm 1)}$ in Eq. (4.32), we may rewrite the flux tensor. This involves second-order derivatives, and we introduce the anisotropic second-order differential operators

$$\bar{\partial}^2_{\alpha\beta} = \bar{\partial}_{\alpha\beta}\bar{\partial}_{\beta\gamma} = \begin{pmatrix}\partial_x^2-\partial_y^2 & -2\partial_x\partial_y\\ 2\partial_x\partial_y & \partial_x^2-\partial_y^2\end{pmatrix} \quad (4.33)$$

$$\partial^2_{\alpha\beta} = \partial_{\alpha\beta}\partial_{\beta\gamma} = \begin{pmatrix}\partial_x^2-\partial_y^2 & 2\partial_x\partial_y\\ -2\partial_x\partial_y & \partial_x^2-\partial_y^2\end{pmatrix} \quad (4.34)$$

$$\bar{\partial}_{\alpha\beta}\partial_{\beta\gamma} = \partial_{\alpha\beta}\bar{\partial}_{\beta\gamma} = \begin{pmatrix}\partial_x^2+\partial_y^2 & 0\\ 0 & \partial_x^2+\partial_y^2\end{pmatrix} = \partial^2_\beta\delta_{\alpha\gamma} \equiv \nabla^2. \quad (4.35)$$

Mixing the Wirtinger derivatives results in the Laplacian operator in 2D. Using Eq. (4.32), we write $\partial_\beta P^{(m_o)}_{\alpha\beta}$, for odd integers $m_o > 1$, as

$$\begin{aligned}\partial_\beta\hat{P}^{(m_o)}_{\alpha\beta} &= -\frac{v_F^2}{4}\left(\frac{1+F_{m_o-1}}{\gamma_{m_o-1}}\bar{\partial}_{\alpha\beta}\left[\left(1+F_{m_o-2}\right)\bar{\partial}_{\beta\gamma}\Phi^{(m_o-2)}_{\gamma} + \left(1+F_{m_o}\right)\partial_{\beta\gamma}\Phi^{(m_o)}_{\gamma}\right]\right.\\ &\qquad\left.+\frac{1+F_{m_o+1}}{\gamma_{m_o+1}}\partial_{\alpha\beta}\left[\left(1+F_{m_o}\right)\bar{\partial}_{\beta\gamma}\Phi^{(m_o)}_{\gamma} + \left(1+F_{m_o+2}\right)\partial_{\beta\gamma}\Phi^{(m_o+2)}_{\gamma}\right]\right)\\ &= -\frac{v_F^2}{4}\left[\Gamma^-_{m_o-1}\bar{\partial}^2_{\alpha\beta}\Phi^{(m_o-2)}_{\beta} + \left(\Gamma^+_{m_o-1}+\Gamma^-_{m_o+1}\right)\partial^2_\beta\Phi^{(m_o)}_{\alpha} + \Gamma^+_{m_o+1}\partial^2_{\alpha\beta}\Phi^{(m_o+2)}_{\beta}\right],\end{aligned} \quad (4.36)$$

where the parameters $\Gamma^{\pm}_m$ are defined as

$$\Gamma^{\pm}_m = \left(\frac{1+F_m}{\gamma_m}\right)\left(1+F_{m\pm1}\right). \quad (4.37)$$

By adiabatically eliminating the even modes, the flux tensor instead has three terms. Two of them describe anisotropic second-order derivative couplings to the $m_o \pm 2$ modes, and one describes diffusion of the m_o mode.

Density Equation

Using Eqs. (4.30) and (4.26), we derive an equation for $\Phi_x^{(0)}$ by setting $m = 0$:

$$\partial_t \Phi_x^{(0)} + v_F (1 + F_1) \partial_\beta \Phi_\beta^{(1)} = 0 \tag{4.38}$$

This equation is rewritten in terms of the density perturbation $\delta\rho$ and the current j_β, which leads to the density equation

$$\partial_t \delta\rho + \partial_\beta j_\beta = 0. \tag{4.39}$$

This is exactly the linearized continuity equation for the lattice gas (Eq. (3.73)). The main difference lies in the inclusion of the Landau parameter F_1 in the definition of the current (Eq. (4.17)).

Current Equation

Using Eqs. (4.30) and (4.3), we derive an equation for $\Phi_x^{(1)}$ by setting $m = 1$ with an adiabatically eliminated $m = 2$ mode:

$$\partial_t \Phi_\alpha^{(1)} + \frac{v_F}{2} (1 + F_0) \bar{\partial}_{\alpha\beta} \Phi_\beta^{(0)} - \frac{v_F^2}{4} \left[\Gamma_2^- \partial_\beta^2 \Phi_\alpha^{(1)} + \Gamma_2^+ \partial_{\alpha\beta}^2 \Phi_\beta^{(3)} \right] = 0. \tag{4.40}$$

Multiplying Eq. (4.40) by $v_F (1 + F_1)$ leads to the current equation:

$$\partial_t j_\alpha + \frac{v_F^2}{2} (1 + F_0) (1 + F_1) \partial_\alpha \delta\rho = \frac{v_F^2}{4} \left[\Gamma_2^- \partial_\beta^2 j_\alpha + v_F (1 + F_1) \Gamma_2^+ \partial_{\alpha\beta}^2 \Phi_\beta^{(3)} \right]. \tag{4.41}$$

We find that the speed of sound is $c_s = \sqrt{\frac{v_F^2}{2} (1 + F_0) (1 + F_1)}$. The kinematic viscosity is identified as

$$\nu = \frac{v_F^2}{4} \frac{1 + F_2}{\gamma_2} (1 + F_1). \tag{4.42}$$

In the lattice gas, there is no interaction energy between particles. In the limit $F_m = 0$ for all m, the speed of sound is $c_s = v_F/\sqrt{2}$ and the viscosity is $\nu = v_F^2/(4\gamma_2)$. Interpreting the Fermi velocity v_F as the speed of the particles c, both the speed of sound and the viscosity are the same in the lattice gas (Eqs. (3.72) and (3.70)). Specifically, the viscosity is the same as the collision viscosity in the lattice gas.

Further, setting $\Phi_y^{(3)} = 0$, the $m = 3$ mode becomes equivalent to the scalar hexapolar mode ϕ. Eq. (4.41) then reduces to the linearized momentum equation in Eq. (3.74) for the lattice gas.

Hexapolar Equation

Using Eqs. (4.30) and (4.3), we derive an equation for $\Phi_x^{(3)}$. We do this by setting $m = 3$, with the $m = 2, 4$ modes adiabatically eliminated:

$$\partial_t \Phi_\alpha^{(3)} - \frac{v_F^2}{4} \left[\Gamma_2^- \bar{\partial}_{\alpha\beta}^2 \Phi_\beta^{(1)} + \left(\Gamma_2^+ + \Gamma_4^- \right) \partial_\beta^2 \Phi_\alpha^{(3)} + \Gamma_4^+ \partial_{\alpha\beta}^2 \Phi_\beta^{(5)} \right] = -\gamma_3 \Phi_\alpha^{(3)}. \tag{4.43}$$

To get the hexapolar equation for the lattice gas (Eq. (3.68)), we first assume that we have no interaction energies such that $F_m = 0$ for all m. In the FHP model limit, we replace θ with θ_j as defined in Eq. (2.2) with $b = 6$. We find that $\Phi_x^{(5)} = \Phi_x^{(1)}$ and $\Phi_y^{(5)} = -\Phi_y^{(1)}$. Doing this replacement, we see that

$$\partial^2_{\alpha\beta}\Phi_\beta^{(5)} = \begin{pmatrix} \partial_x^2 - \partial_y^2 & -2\partial_x\partial_y \\ -2\partial_x\partial_y & -\partial_x^2 - \partial_y^2 \end{pmatrix} \Phi_\beta^{(1)}. \tag{4.44}$$

In this limit, we have a scalar hexapolar mode $\Phi_x^{(3)} = \phi$ and $\Phi_y^{(3)} = 0$, so the only relevant part of Eq. (4.44) is the first row of the matrix, which has the form $\bar{\partial}^2_{x\beta}\Phi_\beta^{(1)}$. The decay rates satisfy $\gamma_2 = \gamma_4$. Using this, we write the x-component part of Eq. (4.43) in terms of $\mathbf{j}$ and ϕ. Replacing $v_F^2/(4\gamma_2)$ with ν leads to

$$\partial_t\phi = 2\nu\partial_\beta^2\phi + \frac{2}{v_F}\nu\bar{\partial}^2_{x\beta}j_\beta - \gamma_3\phi. \tag{4.45}$$

This is exactly the linearized hexapolar equation (Eq. (3.75)). We see that the factors of two that appear are due to the rotational symmetry of the lattice, such that the $m = 5$ mode becomes the conjugate of the $m = 1$ mode.

This additional factor of two, which we may consider a lattice artifact, has the unfortunate consequence that the lattice gas does not accurately model the 2DEG. It gives a stronger coupling to the $\mathbf{\Phi}^{(1)}$ mode in the hexapolar equation. When solving flow in a channel along the x-axis (Sec. 3.6), it also causes a perfect cancellation of the momentum diffusion terms, giving a constant ϕ solution, which is inaccurate for the 2DEG.

5 Conclusion

In this final chapter, we draw various conclusions about our findings of the lattice gas and its connection to the tomographic dynamics observed in two-dimensional Fermi liquids. In Sec. 5.1, we discuss the possibility of using LGCA to simulate tomographic Fermi liquids. There are many discrepancies with the model that hinder it from being fully accurate. In Sec. 5.2, we conclude this thesis by discussing possible research paths to explore in the future. This includes unexplored use cases for LGCA in condensed matter physics. We also suggest how the Fermi liquid equations derived in this work can be expanded upon and used in practice.

5.1 Simulating Tomographic Transport

The lattice gas cellular automaton exhibits dynamics that are reminiscent of those found in two-dimensional Fermi liquids. The model exhibits a two-step relaxation process, with a rapidly relaxing even-parity mode and a long-lived odd-parity mode, which are relaxed by symmetric three-body collisions and head-on collisions, respectively. The difference in relaxation times stems from the rarity of symmetric three-body collisions in comparison to head-on collisions. This effect can be increased by lowering the probability of three-body collisions, or by lowering the background density of particles. In two-dimensional Fermi liquids, odd-parity modes are instead relaxed by small-angle scattering. Thus, the even and odd relaxation rates do not have the same mathematical expressions in the LGCA as in the 2DEG. Still, the resulting odd-even effect is the same in both models, which lets us derive a similar set of macroscopic equations for both systems.

There are, however, some properties of the LGCA that limit its capability of accurately simulating a tomographic 2DEG. Firstly, the hexapolar mode of the LGCA only represents the cosine component of the true hexapolar mode. This limits the LGCA to scenarios where only this component is excited, such as flow in a channel along the x-axis. Secondly, the factor of two in the momentum diffusion term in the LGCA's hexapolar equation is not present in the 2DEG. As we found in Sec. 3.6, this causes a perfect cancellation in the steady-state equations for flow in a channel and a solution with a constant ϕ. In the 2DEG, if one assumes that the $m = 5$ mode is overdamped, the factor of two does not appear and the steady-state solution is different from the corresponding LGCA solution.

The lattice gas model serves as a simple model that exhibits tomographic dynamics, an aspect that was not explored when the model was introduced. Were it not for its lack of rotational symmetry, the dynamics would essentially be the same as those found in the 2DEG, without the effects of the Landau parameters of course. Since there are no regular polygons other than squares and triangles that tile the plane, obtaining more degrees of freedom to unlock higher angular modes seems impossible. For now, the model can still serve as a pedagogical tool to illustrate the odd-even effect on the kinetic level.

5.2 Outlook

There are many directions one can take these lattice gas models and, by extension, lattice Boltzmann methods. The single-speed LGCA with a regular two-dimensional lattice is a good proxy for a homogeneous Fermi liquid with a single circular Fermi surface. However, two-dimensional Fermi liquids can exhibit more exotic Fermi surfaces with more energy bands. A simple way of thinking about band structures in LGCA is to model particles with one of the six velocity vectors in the FHP model as belonging to the lowest band. These six velocity vectors point to the nearest-neighbor nodes, but one could also include the second-nearest-neighbor nodes. If one allows particles to also have velocities that point to the second-nearest neighbors, these particles would belong to a band with higher energy. Implementing multi-speed particles in this way has been done for the HPP model and lattice Boltzmann methods [29]. A challenge would be to model a non-circular Fermi surface, for instance the two oval Fermi surfaces found in d-wave altermagnets [35]. Another possibility is to use LGCA to model electron-hole hydrodynamics, electron-phonon hydrodynamics, or other exotic electron fluids [8], for instance using different species of particles. Besides Fermi liquids, LGCA can be adapted to study other problems in condensed matter physics. For instance, one can study chiral fluids by introducing a bias in the transition probabilities for collisions [36].

There are other aspects of tomographic transport that have not been explored using LGCA in this work. One such effect is that the long relaxation times of odd-parity modes are rapidly suppressed by weak magnetic fields [37]. The resulting Lorentz force from a magnetic field in the z-direction causes the electrons to precess counterclockwise in the xy-plane. In the lattice gas model, one can think of this as each particle having a small probability to change its velocity $c_j \to c_{j+1}$. This angular redistribution of velocities destroys the long-lived odd-parity mode at the rate of rotations. Another aspect that received little attention in this work was the role of kinetic boundary effects, which are affected by the relaxation times of the angular modes [38, 39]. Kinetic boundary layers, also known as Knudsen layers, have been analyzed previously but without the context of the tomographic effect [30].

Finally, the macroscopic Fermi liquid equations derived in Chapter 4 are simply a rewriting of known kinetic equations [33]. Due to the dependence on m in $\gamma_{m,\text{odd}}$, there is some threshold m_{cutoff} that allows one to assume higher modes $m > m_{\text{cutoff}}$ are overdamped. The truncated equations may be useful for experimentalists in flows with few non-overdamped odd-parity modes. We have also seen that the unusual tensor structures appear in the linear terms in the Fermi liquid equations. There are however some nonlinear terms in the macroscopic lattice gas equations that we did not attempt to find in the Fermi liquid. Finding these equations could help predict nonlinear effects in tomographic flows, such as shock waves, vortices, and turbulence.

To do this, one could make a similar expansion to the small perturbation expansion in the LGCA to second order.

Bibliography

[1] P. Drude. “Zur Elektronentheorie der Metalle”. In: *Annalen der Physik* 306.3, (1900), 566–613. eprint: `https://onlinelibrary.wiley.com/doi/pdf/10.1002/andp.19003060312`.

[2] P. Drude. “Zur Elektronentheorie der Metalle; II. Teil. Galvanomagnetische und thermomagnetische Effecte”. In: *Annalen der Physik* 308.11, (1900), 369–402. eprint: `https://onlinelibrary.wiley.com/doi/pdf/10.1002/andp.19003081102`.

[3] A. Sommerfeld. “Zur Elektronentheorie der Metalle auf Grund der Fermischen Statistik”. In: *Zeitschrift für Physik* 47.1, (Jan. 1928), 1–32. ISSN: 0044-3328.

[4] L. D. Landau. “The Theory of a Fermi Liquid”. In: *J. Exptl. Theoret. Phys. (U.S.S.R.)* 30, (June 1956), 1058–1064.

[5] Radii N. Gurzhi. “Minimum of resistance in impurity-free conductors”. In: *Sov. Phys. JETP* 44.771, (Aug. 1963), 045443–045445.

[6] K. S. Novoselov et al. “Electric Field Effect in Atomically Thin Carbon Films”. In: *Science* 306.5696, (2004), 666–669. eprint: `https://www.science.org/doi/pdf/10.1126/science.1102896`.

[7] Georgios Varnavides et al. “Charge transport and hydrodynamics in materials”. In: *Nature Reviews Materials* 8, (Oct. 2023), 726–741.

[8] L. Fritz and T. Scaffidi. “Hydrodynamic Electronic Transport”. In: *Annual Review of Condensed Matter Physics* 15.Volume 15, 2024, (2024), 17–44. ISSN: 1947-5462.

[9] R. Krishna Kumar et al. “Superballistic flow of viscous electron fluid through graphene constrictions”. In: *Nature Physics* 13.12, (Dec. 2017), 1182–1185. ISSN: 1745-2481.

[10] Joseph A. Sulpizio et al. “Visualizing Poiseuille flow of hydrodynamic electrons”. In: *Nature* 576.7785, (Dec. 2019), 75–79. ISSN: 1476-4687.

[11] A. Aharon-Steinberg et al. “Direct observation of vortices in an electron fluid”. In: *Nature* 607.7917, (July 2022), 74–80. ISSN: 1476-4687.

[12] Johannes Geurs et al. “Supersonic flow and hydraulic jump in an electronic de Laval nozzle”. In: *arXiv preprint arXiv:2509.16321*, (2025).

[13] B. Laikhtman. “Electron-electron angular relaxation in a two-dimensional electron gas”. In: *Phys. Rev. B* 45, (3 Jan. 1992), 1259–1266.

[14] R. N. Gurzhi, A. N. Kalinenko, and A. I. Kopeliovich. “Electron-electron momentum relaxation in a two-dimensional electron gas”. In: *Phys. Rev. B* 52, (7 Aug. 1995), 4744–4747.

[15] John von Neumann. “The General and Logical Theory of Automata”. In: *Cerebral Mechanisms in Behavior—The Hixon Symposium*. Ed. by L. A. Jeffress. Collected Works 5.288–328. New York: John Wiley, 1951, 1–41.

[16] John von Neumann. “Probabilistic Logics and the Synthesis of Reliable Organisms from Unreliable Components”. In: *Automata Studies*. Ed. by C. E. Shannon and J. McCarthy. Collected Works 5.329–378. Princeton: Princeton University Press, 1956, 43–98.

[17] John von Neumann. *The computer and the brain*. Yale Univer. Press, 1958.

[18] John von Neumann and Arthur W Burks. *Theory of self-reproducing automata*. University of Illinois Press Urbana, 1966.

[19] S. Ulam. “Random Processes and Transformations”. In: *Proceedings of the International Congress of Mathematicians*. Cambridge, Aug. 1950, 264–275.

[20] Stanislaw Ulam et al. “On some mathematical problems connected with patterns of growth of figures”. In: *Proceedings of symposia in applied mathematics*. Vol. 14. 14. American Mathematical Society Providence, RI, USA. 1962, 215–224.

[21] Stephen Wolfram. “Statistical mechanics of cellular automata”. In: *Rev. Mod. Phys.* 55, (3 July 1983), 601–644.

[22] J. Hardy, Y. Pomeau, and O. de Pazzis. “Time Evolution of a Two-Dimensional Classical Lattice System”. In: *Phys. Rev. Lett.* 31, (5 July 1973), 276–279.

[23] U. Frisch, B. Hasslacher, and Y. Pomeau. “Lattice-Gas Automata for the Navier-Stokes Equation”. In: *Phys. Rev. Lett.* 56, (14 Apr. 1986), 1505–1508.

[24] D. d’Humières, P. Lallemand, and U. Frisch. “Lattice Gas Models for 3D Hydrodynamics”. In: *Europhysics Letters* 2.4, (Aug. 1986), 291.

[25] Guy R. McNamara and Gianluigi Zanetti. “Use of the Boltzmann Equation to Simulate Lattice-Gas Automata”. In: *Phys. Rev. Lett.* 61, (20 Nov. 1988), 2332–2335.

[26] Bruce M. Boghosian et al. “Integer lattice gases”. In: *Phys. Rev. E* 55, (4 Apr. 1997), 4137–4147.

[27] Uriel Frisch et al. “Lattice Gas Hydrodynamics in Two and Three Dimensions”. In: *Complex Systems* 1.4, (1987), 649–707.

[28] B. Hasslacher. “Discrete Fluids”. In: *Los Alamos Science Special Issue* 15, (1987), 175–217.

[29] Dieter A Wolf-Gladrow. *Lattice-gas cellular automata and lattice Boltzmann models: an introduction*. Springer, 2004.

[30] R. Cornubert, D. d’Humières, and D. Levermore. “A Knudsen layer theory for lattice gases”. In: *Physica D: Nonlinear Phenomena* 47.1, (1991), 241–259. ISSN: 0167-2789.

[31] Michel Hénon. “Viscosity of a lattice gas”. In: *Lattice Gas Methods for Partial Differential Equations*. CRC Press, 2019, 181–208.

[32] U. Frisch. “Relation between the lattice Boltzmann equation and the Navier-stokes equations”. In: *Physica D: Nonlinear Phenomena* 47.1, (1991), 231–232. ISSN: 0167-2789.

[33] Johannes Hofmann and Sankar Das Sarma. “Collective modes in interacting two-dimensional tomographic Fermi liquids”. In: *Phys. Rev. B* 106, (20 Nov. 2022), 205412-1 –205412-11.

[34] D. Pines and P. Nozières. *The Theory of Quantum Liquids: Normal Fermi liquids*. Advanced book classics. W.A. Benjamin, 1966. ISBN: 9780201500639.
[35] Habib Rostami and Johannes Hofmann. "Fermi Liquid Theory of d-Wave Altermagnets: Demon Modes and Fano-Demon States". In: *Phys. Rev. Lett.* 135, (23 Dec. 2025), 236701.
[36] Andrew A. Allocca et al. *Odd fluids from chiral cellular automata*. 2026. arXiv: 2606.19431 [cond-mat.stat-mech].
[37] Habib Rostami et al. "Magnetic field suppression of tomographic electron transport". In: *Phys. Rev. B* 111, (15 Apr. 2025), 155434.
[38] Nitay Ben-Shachar and Johannes Hofmann. *Magnetotransport of tomographic electrons in a channel*. 2025. arXiv: 2503.14431 [cond-mat.mes-hall].
[39] Nitay Ben-Shachar and Johannes Hofmann. *Tomographic electron flow in confined geometries: Beyond the dual-relaxation time approximation*. 2025. arXiv: 2503.14461 [cond-mat.mes-hall].

A

Supplementary Lattice Gas Details

These appendices contain details of general non-deterministic lattice gas cellular automata. The following is based on the review by Frisch *et al.* [27].

A.1 Properties

There are several properties that hold for the discussed class of deterministic and non-deterministic LGCA, many of which involve velocity moments, also called lattice tensors [27, 29]. The velocity moment of order m is defined as

$$\sum_{j=0}^{b-1} c_{j\alpha_1} c_{j\alpha_2} \cdots c_{j\alpha_m}, \tag{A.1}$$

where the Roman and Greek indices refer to velocity labels and components, respectively. An important property is that odd-order velocity moments are zero and second-order velocity moments are given by

$$\sum_{j=0}^{b-1} c_{j\alpha} c_{j\beta} = \frac{bc^2}{d} \delta_{\alpha\beta}. \tag{A.2}$$

The proofs, as well as a discussion of more lattice properties, are provided by Frisch *et al.* [27].

The w_j introduces a new set of anisotropic velocity moments. Without any formal proofs, for a triangular lattice with $b = 6$, the new moments up to third order are computed as

$$\sum_{j=0}^{5} w_j = 0, \tag{A.3}$$

$$\sum_{j=0}^{5} c_{j\alpha} w_j = 0, \tag{A.4}$$

$$\sum_{j=0}^{5} c_{j\alpha} c_{j\beta} w_j = 0, \tag{A.5}$$

$$\sum_{j=0}^{5} c_{j\alpha} c_{j\beta} c_{j\gamma} w_j = R_{\alpha\beta\gamma} \neq 0. \tag{A.6}$$

Note that the third-order tensor $R_{\alpha\beta\gamma}$ is nonzero, which means that equations containing this tensor have broken isotropy. The tensor is symmetric and identified in Eq. (3.50).

A.2 Foundations of the Probabilistic Description

In this appendix, we establish a probabilistic description of the LGCA. We do so by considering an ensemble of similar models on a finite lattice $\mathcal{L}$ and defining an ensemble average over all realizations. To simplify the notation, we define the collision operator $\mathcal{C}$ and streaming operator $\mathcal{S}$ as

$$\mathcal{C}: \quad n_j(\mathbf{r}_*) \mapsto n_j(\mathbf{r}_*) + \Delta_j(\mathbf{n}(\mathbf{r}_*)), \tag{A.7}$$

$$\mathcal{S}: \quad n_j(\mathbf{r}_*) \mapsto n_j(\mathbf{r}_* - \mathbf{c}_j). \tag{A.8}$$

The composite of $\mathcal{C}$ and $\mathcal{S}$ is the evolution operator $\mathcal{E}$, defined as

$$\mathcal{E} = \mathcal{S} \circ \mathcal{C}. \tag{A.9}$$

It describes the dynamics of the lattice gas during one time step. We then write the dynamics of the whole system as two separate steps using $\mathcal{C}$ and $\mathcal{S}$ as

$$\mathbf{n}(t_* + 1/2, \cdot) = \mathcal{C}\mathbf{n}(t_*, \cdot), \tag{A.10}$$

$$\mathbf{n}(t_* + 1, \cdot) = \mathcal{S}\mathbf{n}(t_* + 1/2, \cdot), \tag{A.11}$$

where the $\cdot$ in the second argument of $\mathbf{n}$ represents every site on the lattice. We may also write this as a single operation using $\mathcal{E}$ as

$$\mathbf{n}(t_* + 1, \cdot) = \mathcal{E}\mathbf{n}(t_*, \cdot). \tag{A.12}$$

We introduce the phase space Γ, defined as the set of all possible assignments, or realizations, $s(\cdot) = \{s_j(\mathbf{r}_*) = 0 \text{ or } 1,\ j = 0, 1, \ldots, b-1,\ \mathbf{r}_* \in \mathcal{L}\}$. Using the phase space, we define an ensemble of initial conditions at time $t_* = 0$, each with an initial probability $P\left(0, s(\cdot)\right) \geq 0$ that is normalizable as

$$\sum_{s(\cdot)\in\Gamma} P\left(0, s(\cdot)\right) = 1. \tag{A.13}$$

If we let each initial condition evolve according to the non-deterministic evolution operator $\mathcal{E}$, the probabilities evolve according to the following Liouville equation, or Chapman-Kolmogorov equation,

$$P\left(t_* + 1, \mathcal{S}s'(\cdot)\right) = \sum_{s(\cdot)\in\Gamma} \prod_{\mathbf{r}_*\in\mathcal{L}} A\left(\mathbf{s}(\mathbf{r}_*) \to \mathbf{s}'(\mathbf{r}_*)\right) P\left(t_*, s(\cdot)\right), \tag{A.14}$$

where $A(\mathbf{s}' \leftarrow \mathbf{s})$ is the transition probability from state $\mathbf{s}$ to $\mathbf{s}'$. If $\mathcal{E}$ is deterministic, the Liouville equation simplifies to

$$P\left(t_* + 1, \mathcal{S}s(\cdot)\right) = P\left(t_*, \mathcal{C}^{-1}s(\cdot)\right) \tag{A.15}$$

or

$$P\left(t_*+1, s(\cdot)\right) \quad = P\left(t_*, \mathcal{E}^{-1}s(\cdot)\right). \tag{A.16}$$

Using this probabilistic description of the time evolution, we define the ensemble average of an observable $q\left(n(t_*, \cdot)\right)$, which depends on the Boolean field at time t_*, as

$$\langle q\left(n(t_*, \cdot)\right)\rangle = \sum_{s(\cdot)\in\Gamma} q\left(s(\cdot)\right) P\left(t_*, s(\cdot)\right). \tag{A.17}$$

Using the ensemble average, we may define the mean occupation N_j as the ensemble average of n_j:

$$N_j(t_*, \mathbf{r}_*) = \langle n_j(t_*, \mathbf{r}_*)\rangle = \sum_{\mathbf{s}(\cdot)\in\Gamma} s_j(\mathbf{r}_*) P\left(t_*, s(\cdot)\right). \tag{A.18}$$

A.3 Steady-State Solutions

It is of interest to find steady-state solutions, or equilibrium solutions, to the Liouville equation (A.14). For this, we assume a finite, periodically wrapped around lattice $\mathcal{L}$. Since there are no physical boundaries, and collisions are purely local, the solutions are expected to be translation invariant and thus independent of the nodes $\mathbf{r}_*$. Such solutions can be written as

$$P\left(s(\cdot)\right) = \prod_{\mathbf{r}_*\in\mathcal{L}} p\left(\mathbf{s}(\mathbf{r}_*)\right), \tag{A.19}$$

where $p(\mathbf{s})$ is the probability of a given state $\mathbf{s}$. Inserting the steady-state solution of $P\left(s(\cdot)\right)$ (Eq. (A.19)) into the Liouville equation (Eq. (A.14)) leads to

$$\begin{aligned}\prod_{\mathbf{r}_*\in\mathcal{L}} p\left(\mathbf{s}'(\mathbf{r}_*)\right) &= \sum_{s(\cdot)\in\Gamma}\prod_{\mathbf{r}_*\in\mathcal{L}} \left[A\left(\mathbf{s}(\mathbf{r}_*)\to\mathbf{s}'(\mathbf{r}_*)\right) p\left(\mathbf{s}(\mathbf{r}_*)\right)\right] \\ &= \prod_{\mathbf{r}_*\in\mathcal{L}}\sum_{\mathbf{s}(\mathbf{r}_*)} \left[A\left(\mathbf{s}(\mathbf{r}_*)\to\mathbf{s}'(\mathbf{r}_*)\right) p\left(\mathbf{s}(\mathbf{r}_*)\right)\right].\end{aligned} \tag{A.20}$$

Since the factor $f(\mathbf{s}(\mathbf{r}_*)) \equiv A\left(\mathbf{s}(\mathbf{r}_*)\to\mathbf{s}'(\mathbf{r}_*)\right) p\left(\mathbf{s}(\mathbf{r}_*)\right)$ only depends on the local state $\mathbf{s}(\mathbf{r}_*)$, one can write $\sum_{s(\cdot)\in\Gamma}\prod_{\mathbf{r}_*\in\mathcal{L}}$ as a product of sums.

The $p(\mathbf{s})$ can be written in terms of the cells N_j using an H-theorem for lattice gases established by Hénon [27]. This theorem proves that $p(\mathbf{s})$ must be factorized over the b cells N_j, such that

$$p(\mathbf{s}) = \prod_j N_j^{s_j}\left(1-N_j\right)^{(1-s_j)}. \tag{A.21}$$

Eq. (A.21) is used to define the local entropy H in Eq. (2.26), which is non-decreasing over time. Since the probability $p(\mathbf{s})$ depends only on the local state and is independent of $\mathbf{r}_*$, inserting Eq. (A.21) into Eq. (A.20) gives

$$\prod_k N_k^{s'_k}\left(1-N_k\right)^{(1-s'_k)} = \sum_{\mathbf{s}} A\left(s\to s'\right)\prod_k N_k^{s_k}\left(1-N_k\right)^{(1-s_k)}, \quad \forall\mathbf{s}'. \tag{A.22}$$

These are 2^b independent equations, one for each configuration of $\mathbf{s}'$. Deriving the steady-state solution of Eq. (A.22) is not trivial [27]. One finds that the solutions are Fermi-Dirac distributed, given by Eq. (2.27) (see [27]). The steady states N_j^{eq} are also solutions to the following b equations:

$$\sum_{\mathbf{s}\mathbf{s}'} \left(s_j' - s_j\right) A(\mathbf{s}' \leftarrow \mathbf{s}) \prod_k N_k^{s_k} \left(1 - N_k\right)^{(1-s_k)} = 0, \quad \forall j. \tag{A.23}$$

The solutions N_j^{eq} annihilate the collision function, such that $\Delta_j(\mathbf{N}^{\mathrm{eq}}) = 0$.

B

Macroscopic Derivations

B.1 Small Perturbation Expansion Coefficients

To derive the small perturbation approximation to the equilibrium distribution with a long-lived ϕ, the expansion coefficients and the derivatives of the Fermi-Dirac distribution in Eq. (3.30) need to be determined. We begin by determining the derivatives $f_0^{(1)}$ and $f_0^{(2)}$, defined in Eq. (3.31). From Sec. 3.3, we already know that

$$f_0^{(0)} = \frac{1}{1+e^{h^{(0)}}} = \frac{\rho_0}{b} \quad \Rightarrow e^{h^{(0)}} = \frac{b-\rho_0}{\rho_0}. \tag{B.1}$$

We evaluate the first- and second-order derivatives $f_0^{(1)}$ and $f_0^{(2)}$ as

$$f_0^{(1)} = \frac{-e^{h^{(0)}}}{(1+e^{h^{(0)}})^2} = \frac{\rho_0(\rho_0-b)}{b^2}, \tag{B.2}$$

$$f_0^{(2)} = \frac{e^{h^{(0)}}\left(e^{h^{(0)}}-1\right)}{(1+e^{h^{(0)}})^3} = \frac{\rho_0(\rho_0-b)(2\rho_0-b)}{b^3}. \tag{B.3}$$

Inserting Eqs. (B.2) and (B.3) into Eq. (3.30) leads to

$$\begin{aligned} N_j = \frac{\rho_0}{b} + \frac{\rho_0(\rho_0-b)}{b^2}&\left(h^{(\delta\rho)}\delta\rho + h^{(\delta\rho,\delta\rho)}\delta\rho^2 + h^{(u,u)}u^2 + h^{(\phi,\phi)}\phi^2 + \right.\\ &\left.\left(q^{(u)} + q^{(\delta\rho,u)}\delta\rho\right)c_{j\alpha}u_\alpha + \left(z^{(\phi)} + z^{(\delta\rho,\phi)}\delta\rho\right)w_j\phi\right)\\ &+ \frac{\rho_0(\rho_0-b)(2\rho_0-b)}{2b^3}\left((q^{(u)})^2c_{j\alpha}c_{j\beta}u_\alpha u_\beta + 2q^{(u)}z^{(\phi)}c_{j\alpha}w_ju_\alpha\phi + (z^{(\phi)})^2\phi^2\right). \end{aligned} \tag{B.4}$$

The expansion coefficients $h^{(\delta\rho)}$, $h^{(\delta\rho,\delta\rho)}$, $h^{(u,u)}$, $h^{(\phi,\phi)}$, $q^{(u)}$, $q^{(\delta\rho,u)}$, $z^{(\phi)}$, and $z^{(\delta\rho,\phi)}$ are determined using the definitions of the mean quantities. Starting with the density, inserting Eq. (B.4) into Eq. (2.21) leads to

$$\begin{aligned} \rho_0 + \delta\rho = \rho_0 + bf_0^{(1)}&\left(h^{(\delta\rho)}\delta\rho + h^{(\delta\rho,\delta\rho)}\delta\rho^2 + h^{(u,u)}u^2 + h^{(\phi,\phi)}\phi^2\right)\\ &+ \frac{b}{2}f_0^{(2)}\left(\frac{c^2}{d}(q^{(u)})^2\delta_{\alpha\beta}u_\alpha u_\beta + (z^{(\phi)})^2\phi^2\right) \end{aligned} \tag{B.5}$$

Many terms disappear due to the properties of velocity moments and moments involving w_j in Appendix A.1. Subtracting ρ_0 on both sides of (B.5) and separating the $\delta\rho$, $\delta\rho^2$, u^2 and ϕ^2 terms into separate equations leads to

$$1 = bf_0^{(1)}h^{(\delta\rho)}, \tag{B.6}$$

$$0 = h^{(\delta\rho,\delta\rho)}, \tag{B.7}$$

$$0 = bh^{(u,u)} + \frac{c^2}{2d}(2\rho_0 - b)(q^{(u)})^2, \tag{B.8}$$

$$0 = 2bh^{(\phi,\phi)} + (2\rho_0 - b)(z^{(\phi)})^2. \tag{B.9}$$

From Eq. (B.7), we see that the $\delta\rho^2$ term is zero. Using Eq. (B.6), we identify $h^{(\delta\rho)}$ as

$$h^{(\delta\rho)} = \frac{1}{bf_0^{(1)}} = \frac{b}{\rho_0(\rho_0 - b)}. \tag{B.10}$$

Writing the momentum as $\rho\mathbf{u} = (\rho_0 + \delta\rho)\,\mathbf{u}$ and inserting Eq. (B.4) into Eq. (2.22) leads to

$$(\rho_0 + \delta\rho)\,u_\alpha = \frac{bc^2}{d} f_0^{(1)} \left(q^{(u)} + q^{(\delta\rho,u)}\delta\rho\right)\delta_{\alpha\beta}u_\beta. \tag{B.11}$$

Eq. (B.11) contains a Kronecker delta on the RHS which destroys any non-isotropic terms. It is therefore clear that our ansatz that $q^{(u)}_{\alpha\beta}(\rho_0)u_\beta + q^{(\delta\rho,u)}_{\alpha\beta}(\rho_0)\delta\rho u_\beta = q^{(u)}(\rho_0)u_\alpha + q^{(\delta\rho,u)}(\rho_0)\delta\rho u_\alpha$ holds.

Using the Kronecker delta and separating the u_β and $\delta\rho u_\beta$ parts in Eq. (B.11) identifies the expansion coefficients $q^{(u)}$ and $q^{(\delta\rho,u)}$ as

$$q^{(u)} = \frac{d\rho_0}{bc^2 f_0^{(1)}} = \frac{db}{c^2(\rho_0 - b)}, \tag{B.12}$$

$$q^{(\delta\rho,u)} = \frac{d}{bc^2 f_0^{(1)}} = \frac{db}{c^2\rho_0(\rho_0 - b)}. \tag{B.13}$$

We insert Eq. (B.4) into the equation for the hexapolar mode (Eq. (3.8)), which leads to

$$\phi = bf_0^{(1)}\left(z^{(\phi)} + z^{(\delta\rho,\phi)}\delta\rho\right)\phi. \tag{B.14}$$

For Eq. (B.14) to hold, $z^{(\delta\rho,\phi)}$ must be zero since there is only one term proportional to $\delta\rho\phi$. Taking the ϕ part of Eq. (B.14), we may solve for the expansion coefficient $z^{(\phi)}$ as

$$z^{(\phi)} = \frac{1}{bf_0^{(1)}} = \frac{b}{\rho_0(\rho_0 - b)}. \tag{B.15}$$

Inserting Eqs. (B.12) and (B.15) into Eqs. (B.8) and (B.9) allows us to identify $h^{(u,u)}$ and $h^{(\phi,\phi)}$ as

$$h^{(u,u)} = -\frac{db(2\rho_0 - b)}{2c^2(\rho_0 - b)^2}, \tag{B.16}$$

$$h^{(\phi,\phi)} = -\frac{b(2\rho_0 - b)}{2\rho_0^2(\rho_0 - b)^2}. \tag{B.17}$$

Inserting the values of the expansion coefficients (Eqs. (B.12), (B.15), (B.16), and (B.17)) into Eq. (B.4) leads to

$$\begin{aligned} N_j = \frac{\rho_0 + \delta\rho}{b} - \frac{d\rho_0(2\rho_0 - b)}{2bc^2(\rho_0 - b)}u^2 - \frac{2\rho_0 - b}{2b\rho_0(\rho_0 - b)}\phi^2 + \frac{d\,(\rho_0 + \delta\rho)}{bc^2}c_{j\alpha}u_\alpha + w_j\frac{\phi}{b} \\ + \frac{d^2\rho_0(2\rho_0 - b)}{2bc^4(\rho_0 - b)}c_{j\alpha}c_{j\beta}u_\alpha u_\beta + \frac{d(2\rho_0 - b)}{bc^2(\rho_0 - b)}c_{j\alpha}w_j u_\alpha\phi + \frac{2\rho_0 - b}{2b\rho_0(\rho_0 - b)}\phi^2 \end{aligned} \tag{B.18}$$

The two ϕ^2-terms in Eq. (B.18) perfectly cancel. Rearranging the terms and substituting $b = 6$ and $d = 2$, and introducing the factors $G(\rho)$ and $Q_{j\alpha\beta}$ (as defined in Eqs. (3.33) and (3.3)) results in the small perturbation approximation in Eq. (3.32).

B.2 Deriving the Second-Order Corrections

We want to derive macroscopic equations introduced in Sec. 3.4 to second order in the time scale ϵ. These will describe the diffusive dynamics of the density ρ, momentum $\rho\mathbf{u}$, and hexapolar mode ϕ. We will make use of the small perturbation equilibrium distribution $N_j^{(0)}$ (Eq. (3.32)), momentum-flux tensor $P_{\alpha\beta}$ (Eq. (3.48)), and hexapolar-flux tensor Y_β (Eq. (3.51)). We begin by collecting the ϵ^2 terms in Eq. (3.41), which leads to the three diffusive equations

$$\begin{aligned} 0 = \partial_{t_2}\sum_j N_j^{(0)} + \frac{1}{2}\partial_{t_1}\partial_{t_1}\sum_j N_j^{(0)} + \frac{1}{2}\partial_{1\beta}\partial_{1\gamma}\sum_j c_{j\beta}c_{j\gamma}N_j^{(0)} \\ + \partial_{t_1}\partial_{1\beta}\sum_j c_{j\beta}N_j^{(0)} + \partial_{t_1}\sum_j N_j^{(1)} + \partial_{1\beta}\sum_j c_{j\beta}N_j^{(1)}, \end{aligned} \tag{B.19}$$

$$\begin{aligned} 0 = \partial_{t_2}\sum_j c_{j\alpha}N_j^{(0)} + \frac{1}{2}\partial_{t_1}\partial_{t_1}\sum_j c_{j\alpha}N_j^{(0)} + \frac{1}{2}\partial_{1\beta}\partial_{1\gamma}\sum_j c_{j\alpha}c_{j\beta}c_{j\gamma}N_j^{(0)} \\ + \partial_{t_1}\partial_{1\beta}\sum_j c_{j\alpha}c_{j\beta}N_j^{(0)} + \partial_{1\beta}\sum_j c_{j\alpha}c_{j\beta}N_j^{(1)} + \partial_{t_1}\sum_j c_{j\alpha}N_j^{(1)}, \end{aligned} \tag{B.20}$$

$$\begin{aligned} 0 = \partial_{t_2}\sum_j w_j N_j^{(0)} + \frac{1}{2}\partial_{t_1}\partial_{t_1}\sum_j w_j N_j^{(0)} + \frac{1}{2}\partial_{1\beta}\partial_{1\gamma}\sum_j w_j c_{j\beta}c_{j\gamma}N_j^{(0)} \\ + \partial_{t_1}\partial_{1\beta}\sum_j w_j c_{j\beta}N_j^{(0)} + \partial_{1\beta}\sum_j w_j c_{j\beta}N_j^{(1)} + \partial_{t_1}\sum_j w_j N_j^{(1)}. \end{aligned} \tag{B.21}$$

To capture viscous effects, we keep only terms up to linear order in u and ϕ in $N_j^{(0)}$, $P_{\alpha\beta}$ and Y_β, discarding quadratic terms of order $\mathcal{O}(\epsilon^2 u^2)$, $\mathcal{O}(\epsilon^2 u\phi)$, and $\mathcal{O}(\epsilon^2\phi^2)$. Since $Y_\beta \sim \phi u$ to leading order, it is always zero to this order.

The density diffusion equation (Eq. (B.19)) is simplified using the definitions of ρ and $\mathbf{u}$ in Eqs. (2.21), (2.22), and (2.25). The non-equilibrium contributions $N_j^{(1)}$ disappear using the relations in Eq. (3.35). Expressing time derivatives ∂_{t_1} as spatial derivatives $\partial_{1\alpha}$ using Eqs. (3.45) and (3.46) leads to

$$\partial_{t_2}\rho = 0 \tag{B.22}$$

All momentum terms cancel at order ϵ^2 and we get no further contributions to the time evolution of ρ, resulting in Eq. (3.52). The momentum diffusion equation (Eq. (B.20)) requires more work. We want to express $\partial_{t_2}(\rho u_\alpha)$ in terms of only spatial derivatives. We use the same tricks as in the derivation of the previous equation, as well as the definition of ϕ in Eq. (3.8), leading to

$$\mathcal{O}(\delta^2) = \rho_0\partial_{t_2}u_\alpha + \frac{1}{2}\partial_{t_1}\partial_{1\beta}P_{\alpha\beta} + \frac{1}{2}\partial_{1\beta}\partial_{1\gamma}\sum_j c_{j\alpha}c_{j\beta}c_{j\gamma}N_j^{(0)} + \partial_{1\beta}\sum_j c_{j\alpha}c_{j\beta}N_j^{(1)}. \tag{B.23}$$

We insert our small perturbation approximation of $N_j^{(0)}$ from Eq. (3.32), up to linear order in the small parameters, into Eq. (B.23), which gives

$$\begin{aligned}\mathcal{O}(\delta^2) = {} & \rho_0\partial_{t_2}u_\alpha + \frac{1}{2}\partial_{t_1}\partial_{1\beta}P_{\alpha\beta} + \frac{1}{12}R_{\alpha\beta\gamma}\partial_{1\beta}\partial_{1\gamma}\phi \\ & + \frac{1}{6c^2}\partial_{1\beta}\partial_{1\gamma}\sum_j c_{j\alpha}c_{j\beta}c_{j\gamma}c_{j\delta}(\rho_0 u_\delta) + \partial_{1\beta}\sum_j c_{j\alpha}c_{j\beta}N_j^{(1)}.\end{aligned} \tag{B.24}$$

To continue, we rearrange terms, grouping them by $\partial_{1\beta}$, and expand the momentum flux tensor $P_{\alpha\beta}$ using Eq. (3.48), keeping only terms linear in u and ϕ, which leads to

$$\mathcal{O}(\delta^2) = \rho_0\partial_{t_2}u_\alpha + \partial_{1\beta}\left[\sum_j c_{j\alpha}c_{j\beta}N_j^{(1)} + \frac{1}{6c^2}T_{\alpha\beta\gamma\delta}\rho_0\partial_{1\gamma}u_\delta\right] + \frac{1}{12}R_{\alpha\beta\gamma}\partial_{1\beta}\partial_{1\gamma}\phi. \tag{B.25}$$

The derivation of the hexapolar diffusion equation from Eq. (B.21) follows a similar process to the derivation of the momentum equation, which results in

$$\mathcal{O}(\delta^2) = \partial_{t_2}\phi + \frac{c^2}{4}\partial_{1\beta}\partial_{1\beta}\phi + \frac{1}{6c^2}R_{\beta\gamma\delta}\rho_0\partial_{1\beta}\partial_{1\gamma}u_\delta + \partial_{1\beta}\sum_j c_{j\beta}w_j N_j^{(1)}. \tag{B.26}$$

These equations still contain the non-equilibrium contributions $N_j^{(1)}$. These deviations should vanish in the equilibrium. Therefore, $N_j^{(1)}$ must be a linear combination of gradients of ρ, $\rho\mathbf{u}$, and ϕ with respect to $\mathbf{r}$. To determine the form of the $\mathbf{N}^{(1)}$, we start with the continuous lattice Boltzmann equation (Eq. (3.37)). We expand N_j and the derivatives using Eqs. (3.34) and (3.40). Keeping terms up to first order in ϵ leads to

$$\partial_{t_1} N_j^{(0)} + c_{j\alpha}\partial_{1\alpha} N_j^{(0)} = \Omega_j\left(\mathbf{N}^{(1)}\right). \tag{B.27}$$

Note that $\Omega_j\left(\mathbf{N}^{(0)}\right)$ is zero at equilibrium. We substitute $N_j^{(0)}$ with the small perturbation approximation (Eq. (3.32)). Since quadratic terms are discarded at the order of ϵ^2, we keep only linear terms in u and ϕ and evaluate the LHS as

$$\text{LHS} = -\frac{1}{6}\rho_0\partial_{1\alpha}u_\alpha - \frac{1}{3c^2}c_{j\alpha}\partial_{1\beta}P_{\alpha\beta} + \frac{1}{6}c_{j\alpha}\partial_{1\alpha}\rho + \frac{1}{6}c_{j\alpha}w_j\partial_{1\alpha}\phi + \frac{1}{3c^2}c_{j\alpha}c_{j\beta}\rho_0\partial_{1\alpha}u_\beta. \tag{B.28}$$

The Y_α term disappears since it is quadratic in u and ϕ to leading order. Using Eq. (3.48) to simplify $P_{\alpha\beta}$ and discarding nonlinear terms leads to

$$\text{LHS} = \frac{1}{3c^2}Q_{j\alpha\beta}\rho_0\partial_{1\alpha}u_\beta + \frac{1}{6}c_{j\alpha}w_j\partial_{1\alpha}\phi. \tag{B.29}$$

We linearize the Boltzmann collision function which gives us the equation

$$\frac{1}{3c^2}Q_{j\alpha\beta}\rho_0\partial_{1\alpha}u_\beta + \frac{1}{6}c_{j\alpha}w_j\partial_{1\alpha}\phi = \sum_k \mathcal{L}_{jk}N_k^{(1)}. \tag{B.30}$$

Since the elements $\mathcal{L}_{jk}$ are constants, we assume that $N_j^{(1)}$ contains two terms that are proportional to $Q_{j\alpha\beta}\rho_0\partial_{1\alpha}u_\beta$ and $c_{j\alpha}w_j\partial_{1\alpha}\phi$, respectively. This gives us the ansatz for $N_j^{(1)}$ in Eq. (3.55). Combining this ansatz with Eqs. (B.22), (B.25), and (B.26) gives the second-order corrections to the macroscopic equations (Eqs. (3.52), (3.53), and (3.54)). We may also combine Eq. (B.30) with the ansatz for $N_j^{(1)}$. Separating the ρu_β and ϕ parts leads to

$$\left[\frac{1}{3c^2}Q_{j\alpha\beta} - \sum_k \mathcal{L}_{jk}\psi(\rho_0)Q_{k\alpha\beta}\right]\rho_0\partial_{1\alpha}u_\beta = 0, \tag{B.31}$$

$$\left[\frac{1}{6}c_{j\alpha}w_j - \sum_k \mathcal{L}_{jk}\xi(\rho_0)c_{k\alpha}w_k\right]\partial_{1\alpha}\phi = 0. \tag{B.32}$$

For the equations to hold for arbitrary ρu_β and ϕ, both expressions inside the square brackets must be equal to zero. We multiply the vanishing square bracket in Eq. (B.31) by $Q_{j\alpha\beta}$ and sum over j, α, and β. Similarly, we multiply the vanishing bracket in Eq. (B.32) by $c_{j\alpha}w_j$ and sum over j and α. The resulting equations are given by Eqs. (3.56) and (3.57).

C

Fermi Liquid Kinetic Equation

This appendix contains some supplementary details about the Fermi liquid description of a homogeneous two-dimensional electron gas, introduced in Chapter 4. Sec. C.1 introduces the total energy functional of the system. Sec. C.2 derives the form of the linearized kinetic equation.

C.1 The Energy Functional

The total energy of the system can be written as a functional $E[n_{\mathbf{p}}]$. If the energy is close to the ground-state energy E_0, we may Taylor expand the functional in small $\delta n_{\mathbf{p}}$ as

$$E[n_{\mathbf{p}}] = E_0 + \sum_{\mathbf{p}} \varepsilon_{\mathbf{p}} \delta n_{\mathbf{p}} + \frac{1}{2} \sum_{\mathbf{p}\mathbf{p}'} f_{\mathbf{p}\mathbf{p}'} \delta n_{\mathbf{p}} \delta n_{\mathbf{p}'} + \mathcal{O}(\delta n^3), \tag{C.1}$$

where $f_{\mathbf{p}\mathbf{p}'}$ is the Landau interaction function. It describes the interaction energy between pairs of quasiparticles. In principle, one may take higher-order functional derivatives which describe interaction energies between triplets, quartets, and more quasiparticles. However, in the linearized regime, it is sufficient to expand to second order in $\delta n_{\mathbf{p}}$.

The energy functional allows us to define the local quasiparticle energy $\tilde{\varepsilon}_{\mathbf{p}}(t, \mathbf{r})$, which describes the energy of adding an additional quasiparticle at $\mathbf{r}$. It is defined as

$$\tilde{\varepsilon}_{\mathbf{p}} = \frac{\partial E}{\partial \delta n_{\mathbf{p}}} = \varepsilon_{\mathbf{p}} + \delta \varepsilon_{\mathbf{p}}, \tag{C.2}$$

with

$$\delta \varepsilon_{\mathbf{p}} = \frac{1}{2} \sum_{\mathbf{p}'} \left(f_{\mathbf{p}\mathbf{p}'} + f_{\mathbf{p}'\mathbf{p}} \right) \delta n_{\mathbf{p}'}. \tag{C.3}$$

We may make some assumptions about the Landau function to simplify Eq. (C.3). We assume that the interactions are symmetric such that $f_{\mathbf{p}\mathbf{p}'} = f_{\mathbf{p}'\mathbf{p}}$. We further assume that the Landau function is isotropic such that it only depends on the angular difference $\theta - \theta'$, which leads to

$$\begin{aligned}\delta\varepsilon(\theta) &= \sum_{\mathbf{p}'} f(\theta-\theta')\delta n(\theta') \\ &= \mathcal{N}_0 \int_0^\infty \mathrm{d}\varepsilon' \left(-\frac{\partial n_0}{\partial \varepsilon'}\right) \int_0^{2\pi} \frac{\mathrm{d}\theta'}{2\pi} f(\theta-\theta')\delta\mu(\theta') \\ &\approx \mathcal{N}_0 \int_0^{2\pi} \frac{\mathrm{d}\theta'}{2\pi} f(\theta-\theta')\delta\mu(\theta'). \end{aligned} \tag{C.4}$$

Here, we have used the approximation $n_0(\varepsilon) = \Theta(\mu-\varepsilon)$ at $T=0$. Its derivative is then $\partial n_0/\partial\varepsilon = -\delta(\mu-\varepsilon)$. Defining the dimensionless Landau function as $F(\theta-\theta') = \mathcal{N}_0 f(\theta-\theta')$ leads to Eq. (4.7). If one approximates the distribution function as a step function, which is valid at low temperatures, the integral over ε' is equal to unity.

C.2 Linearized Kinetic Equation

The time evolution of the distribution function $n(\theta) = n(\theta; t, \mathbf{r})$ is governed by the semiclassical kinetic equation

$$\frac{\partial}{\partial t} n(\theta) - \frac{\partial \tilde{\varepsilon}_{\mathbf{p}}}{\partial \mathbf{r}} \cdot \frac{\partial}{\partial \mathbf{p}} n(\theta) + \frac{\partial \tilde{\varepsilon}_{\mathbf{p}}}{\partial \mathbf{p}} \cdot \frac{\partial}{\partial \mathbf{r}} n(\theta) = \mathcal{J}\left[n(\theta)\right], \tag{C.5}$$

where $\mathcal{J}[n(\theta)]$ is the collision integral. As with the collision function in LGCA, the collision integral describes weak interactions via electron-electron scattering. We linearize Eq. (C.5) by evaluating the derivatives of the local quasiparticle energy and dropping terms of order $\mathcal{O}(\delta n^2)$:

$$\frac{\partial \tilde{\varepsilon}_{\mathbf{p}}}{\partial \mathbf{r}} \cdot \frac{\partial n(\theta)}{\partial \mathbf{p}} = \frac{\partial \delta\varepsilon(\theta)}{\partial \mathbf{r}} \cdot \frac{\partial}{\partial \mathbf{p}} \left(n_0 + \delta n(\theta)\right) = \frac{\partial \delta\varepsilon(\theta)}{\partial \mathbf{r}} \cdot \frac{\partial n_0}{\partial \mathbf{p}} + \mathcal{O}(\delta n^2) \tag{C.6}$$

$$\frac{\partial \tilde{\varepsilon}_{\mathbf{p}}}{\partial \mathbf{p}} \cdot \frac{\partial n(\theta)}{\partial \mathbf{r}} = \frac{\partial}{\partial \mathbf{p}} \left(\varepsilon_{\mathbf{p}} + \delta\varepsilon(\theta)\right) \cdot \frac{\partial \delta n(\theta)}{\partial \mathbf{r}} = \mathbf{v}_\theta \cdot \frac{\partial \delta n(\theta)}{\partial \mathbf{r}} + \mathcal{O}(\delta n^2), \tag{C.7}$$

where, in the final line, we used $\partial\varepsilon_{\mathbf{p}}/\partial\mathbf{p} = \mathbf{v}_\theta$. Eq. (C.6) is further rewritten as

$$\frac{\partial n_0}{\partial \mathbf{p}} = \frac{\partial \varepsilon_{\mathbf{p}}}{\partial \mathbf{p}} \frac{\partial n_0}{\partial \varepsilon_{\mathbf{p}}} = \mathbf{v}_\theta \frac{\partial n_0}{\partial \varepsilon_{\mathbf{p}}}. \tag{C.8}$$

This leads us to the linearized kinetic equation (Eq. (4.5)).

DEPARTMENT OF PHYSICS
CHALMERS UNIVERSITY OF TECHNOLOGY
Gothenburg, Sweden
www.chalmers.se